Escola Universitària d'Enginyeria
Tècnica Industrial de Barcelona
Consorci Escola Industrial de Barcelona
UNIVERSITAT POLITÈCNICA DE CATALUNYA

Volume I
Report – Annex

THESIS

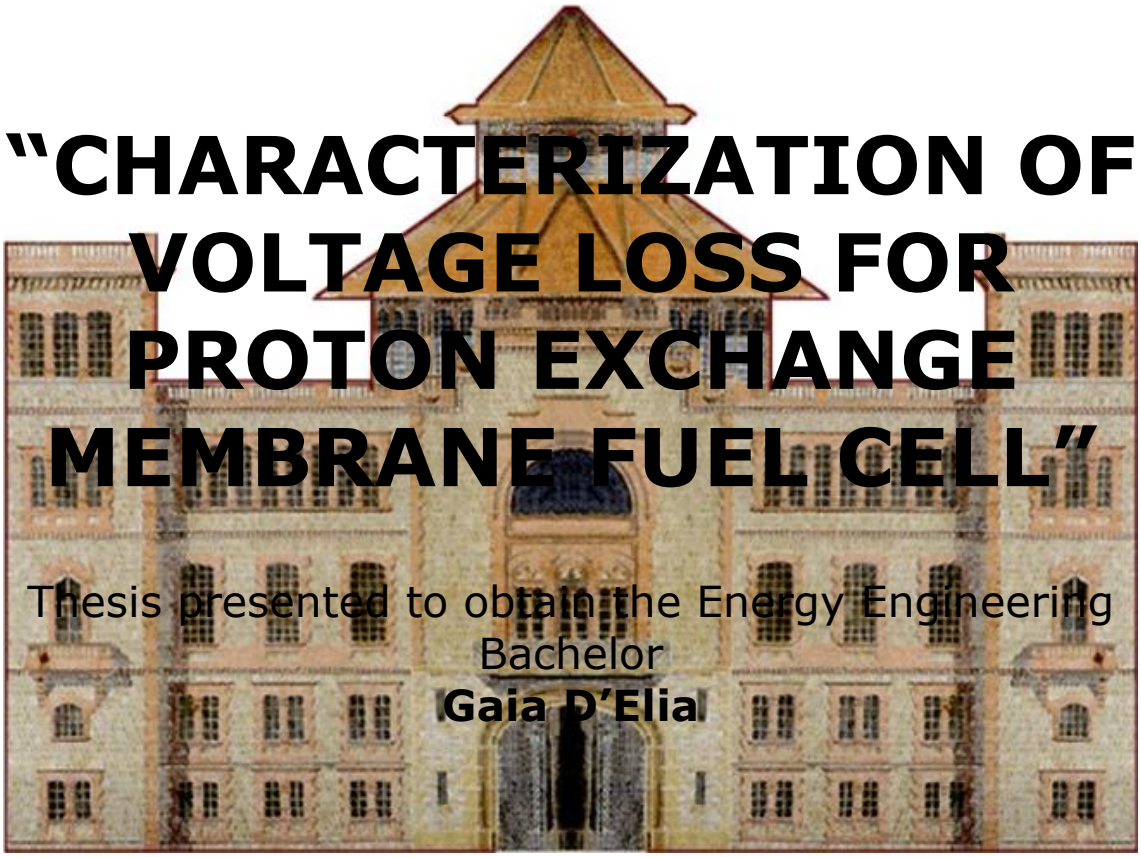

"CHARACTERIZATION OF VOLTAGE LOSS FOR PROTON EXCHANGE MEMBRANE FUEL CELL"

Thesis presented to obtain the Energy Engineering Bachelor

Gaia D'Elia

Barcelona, 9th June 2015

Director: Prof. Dr. Vicente Bitrián Varea
Department of Fluid Mechanics (D729)
Universitat Politècnica de Catalunya (UPC)

Codirector: Dr. Attila Husar
Institut de Robòtica i Informàtica industrial (UPC-CSIC)

DECLARATION OF AUTORSHIP

I, Gaia D'Elia, declare that this thesis and the work presented in it are my own.

I confirm that:

- All the published works of others that I have consulted, is always clearly attributed.
- All references and verbatim extracts have been quoted.
- All sources of information, including graphs and data sets, have been specifically acknowledged.

Barcelona, 9th of June 2015

ACKNOWLEDGMENTS

I would like to express my gratitude to all those who made this diploma thesis possible. I want to thank the fuel cell laboratory of the *Institut de Robòtica i Informàtica Industrial* (CSIC/UPC) for allowing me to collaborate with their studies, using their laboratories and providing me help.

I am warmly thankful to my project director post-Doc. Attila Husar, who orientated me during all my thesis development, helping me to discover the fuel cell world. Furthermore I would like to thank Prof. Vicente Bitrian for the project supervision and the support received. I don't want to forget to thank Stephan Strahl who encouraged me to start my thesis in this field of study and helped me from the beginning to the very end, even from a distance.

Moreover, I would like to thank Prof. Dr. Jordi Riera for allowing me to work in their laboratories with the collaboration of all the team, in a friendly and stimulating environment. I would specially thank Miguel Allué and Vicente Roda who assisted me in my daily work in the laboratory, helping me to overcome problems, finding the best solutions.

Finally I would like to thank Prof. Dr. Ricardo Torres for offering me to work in this thesis, opening all these doors that lead me to work with all these people in this extraordinary conditions for my scientific development and personal growth.

RESUM

Les piles de combustible són, cada dia més, una alternativa als clàssics vectors energètics. La utilització de l'hidrogen com a font energètica suposa una important reducció d'emissions i costos, tot i que la tecnologia es encara massa cara per entrar en competició directa amb fonts i vectors energètics tradicionals.

En aquest context es desenvolupa aquesta tesis, més en concret, en el marc del programa PUMA MIND, un programa d'investigació europeu que cerca optimitzar el funcionament de les piles de combustible de membrana polimèrica (PEM) i reduir-ne els costos associats per aplicacions en el sector de l'automoció.

El treball es centra en la consolidació i reproducció de mètodes d'identificació i caracterització de les pèrdues de voltatge i els seus indicadors associats a partir de dades experimentals obtingudes al laboratori de piles de l'Institut de Robòtica i Informàtica Industrial (UPC – CSIC). Especialment interessant és l'estudi de la variació de la densitat de corrent d'intercanvi al càtode, relacionada amb les pèrdues de concentració d'oxigen a la capa catalitzadora del càtode. A més a més, aquestes dades experimental es poden utilitzar per validar models fluidodinàmics computacionals, tasca que s'inicia en aquest PFG i es continuarà en futurs estudis.

RESUMEN

Las pilas de combustible son, cada día más, una alternativa a los clásicos vectores energéticos. La utilización del hidrogeno como fuente energética supone una importante reducción de emisiones y costes; aun así el precio de esta nueva tecnología sigue siendo demasiado elevado para entrar en competición directa con las fuentes y vectores energéticos tradicionales.

En este contexto se desarrolla esta tesis, más en concreto, en el marco del programa PUMA MIND, un programa de investigación europeo que busca optimizar el funcionamiento de las pilas de combustible de membrana polimérica (PEM) y reducir sus costes asociados para aplicaciones en el sector de la automoción.

En concreto, esta tesis se centra en la consolidación y reproducción de métodos de identificación y caracterización de la perdidas de voltaje y de sus indicadores asociados a partir de datos experimentales obtenidos en el laboratorio de pilas del Instituto de Robótica (UPC – CSIC). Especialmente interesante es el estudio de la variación de la densidad de corriente de intercambio del cátodo, relacionada con las pérdidas de concentración de oxígeno en la capa catalizadora del cátodo. Además, estos datos experimentales se pueden utilizar para validar modelos de dinámica de fluidos computacional, tarea que se inicia con este PFG y que seguirá en futuros estudios.

ABSTRACT

Fuel cells are, every day more and more, an alternative to the usual energy vectors. Using hydrogen as source, the fossil costs and the emissions are highly reduced. Despite this, the investment costs of this new technology are still too high to compete with the traditional energy vectors.

In this context is where this thesis is developed, more specifically, as part of the European investigation program PUMA MIND which aim is to optimize the performance of the polymeric exchange membranes fuel cells (PEMFC) and reduce the associated costs for applications in the automotive sector.

This work is centred in the consolidation and reproduction of methods for identification and characterization of voltage losses and the associated indicators starting from experimental data obtained in the Fuel Cell laboratory at the *Institut de Robòtica i Informàtica Industrial (UPC – CSIC)*. Especially interesting is the study of the cathode exchange current density variation, related with the reduction of the oxygen concentration at the cathode's catalyst. Moreover, this experimental data can be used to validate computational fluid dynamics (CFD) models, work that starts whit this thesis and will continue in future studies.

CONTENTS

LIST OF FIGURES

LIST OF TABLES

LIST OF ABBREVIATIONS

IRI	Institut de Robòtica i Informàtica Industrial
CSIC	Centro Superior de Investigación Científica
PUMA MIND	Physical bottom Up Multi-scale Modelling for Automotive PEMFC Innovative performance and Durability optimization
CHP	Combined Heat and Power
FEM	Finite Element Method
GDL	Gas Diffusion Layer
MPL	Micro-Porous Layer
CL	Catalyst Layer
MEA	Membrane Electrode Assembly
PEM	Proton Exchange Membrane
CFD	Computational Fluid Dynamics
FC	Fuel Cell
FPGA	Field Programmable Gate Array
Rtos	Real Time Operation System
GUI	Graphical User Interface
EIS	Electrochemical Impedance Spectroscopy
CS	Current Sweep
PC	Polarization Curve
CEA	Atomic Energy Commission

SYMBOLS

α	Charge transfer coefficient	Dimensionless
X	Molar fraction	Dimensionless
E	Potential	[V]
G	Gibbs free energy	[kJ/mol]
H	Enthalpy	[kJ/mol]
S	Entropy	[kJ/mol·K]
h_f	Enthalpy of formation	[kJ/mol]
s_f	Entropy of formation	[kJ/mol·K]
H_{HHV}	Hydrogen's higher heating value	[kJ/mol]
H_{HHL}	Hydrogen's lower heating value	[kJ/mol]
I	Current	[A]
i	Current Density	[A/m]
i_0	Exchange Current Density	[A/m]
i_L	Limiting current density	[A/m]
M	Molar Mass	[kg/mol]
m	Mass	[kg]
$\dot{m}$	Mass flow rate	[kg/s]
μ	Dynamic viscosity	[Pa·s]
n	Number of electrones	Dimensionless
R_{ohm}	Ohmic resistance	[Ω]
ρ	Density	[kg/m^3]
T	Temperature	[K]
t	Time	[s]
W	Work	[W]
x	Mass fraction	Dimensionless
ϕ_l	Electrolyte potential	[V]
ϕ_s	Electronic phase potential	[V]
σ	Conductivity	[S/m]
Q	Charge	[Coulombs]
P	Pressure	[Pa]
V	Voltage	[V]
J	Molar flux	[mol/s·m^2]
C	Capacitor	[F]
F	Faraday's constant	[J/V/mol]
R	Universal gas constant	[J/molK]
u	Velocity	[m/s]

CHAPTER 1: INTRODUCTION

In the globalized society in which we live, that grows and develops more and more, the human life needs energy to survive and progress. This fact, added to the finite natural sources to cover today's energy consume, open the door to development of new ways to generate, as well as to new technologies that were not developed before because of economic reasons. The research in new fields of the energy generation, distribution and storage is not only due to the needing of finding alternatives to the finite fossil fuels, it is also a response to the needing of finding new energies environmental friendly and with a good social impact. In this context is where the research in hydrogen as an energetic vector is developed. Hydrogen can be used as a constant generation source, or what is more common, as a way to storage energy; in all of these cases hydrogen is used through fuel cells.

Hydrogen has lot of advantages, like the reduced C/H ratio (0/1). Since hydrogen can be used pure, the energy content of this vector is really high, at the same time that the carbon emissions are null. Since it is a gas, his weight is low and it can be compressed occupying reduced volume. It is 100% reusable: producing energy from hydrogen only generates water, which is easily recyclable as a raw material to produce hydrogen. Furthermore, hydrogen can be transformed in thermal, mechanical or electrical energy, even though the principal use of this vector is for

electricity generation, sometimes taking profit at the same time of the thermal generation (like a cogeneration process).

One of the problems of this technology is that hydrogen does not exist free, thus energy is needed to obtain it; this reduces the global energy efficiency of the process. What has been largely studied is the implementation of the fuel cell as a support for renewable generation like solar, wind or geothermal energy in order to have a more reliable generation. The use of the surplus generation of these sources to obtain pure hydrogen is a way to improve both technologies efficiencies in a global process.

Another problem is that it is still an expensive technology: some of the materials used are expensive so a research to optimize the investment costs as well as operational costs is needed to reach a low cost energy vector. In the last 25 years there has been a significant progress in terms of materials, component design or production, but there is still a lot of margin to improve, especially in the control research in order to better understand the physical phenomena implying a better control of the fuel cell to guarantee durability and a better efficiency.

This sphere is one of the research areas of the control group of the *Institut de Robòtica i Informàtica Industrial* (IRI). More specifically IRI is nowadays one of the partners of the project PUMA MIND.

1.1. PUMA MIND

The project PUMA MIND (Physical bottom Up Multi-scale Modelling for Automotive PEMFC Innovative performance and Durability optimization) is an international R&D project that aims to advance the state of knowledge in designing new tools for Proton Exchange Membrane Fuel Cells (PEMFCs).

The PUMA MIND approach, consisting in building up a diagnostic and control-dedicated physical model with large prediction capabilities, enables:

- reduction of the amount of experiments (and thus the cost) currently needed to build up classical empirical models with limited prediction capabilities;
- a better targeting of experimental characterizations in representative conditions of the end user application;
- new operation strategies reducing the performance degradation and also strategies to improve the stability of the materials and components;
- the integration at EU level of modelling efforts usually developed separately. This will be done with the development of a modelling platform for more efficient communication and coordination for higher impact of the use of modelling on the PEMFC optimization in engineering practice.

The Breakthroughs expected from PUMA MIND are:

- A set of simulation tools providing a better understanding of the interplay between mechanisms at different scales regarding the electrochemistry (including degradation such as catalyst dissolution, support corrosion, ionomer degradation), water management and thermo-mechanical stresses, and their related impact on the whole cell behaviour in real automotive application conditions.

- Modelling strategies to scale up detailed physical descriptions of mechanisms into macroscopic models, and providing a better understanding of the relationships between the operation conditions (e.g. type of current cycle, relative humidity, temperature, pressures…), the components structural and chemical properties, and the long-term cell durability.

- Cell level models, in particular 3D CFD models, predicting durability as function of the materials chemical and structural properties, components and operation conditions.

- On-line diagnostic model allowing to maintain the PEMFC operation under the appropriate conditions at a given current cycle for enhanced durability; in strong connection with novel validation experiments in ex-situ and in-situ conditions, control strategies to enhance the PEMFC durability and efficiency.

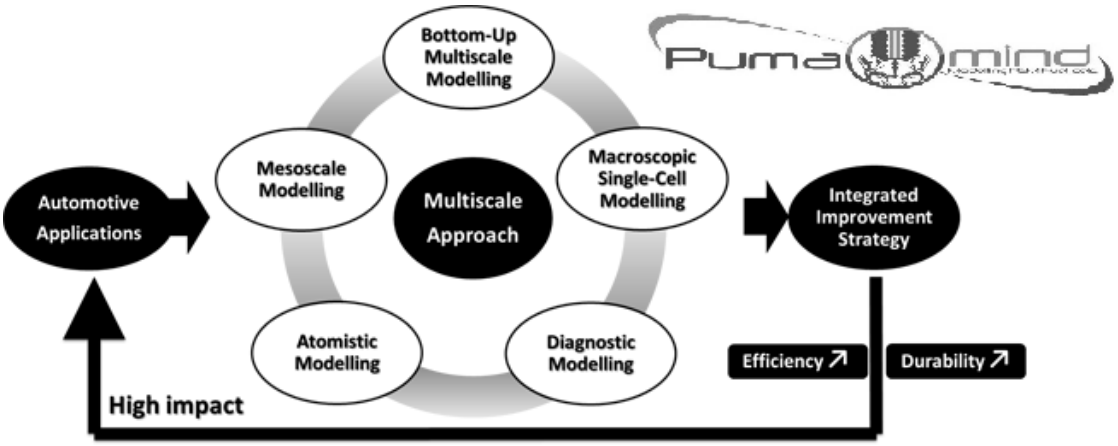

Fig 1: Puma mind project scheme [PUMA-MIND 2014]

The task of the Automatic Control team at IRI is to work on the Real-Time Diagnostic Model. The goals of these assignments are:

- to develop a control oriented model described by ordinary differential equation (ODE) based on the mathematical reduced version by the partners for real time diagnostic purpose.
- to develop and implement on-board monitoring tools to determine fuel cell performance and degradation indicators based on the mathematical model.
- to develop model based control strategies with the purpose of enhancing the PEMFC performance and durability. Design observers for the estimation of states and performance variables in the PEMFC [IRI 2012].

This diploma thesis is a contribution to the development and the achievement of the objectives of the Control group of IRI for the project PUMA MIND. Specifically this work is dedicated to the estimation of the internal voltage losses inside the fuel cell, defining dynamic observers associated to the estimation of states. Moreover, with the purpose of enhancing the PEMFC performance, a CFD model is started to develop.

CHAPTER 2: OBJECTIVE

The objective of this thesis is the experimental characterization of the main voltage loss indicators of the PUMA MIND PEMFC from Alternative Energies and Atomic Energy Commission (CEA) and the adaptation of existing CFD models, starting from these experimental values, in order to optimize the performance of the FC.

Studying the main voltage loss indicators at different operating conditions like temperature, pressure and anode and cathode stoichiometry is possible to define which is the best combination to obtain the best operation condition of the PEMFC. In like manner the CFD model in COMSOL Multiphysics allows for determining the best combination of external condition with a larger range of option than in the experimental case.

Furthermore, the CFD model is a necessary tool in order to determine the related energy costs, identifying optimal operating conditions for the FC that comply at the same time with the durability criteria and the economic requirement.

CHAPTER 3:

LITERATURE REVIEW

This chapter intends to put the basis for a good understanding of the work done throughout the thesis. Understanding what a fuel cell is, how it works and which the principal applications of this technology are is essential to have a panoramic view on the topic, reaching a holistic knowledge.

Since the object of this thesis is a single cell PEMFC everything is explained focusing in this particular kind of fuel cell, without renouncing to have a global review. The electrochemical and physical phenomena are the basis to understand the experimental work done, as well as the main body of the model.

3.1. Fuel Cells

A fuel cell is an electrochemical converter that transforms the chemical energy of the fuel directly in DC current. This singular and straight step makes of fuel cells one of the energy converters with higher efficiency.

What happens in a fuel cell is the reverse process of electrolysis (Fig 2). For the electrolysis you need energy (electricity) to separate hydrogen and oxygen from a molecule of water. In a fuel cell the recombination of hydrogen and oxygen into water takes place, generating energy (electricity and thermal energy).

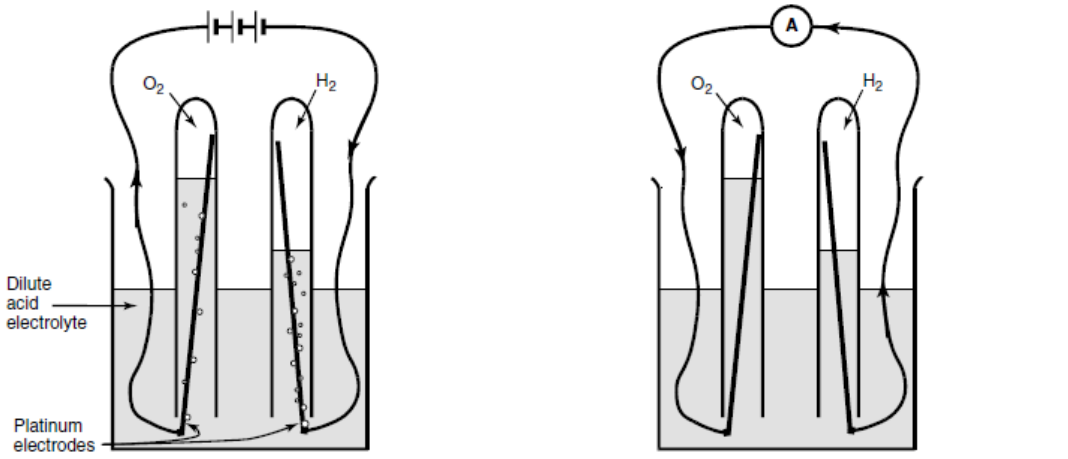

(a) Electrolysis of water (b) Oxygen and hydrogen recombining

Fig 2: Fuel cell principle [Larminie and Dicks 2003]

The first scientist to demonstrate this process was William Groove in 1839. After him, the biggest improvements in these fields were carried on by the military intelligence and space programmes that have been working with different kinds of fuel cells since 1960's.

Nowadays, it is possible to catalogue the existing fuel cell distinguishing the electrolyte or the application.

There are basically 6 types of fuel cell: all of them have the same electrochemical and physics basis, what changes is the inlet fuel, the membrane, and the mobile ion.

Table 1: Fuel cell types and characteristics

Fuel Cell Type		Mobile Ion	Operating Temperature	Electrolyte	Applications
Proton Exchange Membrane Fuel Cell	PEMFC	H+	80°C – 200°C	Polymeric membrane	Transport (cars) Mobile applications
Direct Methanol Fuel Cell	DMFC	H+	60°C – 130°C	Polymeric membrane	Mobile applications
Solid Oxide Fuel Cell	SOFC	O2-	800°C – 1000°C	Ceramics	Stationary applications (CHP)
Alkaline Fuel Cell	AFC	OH-	70°C – 250°C	Alkaline (Potassium hydroxide)	Space vehicles
Molten Carbonate Fuel Cell	MCFC	CO32-	650°C	Porous ceramic	Stationary applications (CHP)
Phosphoric Acid Fuel Cell	PAFC	H+	180°C	Phosphoric acid	Stationary applications (CHP) Transport (buses)

It is possible to observe in the table that the PEMFC (Fig 3) are the ones that work at lower temperatures, reducing the operational costs. This is one of the main advantages since it also reduces the costs of the components. Other advantages are the high efficiency, the short start up and the compactness that make them one of the best for transport applications. Besides, they have also some disadvantages as the short time life and the high costs for some components as the membrane or the catalyst layer.

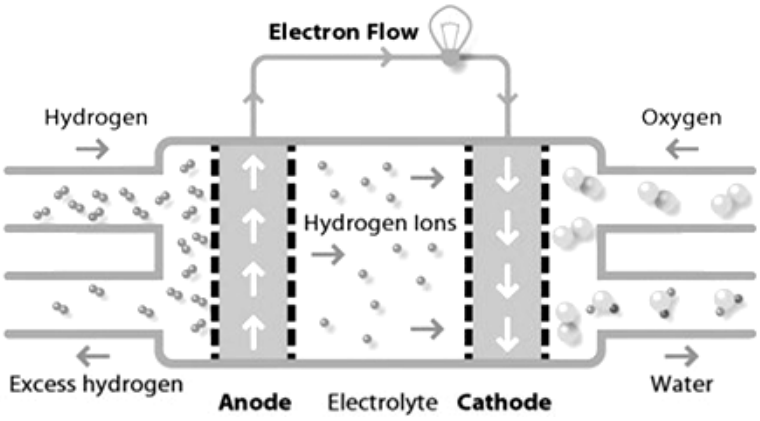

Fig 3: PEMFC scheme [Matthey 2015]

The project PUMA MIND is focused in the PEMFC, and thus this thesis as well. Thus all the following topics are centred in this type of FC.

3.2. PEM fuel cell applications

Fuel Cell applications are mainly three: transport, stationary generation and portable generation.

1. **Automotive systems:** in this field private and public transport are included. There are a lot of cities in the world that have buses working with fuel cells: more silent, environmental friendly and cheaper from the fuel point of view.

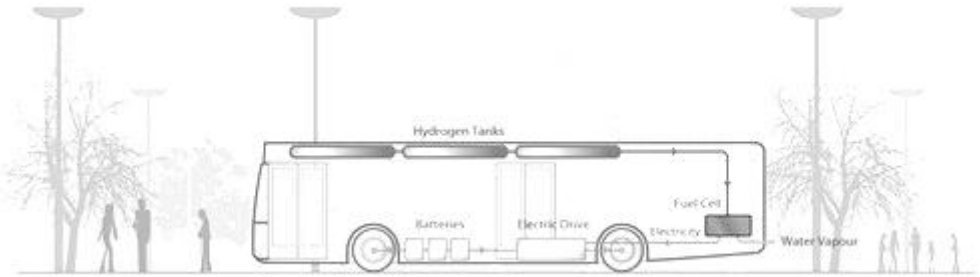

Fig 4: FC system applied to a bus [Matthey 2015]

In the private market, most of the manufacturers have their own car that works, totally or partially (hybrids), ran by FC or they are working on prototypes to sell soon. This is the case of BWM, Ford, General Motors, Honda, Nissan, Hyundai, Ferrari and others.
Due to the need for high power densities, low weight and function in rigorous environmental conditions, automotive systems are obviously the most complex and challenging [S. Strahl 2010]. This is why there is a public financed line of investigation in this field; there is still a lot of work to do with the dynamic response and control of the FC for a longer time life and reducing the primary costs.

2. **Portable Systems**: electronic devices, computers or mobile phones are the main objects where is possible to use FC, even though this is application is not commercial yet. What has been distributed as a portable use of FC is for military devices.

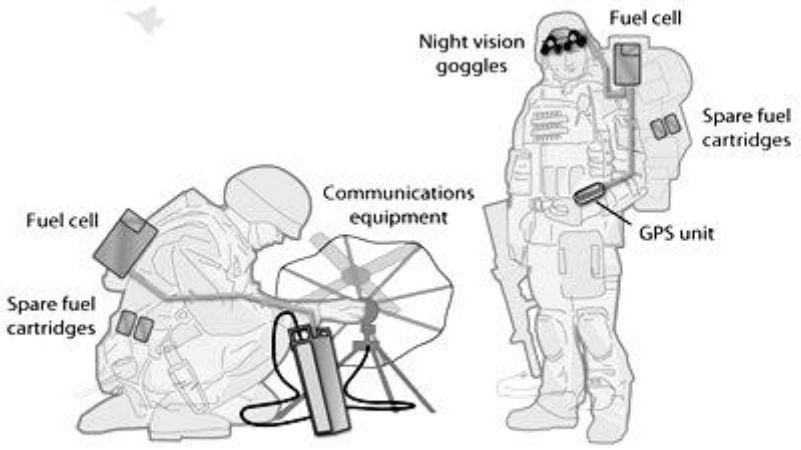

Fig 5: Portable FC applied to military devices [Matthey 2015]

The main advantage of FC for this application is the durability of the power device, which can provide large autonomy.
This is the field where more work has to be done, to reduce the dimensions of the FC and improve the refuel, control and management of this small devices.

3. **Stationary applications:** for high power demands, from a few kW to some MW, the FC are used specially to cover domestic demand, critical demand (like hospitals) or distributed generation.

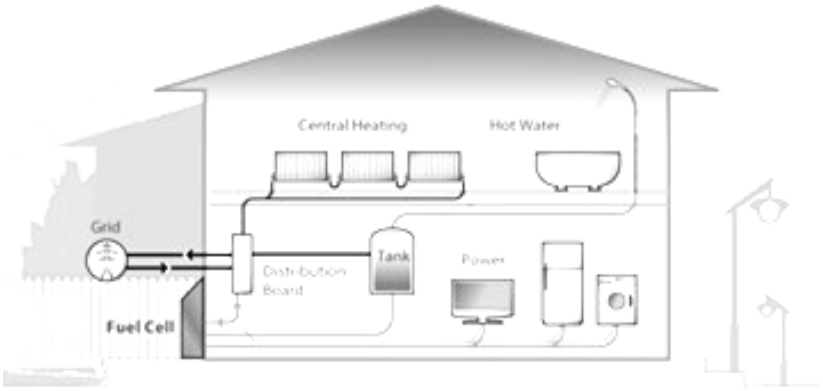

Fig 6: Domestic stationary application of FC [Matthey 2015]

The combine heat and power (CHP) application in domestic buildings is the most commercialized FC. Despite this the use of FC in buildings like hospitals or fireman stations has an important role in case of problems with the power supply from the grid. Moreover, in the U.S.A. and in Japan is possible to find the first substations of power generation and distribution throughout FC

that work like ramification of the common power grid where this do not arrive for logistical reasons.
What is common for this application is the utilization of natural gas (or liquid natural gas) to provide the fuel, even though in Europe methanol is being tested for this application.

Usually, high temperature FC are used for stationary applications (CHP) while on the other hand low temperature FC are used for portable applications or transport, where the size, the weight and the temperature have an important role.

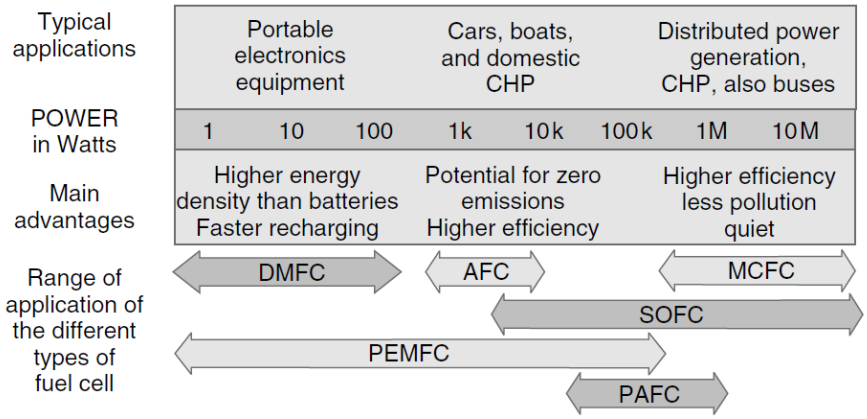

Fig 7: FC types and applications [Larminie and Dicks 2003]

Moreover, fuel cells are used as a support for renewable energy generation. One drawback of these energy sources is their variability, thus renewable power plants must be supported by spinning reserve power stations, typically fast-response open-cycle gas turbines – which goes against the environmental aims of the projects. In a case of oversized plant, the excess renewable energy generated during times of plenty can be stored and then used when sufficient energy is not available. On way of storing this energy is throughout batteries or similar technologies, but these only perform well over short timescales. Storing energy in hydrogen is another alternative: excess electricity is fed into an electrolyser to split water into its constituent parts, oxygen and hydrogen. The hydrogen is then used in fuel cells to produce electricity when needed. The most efficient way to convert hydrogen back to electricity is via fuel cells.

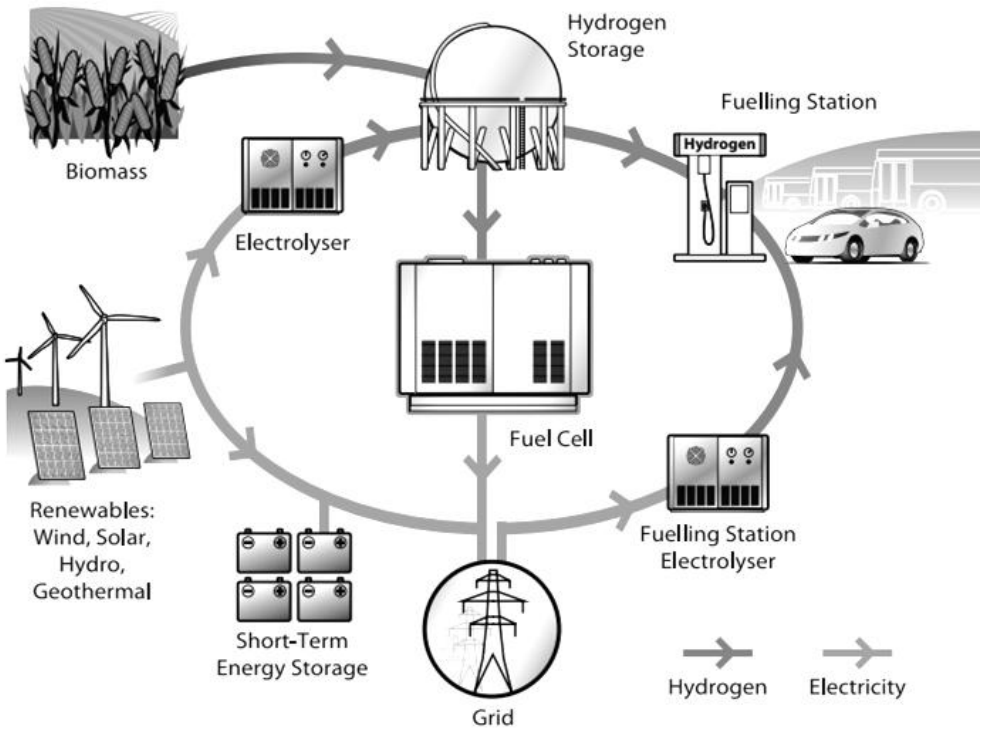

Fig 8: Fuel cell integration in a renewable energy plant [Matthey 2015]

This process allows excess energy produced in wind farms and solar power plants to be stored and used, instead of wasted. Increasing the utilisation of renewable power plants helps to maximise the return on investment and lower the cost of electricity. Hydrogen can also be produced in a number of ways from biomass, allowing for the integration of this energy source in a complete renewable energy system [Matthey 2015].

3.3. PEMFC basics

The main component of a PEM fuel cell is a polymer membrane that is impermeable to gases and electrically insulated but conductive to protons (proton exchange membrane), and thus acts as the electrolyte [S. Strahl 2010]. The inlets of this particular FC are pure hydrogen and oxygen, mixed into air. The FC is symmetric starting from the bipolar collector plates that contain the flow channels of the gases. Then the gas diffusion layer (GDL), together with the catalyst, forms the porous electrodes. Finally the multilayer assembly shape the membrane (MEA: membrane electrode assembly). Usually a PEMFC is a stack formed by more than one single cell. The Puma mind case is exceptional since it only has one cell.

3.3.1. PEMFC components

The material science is crucial in order to improve FC performance, reduce maintenance and investment costs. Studying the different Puma Mind parts is possible to understand how it works and which the operational conditions of the fuel cell are.

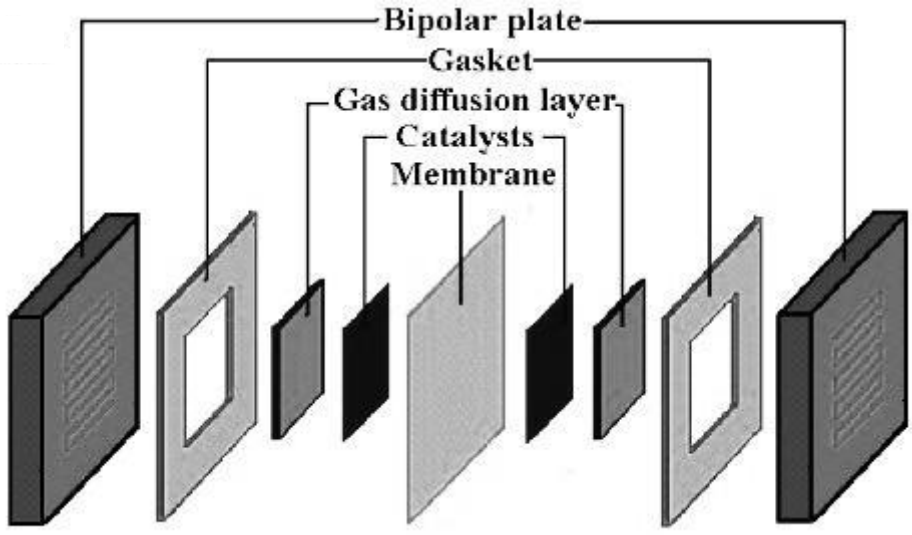

Fig 9: PEMFC components

Membrane

A fuel cell membrane must exhibit relatively high proton conductivity, must present an adequate barrier to mixing of fuel and reactant gases, and must be chemically and mechanically stable in the fuel cell environment [Barbir 2005]. The higher the proton conductivity is, the easier is to reach good efficiency. The membrane has a important role separating the gases and preventing them to mix, in order to avoid catastrophic accidents.

The Puma Mind membrane, as well as the majority of the PEMFC, has a Nafion membrane made of perfluoro-sulfonylfluoride ethyl-propyl-vinyl ether.

The material's SO^{-3} subgroup allows the transport of protons H^{+} through the membrane. However, the resistance of this transport is strongly dependent on the membrane water content, which is defined as the number of water molecules per number of sulphuric subgroups [Barbir 2005].

Catalyst layer

A fuel cell electrode is essentially a thin catalyst layer pressed between the ionomer membrane and porous, electrically conductive substrate. It is the layer where the electrochemical reactions take place [Barbir 2005]. Here electrons, protons and gases are present in order to ensure the reaction, thus the catalyst layer needs to fulfil this requirements:

- It has to be electrically conductive, that electrons can travel through it.
- There must be a direct contact to the membrane so that protons can reach the ionomer.
- The layer has to be porous to allow the reactant gases to travel to the reaction sites [S. Strahl 2010].

Platinum seems to be, until now, the best catalyst for both anode and cathode. Some years ago, it made the FC investment costs really high, but nowadays, techniques like spraying, printing or sputtering have reduced the platinum presence, optimizing its surface thus reducing the PEMFC costs and improving the global efficiency of the fuel cell.

Microporous layer

In the lasts years of study has been proved that a bilayer diffusion medium made up of a hydrophobic-rich microporous layer improves the FC performance. However, the improvement depends on the operating conditions, and the exact reasons are mainly unknown and unquantified.

A carbon microporous layer aims to:

- Minimize the resistance between the GDL and the catalyst.

- Limit the loss of catalyst to the GDL, improving the ohmic resistance of the FC.
- Improve the water management, keeping the water out of the gas diffusion layer and moving it through the anode.

Gas diffusion layer
Connecting the catalyst with the bipolar plates (flow channels) it has to fulfil several electrochemical and physical tasks like:

- Provide reactant gases to the catalyst.
- Distribution of the gas at the catalyst surface.
- Allow the evacuation of the water generated in the catalyst layer.
- Connect electrically the catalyst layer and the bipolar plates.
- Remove the heat from the reaction place.

Thus, the material needs to be porous enough to let the gases pass throughout but small enough to do not allow the catalyst particles to cross. It must have a good thermal and electrical conductivity, as well as being rigid enough to support the MEA structure.

All these requirements are usually fulfilled by carbon fibre papers with porosity between 70% and 80%.

Bipolar plates
In a common fuel cell the bipolar plates are the conjunction between the anode of one cell and the cathode of the next-standing, forming the stack. In the case of the single cell the bipolar plates only have a function of including the flow channels. Thus, they need to be good thermal conductors to remove the heat from the reactant places and need to have high compressive strength, but also low weight.

3.3.2. Basic chemistry

The basic electrochemical reactions developed simultaneously on anode and cathode are the following:

Anode**:** the hydrogen is separated into protons and electrons throughout the oxidation reaction that occurs at the catalyst layer.

$$2H_2 \rightarrow 4H^+ + 4e^- \quad (1)$$

The protons permeate the membrane to the cathode, while the electrons travel in a external circuit to the cathode electrode.

Cathode: in the cathode catalyst layer, the oxygen, through a reduction reaction, combines with the protons coming from the anode and the electrons coming from the external circuit, generation water and heat.

$$O_2 + 4e^- \rightarrow 2O^{2-} \tag{2}$$

$$2O^{2-} + 4h^+ \rightarrow 2H_2O \tag{3}$$

Overall: combining hydrogen and oxygen (pure or mixed into air) is possible to obtain electricity, thermal energy and water.

$$H_2 + {}^1/_2\, O_2 \rightarrow H_2O \tag{4}$$

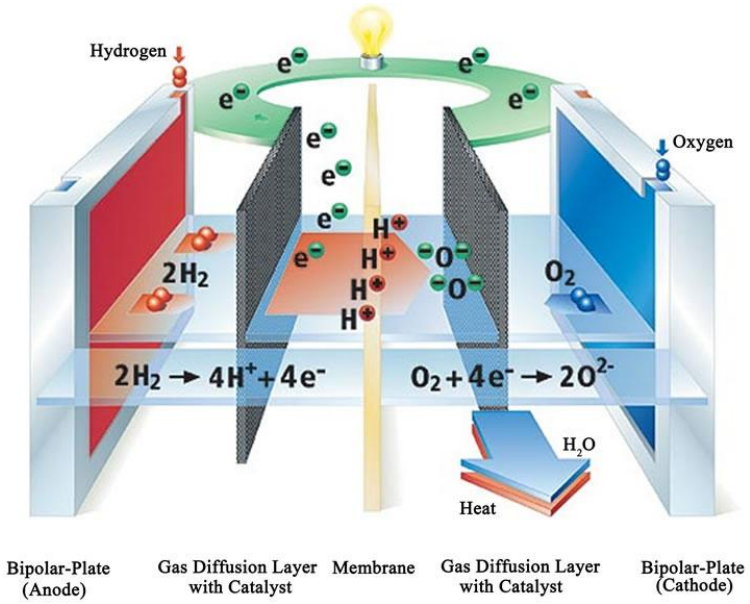

Fig 10: PEMFC chemical reaction

The energy delivered by this reaction is known as the enthalpy of the reaction. The enthalpy of a chemical reaction is the difference between the heat of formation of products and reactants.

Thus, the variation of enthalpy for the equation 4 is:

$$\Delta H = \left(h_f\right)_{H_2O} - \left(h_f\right)_{H_2} - {}^1/_2 \left(h_f\right)_{O_2} \qquad [\mathrm{kJmol^{-1}}] \tag{5}$$

The heat of formation of elements, by definition, is equal to zero, while the heat of formation of liquid water is -286 kJmol^{-1} (at 25°C).

$$\Delta H = -286\ \mathrm{kJmol^{-1}} - 0 - 0 = -286\ \mathrm{kJmol^{-1}} \tag{6}$$

The negative sign in the previous equation means, by convention, that the reaction is delivering heat, so the reaction is exothermic.

$$H_2 + {}^1/_2\, O_2 \rightarrow H_2O + 286\ \mathrm{kJmol^{-1}} \quad (7)$$

Hydrogen heating value is used as a measure of energy input in a fuel cell, it means 286 $\mathrm{kJmol^{-1}}$ is the theoretical thermal energy delivery of the reaction. Then, calculating the real energy delivered by the FC is possible to calculate the fuel cell efficiency. What is obvious, is that the main output of a FC is electrical energy and not thermal energy (which is produced secondarily), thus implies that in the conversion from thermal to electrical there will be losses, as in every kind of energy transformation.

The portion of the reaction enthalpy (or hydrogen's higher heating value) that can be converted to electricity in a fuel cell corresponds to Gibbs free energy and is given by the following equation [Barbir 2005]:

$$\Delta G = \Delta H - T\Delta S \qquad [\mathrm{kJmol^{-1}}] \quad (8)$$

Where ΔG is the Gibbs free energy, T is the temperature of the reaction and ΔS the variation of entropy.

Similarly as the enthalpy, the entropy equation is the following:

$$\Delta S = (s_f)_{H_2O} - (s_f)_{H_2} - {}^1/_2\,(s_f)_{O_2} \qquad [\mathrm{kJmol^{-1}K^{-1}}] \quad (9)$$

The entropies of formation are empirical calculated and they are tabulated in experimental tables from where is possible to get the expressions needed.

Table 2: Entropy of formation

	s_f [$\mathrm{kJmol^{-1}K^{-1}}$]
$H_2O\ (l)$	0.06996
H_2	0.13066
O_2	0.20517

Solving equation 9:

$$\Delta S = 0.06996 - 0.13066 - {}^1/_2\,(0.20517) = -0.163285\ \mathrm{kJmol^{-1}K^{-1}} \quad (10)$$

To know the Gibbs free energy is only necessary to solve equation 8:

$$\Delta G = 286\mathrm{kJmol^{-1}} - (298\mathrm{K} * -0.163285\ \mathrm{kJmol^{-1}K^{-1}}]) = -237.341\ \mathrm{kJmol^{-1}} \quad (11)$$

It is important to notice that the Gibbs free energy is temperature dependent; it means that the theoretical FC potential and the efficiency are temperature dependent.

Equation 8 is the simplified form of Gibbs free energy; the Nerst equation verifies that it is not only time dependent, but also pressure dependent:

$$\Delta G = \Delta H - T\Delta S + RTln\left(\frac{p_{H_2O}}{pH_2 \cdot p_{0_2}^{0.5}}\right) \qquad [\mathrm{kJmol^{-1}}] \tag{12}$$

Where p_{H2O}, p_{H2}, p_{O2} are the partial pressures of the reactant and product gases and *R* is the gas constant.

Knowing the amount of energy that can be converted into electricity, the theoretical fuel cell potential can be calculated.

3.3.3. Theoretical fuel cell potential

The electrical work in a fuel cell reaction per mol of H_2 consumed is equal to:

$$W_{el} = nFE \quad [\mathrm{Jmol^{-1}}] \tag{13}$$

Where *n* is the number of electrons per molecule of H_2 (n=2), F is the Faraday's constant (96,485 Coulombs/electron-mol) and E is the theoretical fuel cell potential.

The electrical work is equal to the maximum electrical energy that is possible to obtain from the fuel cell (the Gibbs free energy), thus:

$$W_{el} = -\Delta G = nFE \quad [\mathrm{Jmol^{-1}}] \tag{14}$$

$$E = -\frac{\Delta G}{nF} \quad [V] \tag{15}$$

At 25°C the theoretical fuel cell potential is equal to 1.23V.

Moreover, explaining the previous equations as temperature and pressure function, the following equation is obtained:

$$E_{T,P} = -\left(\frac{\Delta H^0}{nF} - \frac{T\Delta S^0}{nF}\right) + \frac{RT}{nF}\ln\left[\frac{P_{H2}P_{O2}^{0.5}}{P_{H2O}}\right] [V] \tag{16}$$

Where ΔH^0 and ΔS^0 are the variation of enthalpy and entropy at 25°C.

3.3.4. Fuel cell efficiency

The efficiency of a device is the ratio between the energy output and the energy input. In this case, the maximum output would be the Gibbs free energy, while the energy input is the higher heating value of hydrogen.

$$\eta = \frac{\Delta G}{\Delta H_{HHV}} = \frac{237.341}{286} = 83\% \quad (17)$$

Sometimes, is taken as the maximum efficiency the ratio between the Gibbs free energy and the lower heating value, since, the last one, is the one taken for efficiency calculation of combustion engines. In this case, the maximum theoretical fuel cell efficiency would be:

$$\eta = \frac{\Delta G}{\Delta H_{LHV}} = \frac{237.341}{241.98} = 94.5\% \quad (18)$$

Furthermore, is possible to calculate this efficiency as a ratio between potentials; this means dividing all the terms of the equation 17 by the term *nF*.

$$\eta = \frac{\frac{\Delta G}{nF}}{\frac{\Delta H_{HHV}}{nF}} = \frac{1.23}{1.482} = 83\% \quad (19)$$

Since the denominator term is not temperature and pressure dependent, the efficiency of a fuel cell, at any operational condition, related to the higher heating value, can be expressed as follow:

$$\eta = \frac{V_{cell}}{1.482} \quad (20)$$

3.3.5. Voltage losses

If a fuel cell is not connected to an external circuit, no current is generated, and so the fuel cell potential would be expected to be close to the theoretical potential, respective to the ambient conditions and reactant concentrations [S. Strahl 2010]. Observing a fuel cell open circuit voltage is possible to verify that the real potential is much lower than the theoretical, usually lower than 1V. Therefore, with a load connected to the fuel cell, the potential drops further than expected by the generated current. This implies that there are some voltage losses directly related with the fuel cell performance, further than the losses related with the external circuit.

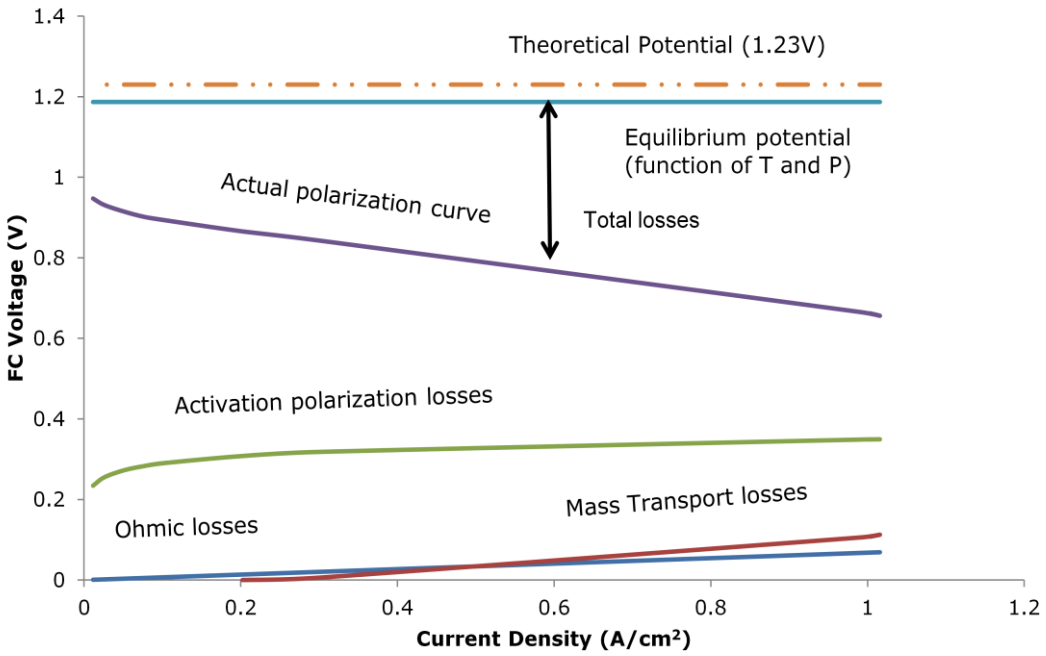

Fig 11: Voltage losses from experimental data

This is due to four main unavoidable losses (Fig 11):

1. **Activation polarization losses**: This corresponds to the voltage lost in driving the chemical reaction that transfers the electrons. These losses occur both on anode and cathode. However, because the reduction of oxygen is a much slower reaction than the oxidation of hydrogen, and therefore requires higher activation polarization, anode side losses can be neglected [S. Strahl 2010]. If only a single reaction is considered then the voltage loss due to activation polarization can be described by the Tafel equation [A. Husar, Strahl, and Riera 2011]:

$$\Delta V_{act} = \frac{RT}{\alpha nF}\ln\left(\frac{i}{i_0}\right) = 2.3\frac{RT}{\alpha nF}\log\left(\frac{i}{i_0}\right) \qquad [V] \qquad (21)$$

The parameter α is the charge transfer coefficient and expresses how the change in the electrical potential across the reaction interface changes the reaction rate. It depends on the type of reaction and the electrode material. Its value is theoretically between 0 and 1 depending on the catalyst material [Larminie and Dicks 2003]. It physically represents the fraction of additional energy that goes toward the cathodic reduction reaction at an electrode. The charge transfer coefficient can also be thought of as a symmetry coefficient of the electrode reaction and it is typically considered to be around 0.5 with hydrogen and oxygen reacting on a platinum catalyst [Wang et al. 2003]. The Exchange current density i_0 (A/cm^2) is the rate at

which the reaction proceeds (simultaneously in both directions) at equilibrium potential ($E_{T,P}$) when the net current equals zero [Barbir 2005]. The exchange current density is a measure of the effectiveness of the electrode in promoting the electrochemical reaction where the higher the exchange current density, the lower the overall activation losses. The fuel cell current density is denoted by i (A/cm^2). The activation losses are generally the dominant effect on the fuel cell voltage, as it is possible to see in Fig 11.
The Tafel slope is the main indicator for activation losses.

2. **Fuel crossover and internal currents**: When the fuel cell is not connected to an external circuit (open circuit voltage), the fuel cell voltage would be expected to be close to the thermodynamic potential, related to the ambient conditions and reactant partial pressure. However, the measured fuel cell voltage is much lower, usually less than 1 V/cell, which can be attributed to hydrogen crossover and internal currents. These losses arise because the membrane in a PEMFC is slightly electronically conductive and permeable to gasses. These losses can be considered as an internal current.

$$I = I_{ext} + I_{loss} \qquad [A] \tag{22}$$

The amount of current that these losses represent is rather small compared to normal operating currents. However, these internal current losses have a large effect on the voltage when the external current is very small [Barbir 2005]. In this study these losses are considered part of the activation losses and should not affect the results.

3. **Ohmic losses**: The resistance to the flow of electrons through the electrically conductive fuel cell components and to the flow of ions through the membrane causes a voltage drop, which can be expressed by Ohm's law:

$$\Delta V_{ohm} = iR_{ohm} \qquad [V] \tag{23}$$

The internal cell resistance R_{ohm} is in Ωcm^2. The electric and contact resistance can be considered constant with respect to current and temperature. Thus any change in the resistance is only dependent on membrane water concentration and membrane temperature.
R_{Ohm} is the indicator for membrane ionic resistance.

4. **Mass Transport losses**: The consumption of reactant gases at the catalyst layers leads to concentration gradients and thus changes the

partial pressure of the reactants, which affects the fuel cell voltage. Referring to Faraday's law of electrolysis, the transferred charge and the molar flux of a reactant *J* are proportional to the current density [Barbir 2005]:

$$J = \frac{i}{nF} \qquad [mol \cdot s^{-1} m^{-2}] \tag{24}$$

The higher the current density, the lower the reactant concentration is at the catalyst layer. The current density at which the reactant concentration reaches zero is called the limiting current density (i_L). Considering this relationship between reactant mass transport and current density, the mass transport losses can be expressed as [Barbir 2005]:

$$\Delta V_{MT} = \frac{RT}{\alpha nF} \ln\left(\frac{i_L}{i_L - i}\right) \qquad [V] \tag{25}$$

However, this expression for mass transport losses does not represent the experimental values well [O'Hayre 2009]. Many studies, and between them Husar studies, have shown that at very low current densities is possible to neglect the mass transport losses, while after an experimental fixed current density value the mass transport losses can be assume to be linear.

With the purpose of determining these linear losses, a R_{mt} (Ω cm^2) indicator is experimentally fixed.

CHAPTER 4: SPECIFIC FUEL CELL CHARACTERISTICS

A PEM single cell is the most basic operational form of the PEM fuel cell. It consists of the two metal current collector plates on either end, two flow field graphite plates on the inside of those, carbon paper further inside, platinum on the inside of that and the Nafion™ based membrane electrode assembly (MEA) in the middle.

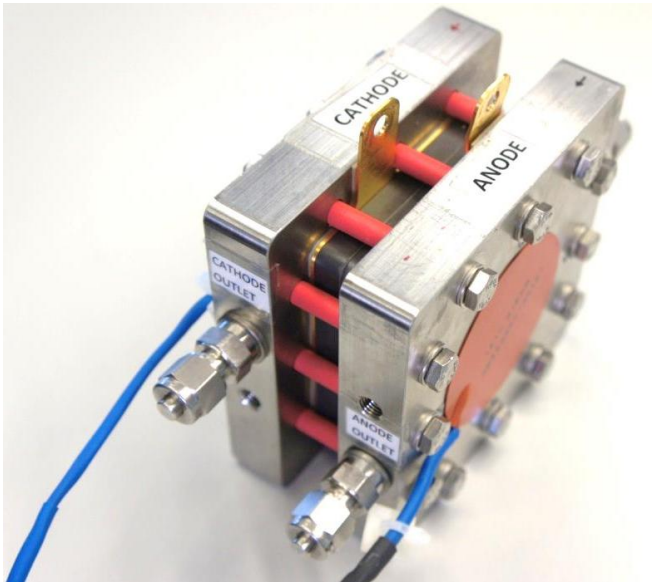

Fig 12: Single Fuel Cell

The electrode consists of a high purity platinum wire inserted into the anode flow field so that it is in direct contact with the input hydrogen gas stream.

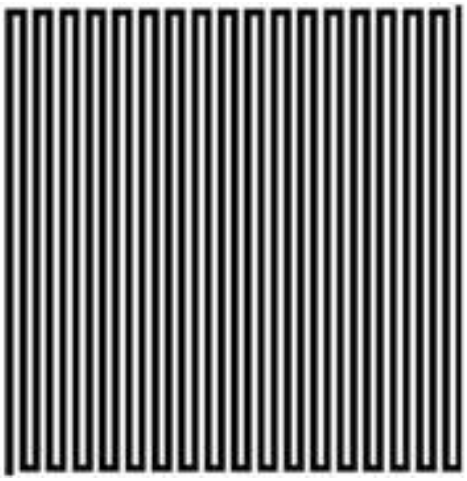

Fig 13: FC single serpentine

The FC has just one channel serpentine, like the one in Fig 13 and it is 1.04 m long.

The membrane is called 7 layers MEA because it is composed of seven parts, as it is possible to see in Fig 14.

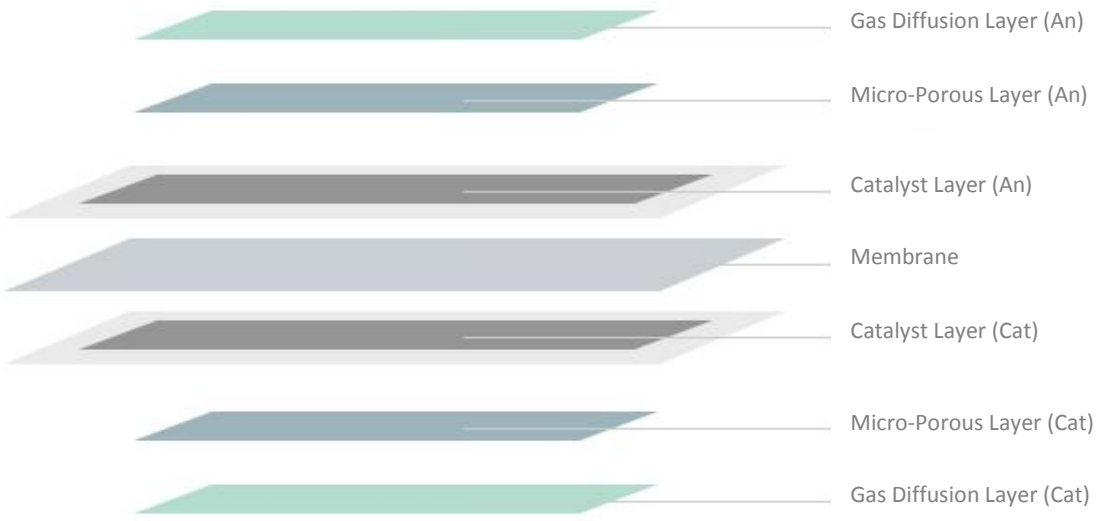

Fig 14: 7 layers MEA

The measured thicknesses of the different layers are listed in Table 3 Additional to the PEM fuel cell components, described in chapter 3.5, the single cell MEA includes a microporous layer between the GDL and the catalyst layer at both cathode and anode. The small pore size of this layer improves the electrical contact to the catalyst and also facilitates the removal of liquid water from the cathode catalyst [Barbir 2005].

In the following tables the specific characteristic of wich part of the fuel cell are presented.

Table 3: MEA component thicknesses [Source: Puma Mind]

Component	Thickness [mm]
Gas Diffusion Layer	0.2
Micro-Porous Layer	0.06
Proton Exchange Membrane	0.025
Cathode Catalyst Layer	0.05
Anode Catalyst Layer	0.05
Membrane Electrode Assemblies	0.055

Table 4: Material parameter of cathode and anode plate: 25cm² graphite plates

[Source: Puma Mind]

Parameter	Value	Unit
Heat transport		
Heat conductivity	8.3	W/(mK)
Heat capacity	708	J/(m^3K)
Electrical		
Conductivity	1.00E+05	S/m

Table 5: Operational parameters cathode and anode gas/channel conditions

[Source: UE reference conditions]

Parameter	Value	Unit
Temperature	353	K
Pressure	2.3	bar
Inlet species composition (e.g. ratio)	<500ppm CO_2 <10ppm CO <2,5ppm NO_x <5ppm SO_2 <0,01mg/m^3 oil	
Mass flow	Current dependent	m/s

Table 6: Structural parameters cathode and anode channel [Source: Puma Mind]

Parameter	Value	Unit
Number of channels	1	-
Channel length	1.04	m
Channel width	1.40E-03	m
Channel depth	1.40E-03	m
Channel area	1.96E-06	m^2
Rib width	8.00E-06	m

Table 7: Material parameter of cathode and anode substrate (GDL SGL24BC)

[Source: Puma Mind]

Parameter	Value	Unit
Thickness	2.46E-04	m
Porosity	77%	
Tortuosity_through plane	0.310	
Tortuosity_in plane	0.179	
Effective tortuosity	3.3	
Pore diameter	1E-5	m
PTFE	5	wt%
Leverett coefficients	Note[1]	
Water contact angle	115	°
Heat capacity (graphite)	708	J/(m^{3}K)
Heat transport parameters		
Thermal conductivity in plane (compressed 1MPa)	11.890	W/m/K
Thermal conductivity through plane (compressed 1MPa)	0.45	W/m/K
Electrical parameters		
Electric conductivity in plane (compressed 1MPa)	4862	S/m
Electric conductivity through plane (compressed 1MPa)	184	S/m
Permeability		
Through plane permeability	6.74E-14	m²
In plane permeability	3.72E-14	m²
Thickness	2.46E-04	m

Note[1]: $$J(s) = 1.417(1-s) - 2.12(1-s)^2 + 1.263(1-s)^3 \quad (26)$$

Table 8: Material parameter of cathode and anode MPL (GDL SGL24BC)

[Source: Puma Mind]

Parameter	Value	Unit
Thickness	4.50E-05	m
Porosity	35%	
Tortuosity	1.690	
Pore diameter	1E-6	m
Particle diameter	5.00E-07	m
PTFE	5%	wt%
Permeability	2.00E-13	S/m
Thermal conductivity	0.4	S/m
Electric conductivity	50	S/m
Heat capacity (graphite)	708	J/(m^{3}K)
Contact angle	105	°

Table 9: Material parameter of cathode catalyst [Source: Puma Mind]

Parameter	Value	Unit
Structural parameters		
Thickness	1.20E-05	m
Porosity (%)	47	
Tortuosity	1.3	
Pore diameter	1.00E-08	m
Particle diameter	4.00E-09	m
Catalytically active areas	2.50E+07	m^2/m^3
Catalyst loading	0.4	mg/cm²
Heat transport parameters		
Heat conductivity	10	W/(mK)
Electrical parameters		
Electrical Conductivity	20	S/m
Permeability	1.00E-12	m^2
Contact angle	95	°
Electrochemical parameters		
Preexponential factors of all reactions	1.00E+13	(various)
Symmetry factors of charge-transfer reactions	0.5	

Table 10: Material parameter of anode catalyst [Source: Puma Mind]

Parameter	Value	Unit
Structural parameters		
Thickness	6.00E-06	m
Porosity (%)	47	
Tortuosity	1.3	
Pore diameter	1.00E-08	m
Particle diameter	4.00E-09	m
Catalytically active areas	5.00E+07	m^2/m^3
Catalyst loading	0.2	mg/cm²
Heat transport parameters		
Heat conductivity	10	W/(mK)
Electrical parameters		
Electrical Conductivity	20	S/m
Permeability	1.00E-12	m^2
Contact angle	95	°
Electrochemical parameters		
Preexponential factors of all reactions	1.00E+13	(various)
Symmetry factors of charge-transfer reactions	0.5	

Table 11: Material parameter of membrane [Source: Puma Mind]

Parameter	Value	Unit
Structural parameters		
Thickness	2.50E-05	m
Equivalentweight	1100	g/equiv
Density (dry)	2.24E+03	kg/m^3
in plane tortuosity	1.00E+00	
through plane tortuosity	1	
Concentration of sulfonic acid groups	2.20E+03	mol/m^3
Mass transport parameters		
Gibbs energy gas absorption in Nafion		
O2	-5.88E+3	J/mol
H2	-9.05E+3	J/mol
N2	-3.74E+3	J/mol
Gas Diffusion coefficients in Nafion		
H_2	DH_2	m^2/s
O_2	DO_2	m^2/s
N_2	DN_2	m^2/s
Heat transport parameters		
Heat conductivity	0.186	W/(mK)
Heat capacity	1046	J/(kgK)
Water diffusion coefficient	D	
Proton conductivity	$Conductivity$	

$$DH_2 = 4.1 \cdot 10^{-3} \cdot e^{-\frac{2602}{T}} \tag{27}$$

$$DO_2 = 3.1 \cdot 10^{-7} \cdot e^{-\frac{2768}{T}} \tag{28}$$

$$DN_2 = 1.1 \cdot 4.02 \cdot 10^{-8} \cdot e^{-\frac{2406}{T}} \tag{29}$$

$$D = 1 \cdot 10^{-4}(1.76 \cdot 10^{-5} + 1.94 \cdot 10^{-4}\lambda_m) \cdot e^{-\frac{2436}{T}} \tag{30}$$

$$Conductivity = (0.51391 \cdot \lambda_m - 0.362) \cdot e^{1268\left(\frac{1}{303.15} - \frac{1}{T}\right)} \quad [S/cm] \tag{31}$$

CHAPTER 5:

TEST CHARACTERIZATION

5.1. Test objective

The objective of the test is to obtain experimental data of the FC performance in order to calculate the characteristic indicators of the fuel cell voltage losses. The study has been done in stationary and dynamic conditions, which are stipulated by the Puma Mind programme.

5.2. Test station

The tests have been done in station 1 (Fig 15) of the fuel cell laboratory at the *Institut de Robòtica i Informàtica Industrial* (UPC - CSIC). This station has a power that reaches 200 W. The inlet gases are hydrogen and nitrogen for the anode and oxygen and synthetic air for the cathode. It has a humidification control of both, anode and cathode, and manual back pressure regulator (up to 4.5 bar) for anode and cathode. It has an electronic load bank from where is possible to control the current, voltage or power demanded.

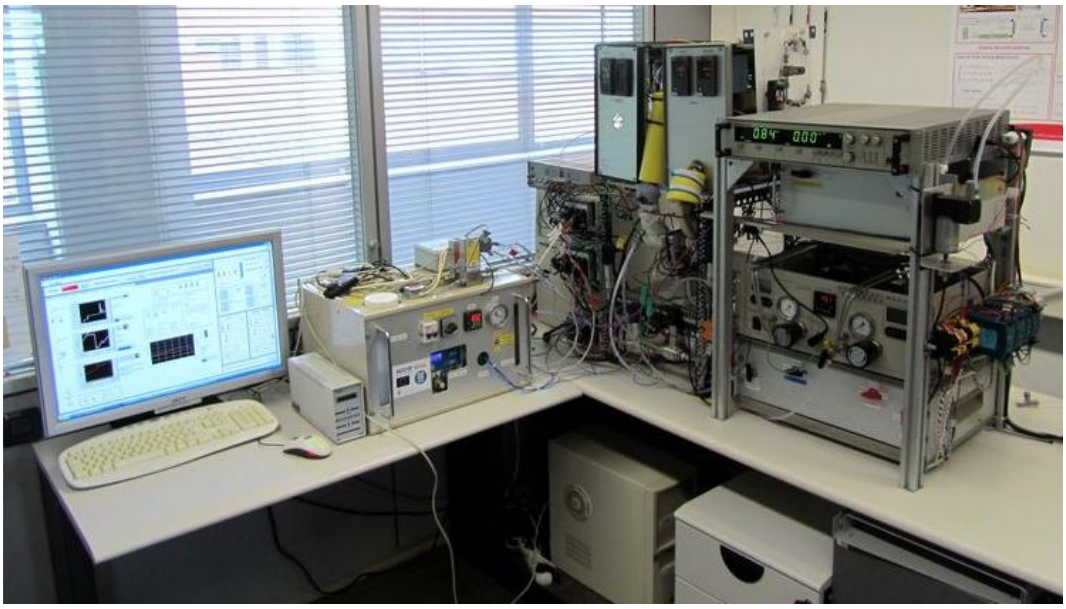

Fig 15: Test Station 1

It is possible to divide the station in four main subsystems: the fuel cell, the anode and the cathode and the control and data acquisition subsystem.

The control and acquisition system as follows the scheme in Fig 16.

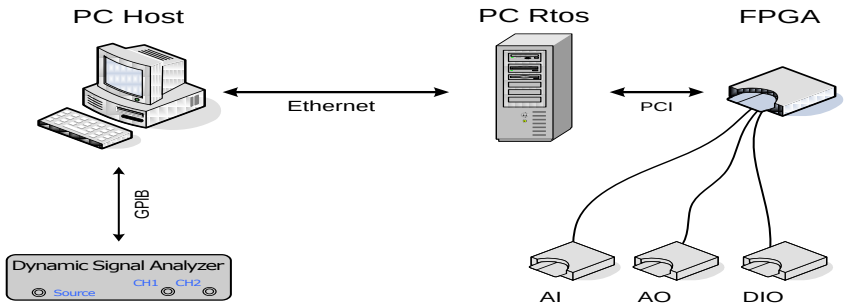

Fig 16: Control and acquisition system scheme

Sensors and actuators of the station are connected to a Field Programmable Gate Array (FPGA) that manages the acquisition and extraction throughout the Labview ® FPGA module. This FPGA is located into the PC R_{tos} (Real Time Operation System).

This PC R_{tos} is the responsible of the communication with the PC Host by Ethernet, the data storing, the communication with the FPGA and the implementation of control strategies.

The PC Host executes the code developed for a friendly GUI (Graphical User Interface). With the possibility of vary the operational points, visualize the variables (numerically and graphically) and configure tests.

In Fig 17 is possible to see the scheme of the station with the single cell.

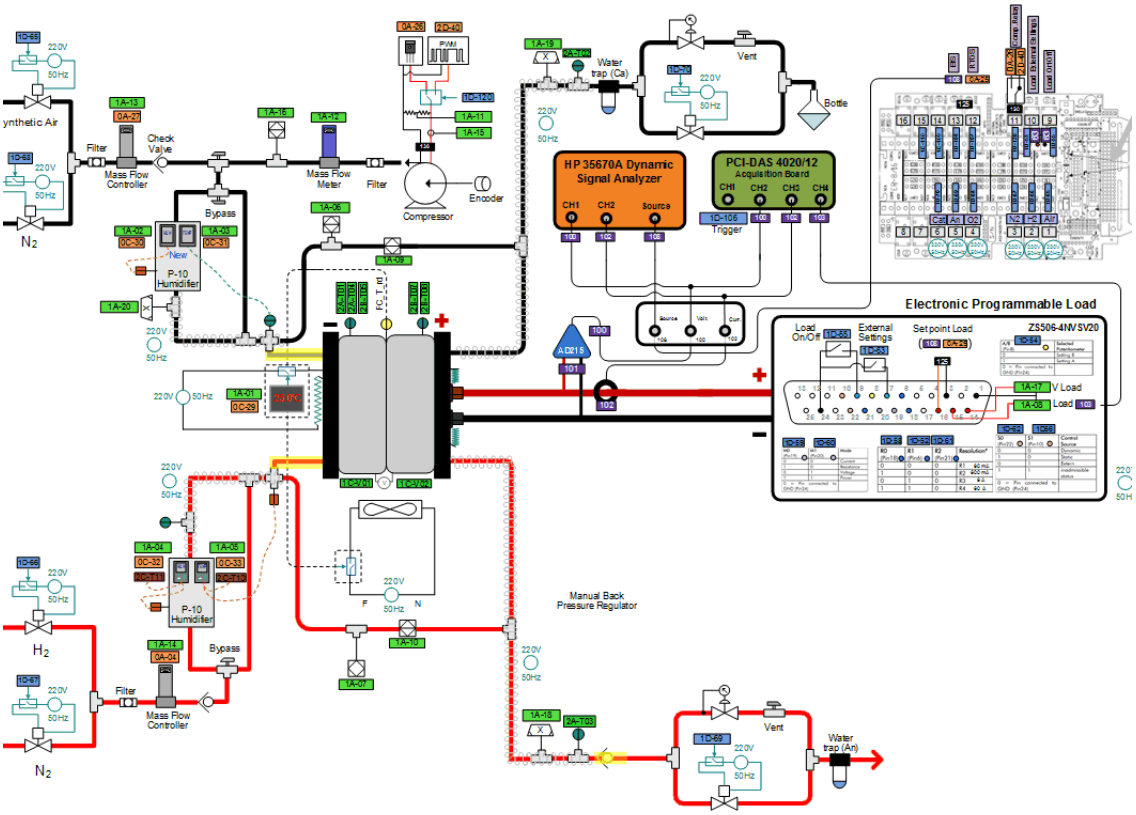

Fig 17: Test Station 1 scheme with Puma Mind FC

In this, all the sensors and actuators are reported:

- Mass flow controllers, both cathode and anode.
- Humidity sensors and humidifiers.
- Temperature sensors, line heater and inlet gas temperature.
- Pressure transducers, absolute inlet pressure and differential pressure between inlet and outlet.
- Solenoid and manual valves, laboratory instrumentation (HP 35670 for EISs), etc.

The pressure control is one of the difficulties of the tests with the test station since it is a manual control, to avoid an overlap and collision between two automatic controllers, the mass flow and the pressure one. The problem is that, due to the low hydrogen flow throughout the single cell, the manual back pressure control is very slow and it takes time to get the desired pressure, and usually this is not stable and accurate.

In the scheme is also possible to see the electronic programmable load and the control and acquisition system.

5.3. Test conditions

The conditions of the tests are described in Table 12. What has to be mentioned is that, especially at low temperature (45°C) the FC is highly unstable, it means that either the temperature, either the relative humidity changes significantly during the test. This affects directly the results of the tests done at these conditions. For this reason those are the less reliable results, thus the ones that have lower weight in the results analysis.

Table 12: PEMFC conditions for the tests

Set point	Value	Units
Anode pressure	1.25, 2.5	bar
Cathode pressure	1.23, 2.3	bar
Anode RH	50	%
Cathode RH	30	%
Anode stoichiometry	1.3	-
Cathode stoichiometry	1.3, 1.5, 2.0	-
FC Temperature	45, 60, 80	ºC
Line heater Temperature	50, 65, 85	ºC

The anode pressure is always a bit higher than the cathode one. These conditions have been set by the PUMA MIND project, but this is probably due to a control reason. If the anode pressure is higher than the cathode one is easier to see if there is a leak or something is broken between the electrodes. With a higher pressure of the anode there is an important voltage drop, due to the fast hydrogen consumption. In the other way, the oxygen consumption is much slower, and the leaks are more difficult to see and the problems due to this kind of leaks are much more dangerous.

What has to be mentioned is that these values, only excepting stoichiometries, can vary during the fuel cell test, but not that much to affect the fuel cell performance. Calculations with the experimental data have been done to ensure this.

5.4. Test routine

In Fig 18 is possible to see the scheme that explains the whole test routine. These starts with the Polarization curve (PC) and once it is finished, after a

time rest, a series of fast Current sweep (CS) and Electrochemical Impedance Spectroscopy (EIS) is done for each current density stable state.

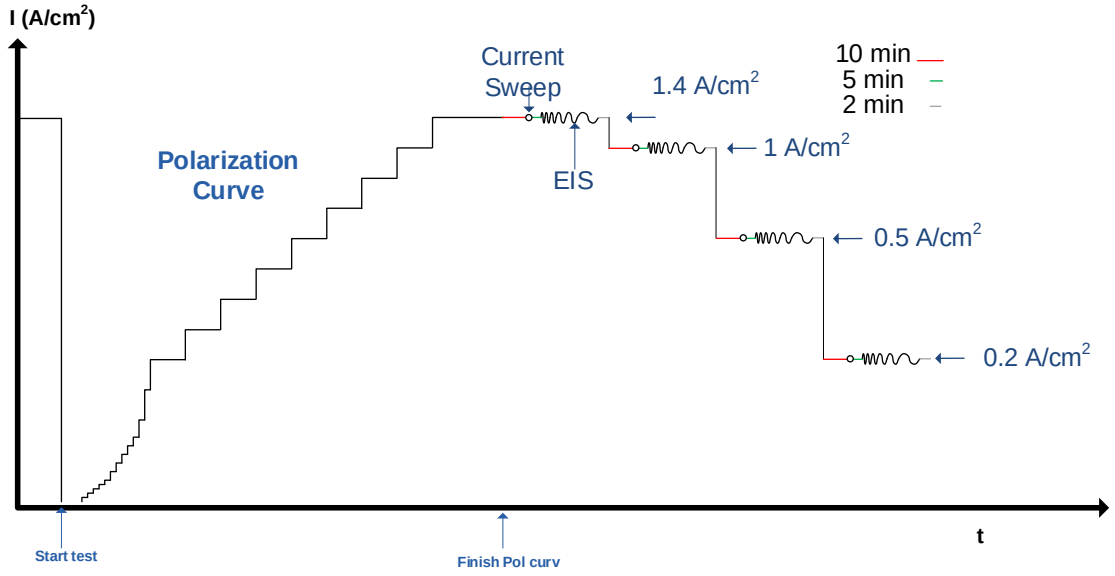

Fig 18: Scheme of the tests, starting with the polarization curve and then the currents sweeps and the EIS at each current density.

The test as a whole lasts between 3 and 4 hours.

Originally the test was supposed to have 4 states at different current density, but this was finally modified depending on the maximum current density that the FC could support in the specific conditions of the test. Before starting each test (before the PC), the fuel cell was tested in order to determine the maximum current density that the FC can support. Sometimes, the FC only arrive to 1.2 A/cm^2 and some others only until 1 A/ cm^2.

In the following table is possible to check at which current densities the CS and the EIS have been done.

Table 13: Current densities (A/ cm^2) of the tests done depending on temperature and stoichiometry (Pressure An-Cat: 1.25-1.23 bar)

	45°C	60°C	80°C
Stoich. An-Cat: 1.3-2	0.2,0.5,1,1.4	0.2,0.5,1	0.2,0.5,1,1.2
Stoich. An-Cat: 1.3-1.5	0.2,0.5,1,1.2	0.2,0.5,1	0.2,0.5,1,1.2
Stoich. An-Cat: 1.3-1.3	0.2,0.5,1	0.2,0.5,1	0.2,0.5,1,1.2

Since the test at higher pressures, 2.5 bar anode and 2.3 bar cathode, were done later on and due to time issues of the laboratory, the sequence of the test changed. First of all, all the polarization curves were done. All the EIS where only done at high frequency, that is the part needed, and then, all the CS where done at different current densities.

Table 14: Current densities (A/ cm^2) of the tests done depending on temperature and stoichiometry (Pressure An-Cat: 2.5-2.3 bar)

	60°C	80°C
Stoich. An-Cat: 1.3-2	0.2,0.5,1,1.4	0.2,0.5,1,1.4
Stoich. An-Cat: 1.3-1.5	0.2,0.5,1,1.4	0.2,0.5,1,1.4
Stoich. An-Cat: 1.3-1.3	0.2,0.5,1,1.2	0.2,0.5,1,1.4

5.4.1. Polarization curve

The polarization curve is the most common method of representing the performance of a fuel cell. The purpose of the Polarization curve (PC) is to obtain the steady state voltage output of the fuel cell. Current and voltage are measured during 180 seconds in order to get an i-V curve that shows the progressive losses of the fuel cell. These results will be compared with the fast Current sweep, which lasts in total less than 2 seconds. The aim is to see the difference since with the slow analysis all the parameters are changing, affecting the fuel cell performance, while with the fast analysis the internal parameters don't change. Between 22 and 24 points are obtained, based on steps starting at low currents up to the max allowed and the other way round. Previous graph this data there is an averaged process. An experimental polarization curve is showed in Fig 19.

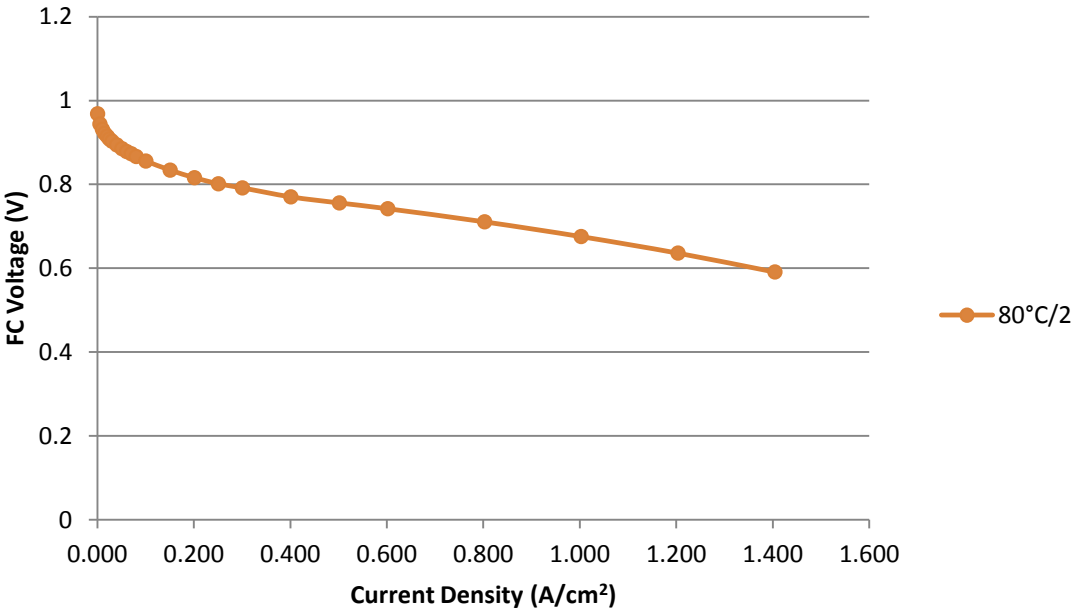

Fig 19: Polarization curves at Pressure An-Cat: 2.5 – 2.3bar, depending on temperature and cathode stoichiometry (2)

5.4.2. Current sweep

As mentioned in the previous section, the purpose of the Polarization curve (PC) is to obtain the steady state voltage output of the fuel cell. Current and voltage are measured during 180 seconds in order to get an i-V curve that shows the progressive losses of the fuel cell.

In Fig 20 is possible to see the scheme of the points of a CS: first three points at high current densities are taken and then more points at low current densities are taken as well.

The points around the operating condition give a good reading of the linear slope of the fuel cell. The others, at low current densities give a good reading on the final nonlinear region of the fuel cell.

The way to determine the points of the curve is based on the current density, more specifically on the first point current density (the one in red), obtaining the others applying a percentage of this first one. However, at low current densities, some problems with this method arose, so the points of the currents sweeps at these current densities were determined adding or subtracting an absolute value. Beyond this, the results of the CS can be compared once against others.

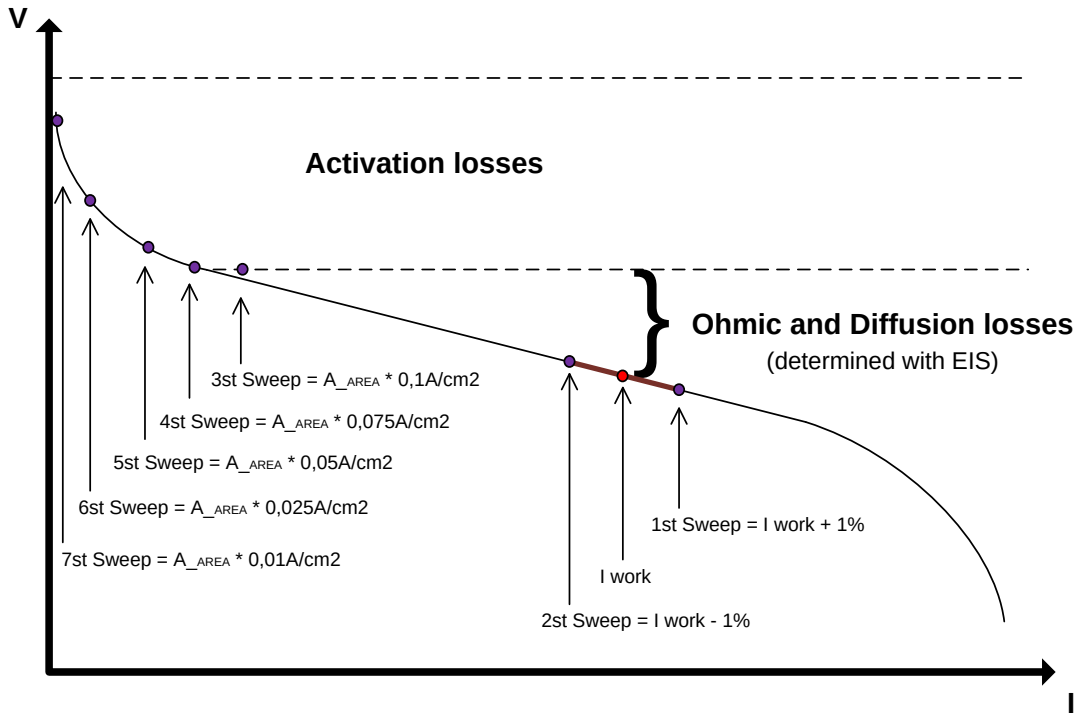

Fig 20: Fast Polarization curve from a Current sweep routine

As can be seen in Fig 21, in this study, the fuel cell is left at each current set point for only 200 ms, which mostly provides enough time for the electrochemical part of the fuel cell to stable out.

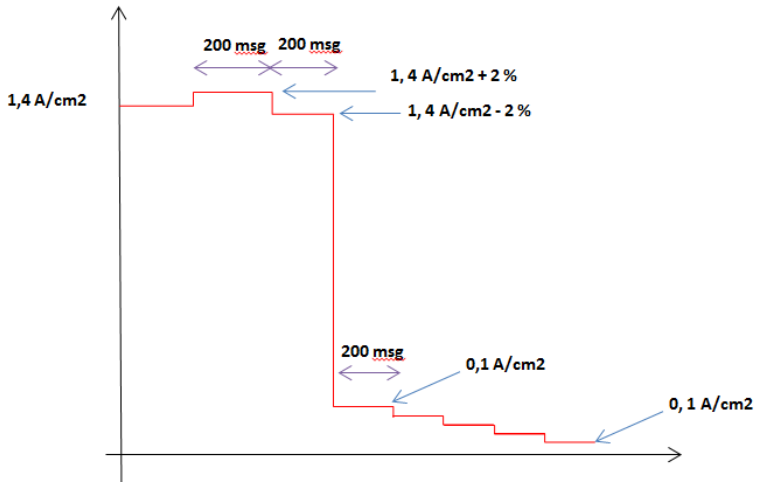

Fig 21: Current sweep current density pattern

As can be seen in Fig 20 there are 8 current rest points, 3 points at high current densities and 5 points in the nonlinear region at lower current densities. The first tests only have 8 point, however, this number was increased in order to have more information on this fast polarization curve, especially in the linear part, having then 3 points in the linear zone and 7 in the non-linear one. The improvement did not reach the objective, but was a good way to have more data, so the majority of the tests have been done taking 10 points.

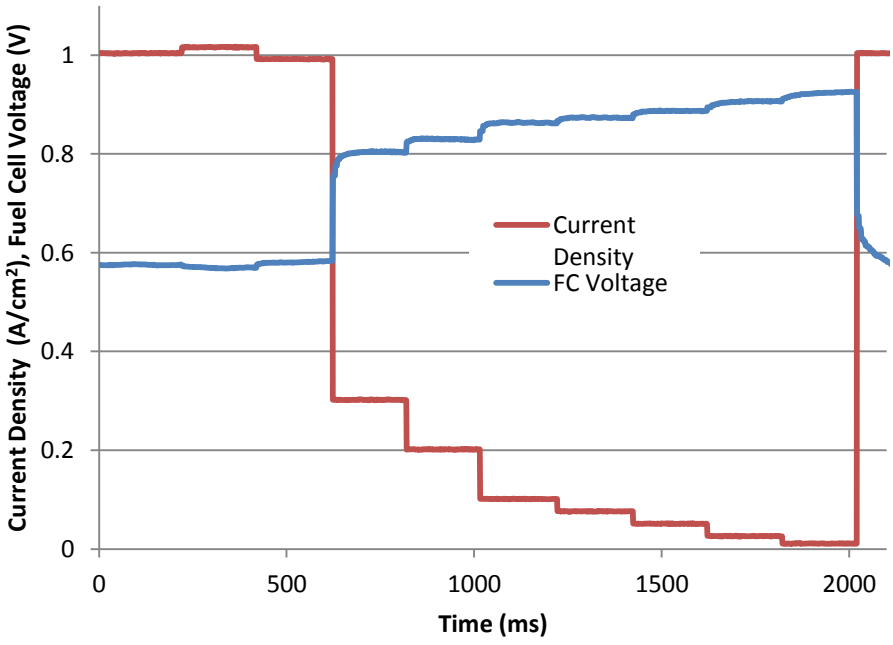

Fig 22: Experimental current sweep at 80ºC, 1.23 – 1.25 bar, cathode's stoichiometry at 2 and 1A/cm^2 (25 A).

In Fig 22 is possible to see all the points and the correspondent values of current density and voltage. Furthermore, in that picture is clear that the points get stabilized in 200ms.

5.4.3. Electrochemical Impedance Spectroscopy

A polarization curve provides useful but not sufficient information about fuel cell dynamics. In a polarization curve is possible to observe all the voltage losses, without any direct method that allow us to distinguish the different losses. This is why other methods are used to define these losses separately. One of these methods is the Electrical Impedance Spectroscopy, used to find the ohmic resistance of the membrane, as well as the total equivalent resistance of the FC. To understand cell resistance measurement, a fuel cell may be represented by a simplified electrical circuit, such as the one shown in Fig 23, consisting of a couple of resistors and a capacitor. The first resistor represents the cell resistance, both electronic and ionic. The second resistor in parallel with a capacitor represents the charge transfer resistance, that is, activation polarization [Barbir 2005].

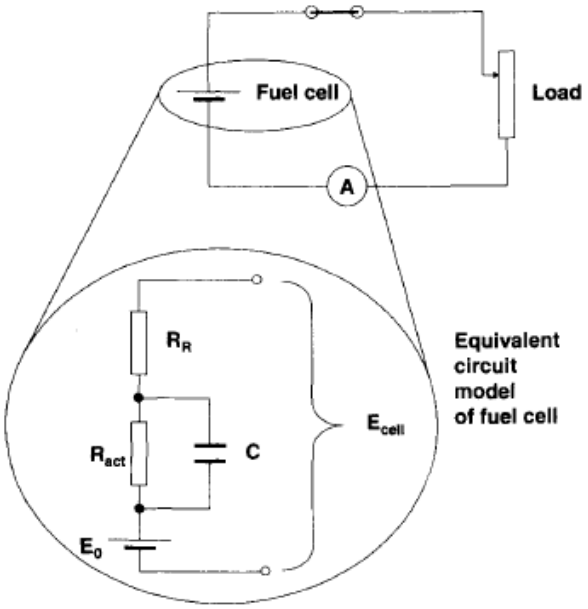

Fig 23: Equivalent circuit representing a fuel cell [Barbir 2005]

For a fuel cell equivalent circuit, such as the one shown in Fig 23, the impedances are:

$$Z_R = R_R; \qquad Z_{act} = R_{act}; \qquad Z_c = -\frac{j}{\omega C} \tag{32}$$

The impedance of the entire circuit is then:

$$Z(\omega) = R_R + \frac{1}{\frac{1}{R_{act}} - \frac{\omega C}{j}} = R_R + \frac{R_{act}}{1 + j\omega C R_{act}} \tag{33}$$

This can be separated in real and complex part, that can be represented in a Nyquist plot diagram:

$$Re\,(Z) = R_R + \frac{R_{act}}{1 + (\omega C R_{act})} \tag{34}$$

$$Im\,(Z) = \frac{\omega C R_{act}^2}{1 + (\omega C R_{act})^2} \tag{35}$$

The Electrical Impedance Spectroscopy consists in sending Alternative Current signals through a frequency spectrum (between 0.05 Hz and 2000 Hz) to obtain a Nyquist diagram that shows the impedance of the equivalent circuit of the fuel cell at various frequencies.

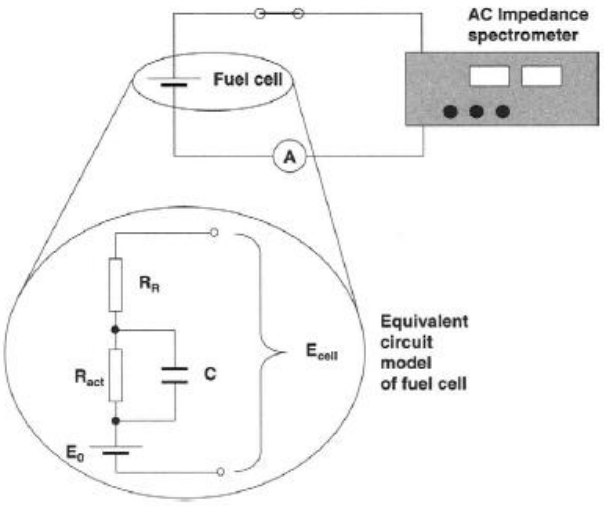

Fig 24: AC impedance spectroscopy setup and fuel cell equivalent circuit.

Plotted in a Nyquist diagram (Im Z vs Re Z), the measurements of complex impedance at various frequencies of this simple fuel cell equivalent circuit result in a semicircle. The Nyquist only gives linear information at the measured point of operation: the low frequencies real axis interception corresponds to the total resistance $Z=R_{tot}$, whereas at high frequency real axis interception corresponds to the ohmic resistance $Z=R_{Ohm}$. Only the high frequency resistances are used to calculate the ohmic losses of the fuel cell.

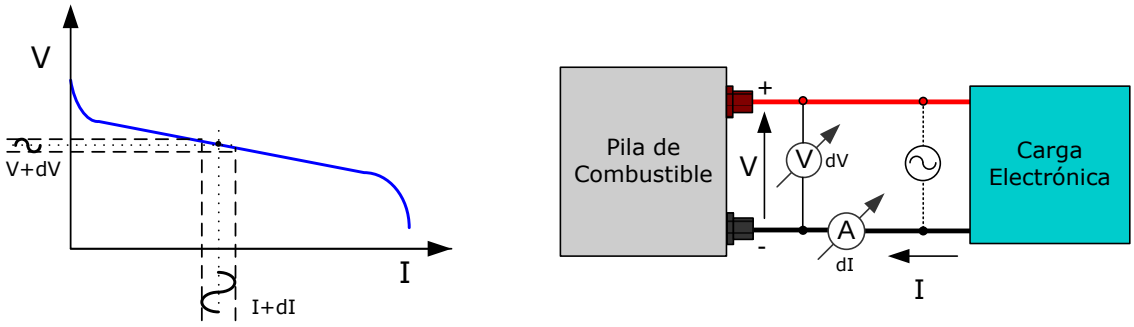

Fig 25: EIS scheme

To obtain the following Nyquist, the Dynamic Signal Analyzer is programmed to work between 0.05 Hz to 2000 Hz, throughout 45 frequencies. At each frequency 12 cycles are done, the firsts four are discarded, and the medium value of the following eight values is the value at that frequency.

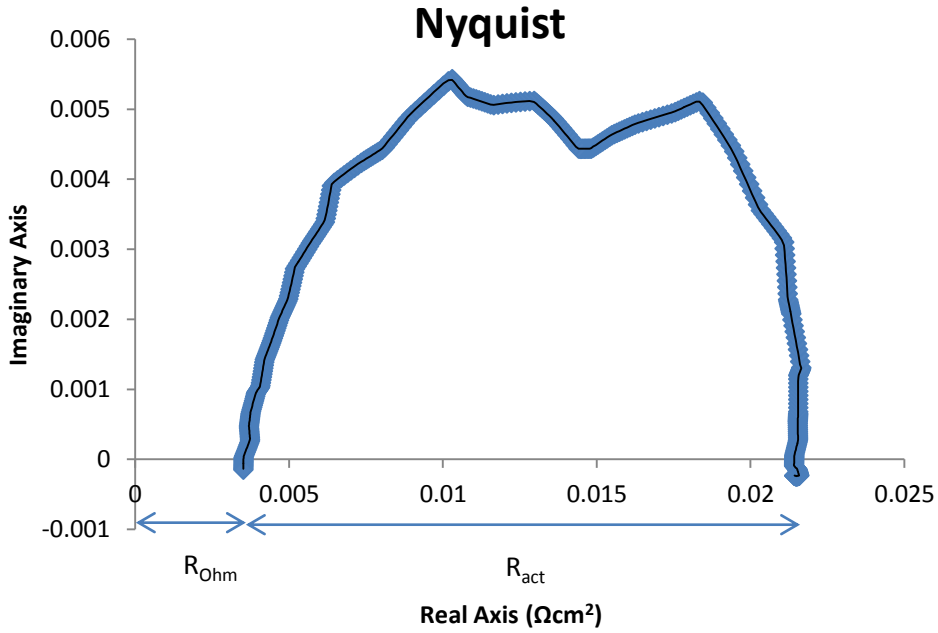

Fig 26: Nyquist (1 A/ cm^2, 80°C, Stoich. An-Cat:1.3 – 2, P An-Cat:1.25-1.23)

As it was said before, for the tests at 2.3 bar in the cathode and 2.5 bar in the anode, the spectroscopies were done only at high frequencies (Fig 27), in order to obtain the R_{ohm}.

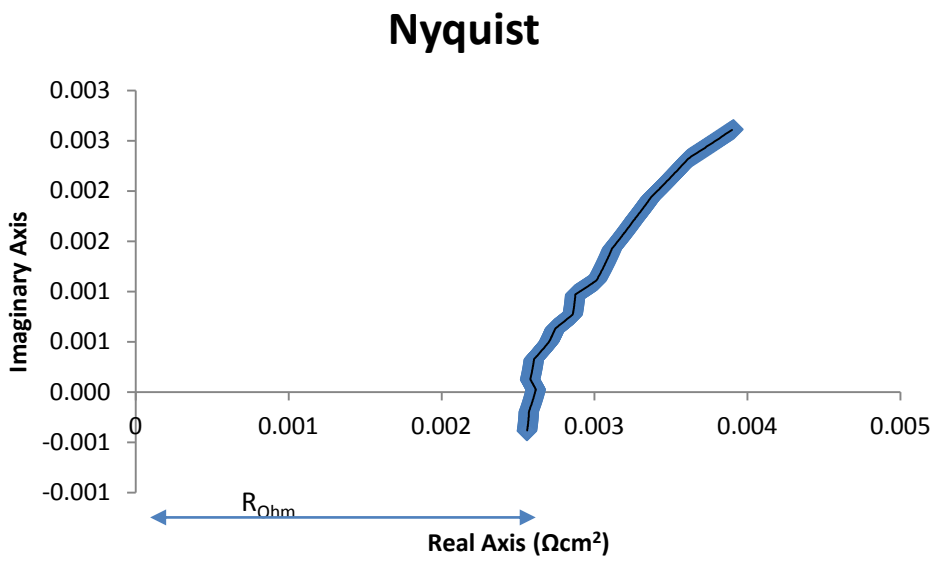

Fig 27: Nyquist (1 A/cm^2, 80°C, Stoich. An-Cat:1.3 – 1.5, P An-Cat: 2.5 – 2.3bar)

5.5. Test Results

As said in the previous chapter, what has been obtained from the tests are: Polarization curves, Current sweeps and Electrochemical Impedance Spectroscopy.

In this chapter, only the polarization curves are presented (Fig 28 - Fig 32). More than 20 CS, as the one in Fig 22, and more than 20 EIS have been done; this high number make those results impossible to present in this thesis. However, all these data are available for the people working at the control line of investigation at IRI.

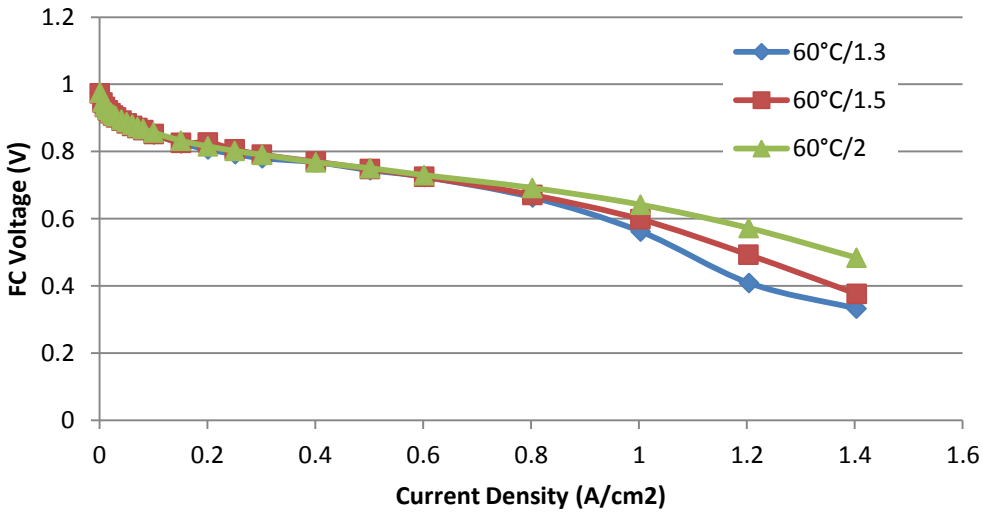

Fig 28: Polarization curve at 60°C (2.3 – 2.5 bar)

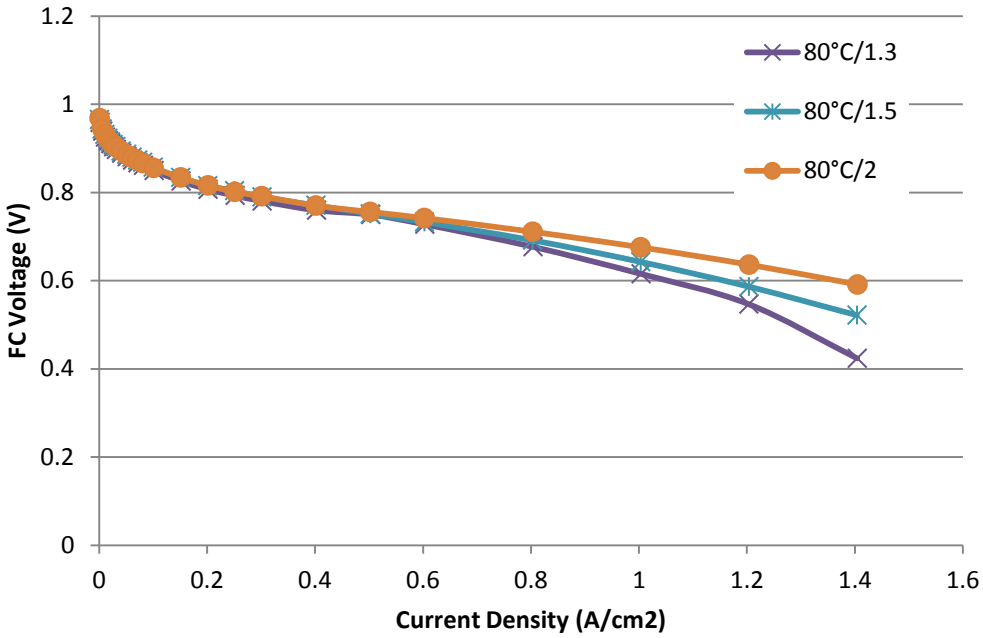

Fig 29: Polarization curve at 80°C (2.3 – 2.5 bar)

As it is possible to see, the results at low pressure seems to be disorganized, specially at 45°C; this is just because working at low pressure and low temperatures the FC is more unstable and it is more difficult to reach higher current densities. This is why, to carry on this study, only the results at 60°C and 80°C are considered.

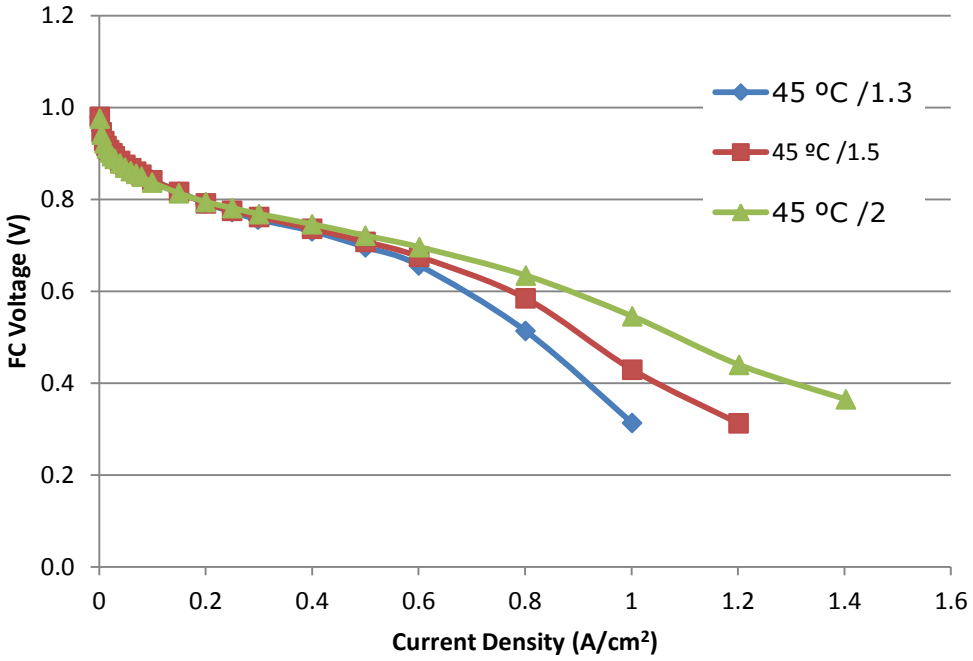

Fig 30: Polarization curve at 45°C (1.23 – 1.25 bar)

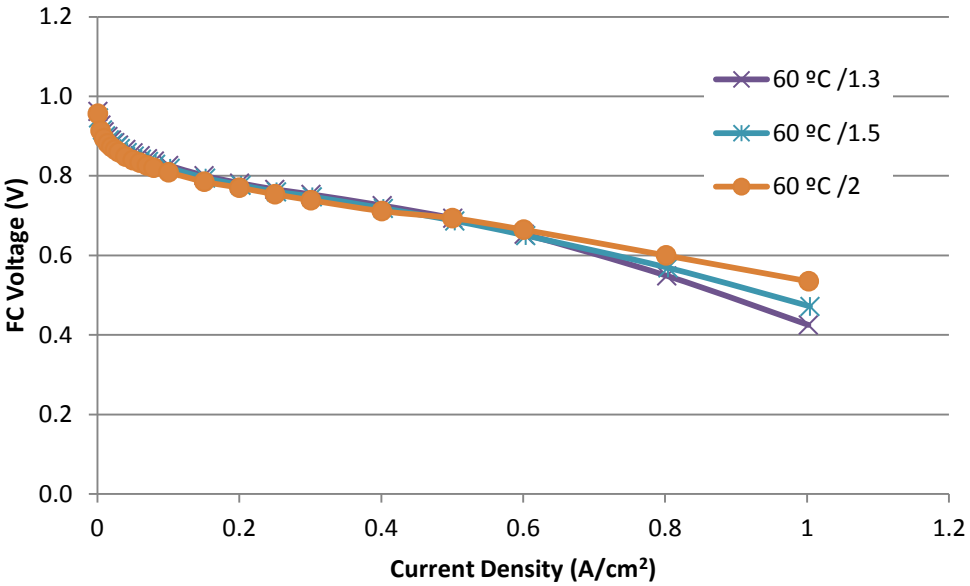

Fig 31: Polarization curve at 60°C (1.23 – 1.25 bar)

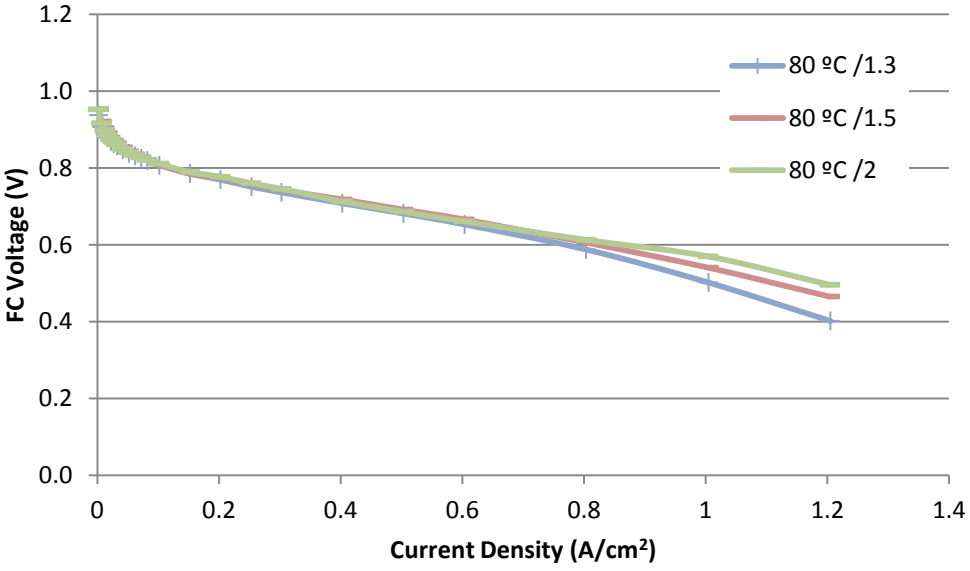

Fig 32: Polarization curve at 80°C (1.23 – 1.25 bar)

These results are a relevant contribution to the fuel cell research, providing empirical data about the fuel cell performance relevant to improve its efficiency. The results, together with the indicators defined and determined in the following chapter, will be presented this summer at the V Iberian Symposium on Hydrogen, Fuel Cells and Advanced Batteries (HYCELTEC 2015).

CHAPTER 6: EXPERIMENTAL DETERMINATION OF COEFFICIENTS

6.1. State of the art

Many studies have been done on optimizing performance of the fuel cells. There is a special need to properly relate the relevant effects of fluid mechanics and thermal dynamics, to the fuel cell voltage. With this purpose, methodologies to determine relevant indicators associated with the voltage drop are developed. The studies published in [Santarelli, Torchio, and Cochis 2006] and [Santarelli and Torchio 2007] have an experimental approach, finding experimental parameters to define the voltage losses further than what is already known and written in literature like [Barbir 2005], [O'Hayre 2009] or [Larminie and Dicks 2003]. What is relevant about these works is the study of the variation of the exchange current density of the cathode, even if no consistent conclusion about that is reported. Moreover, numerous tests have been done changing only the operational variables, like temperature or pressure obtaining polarization curves and power curves.

The work published in [A. P. Husar 2012] treats experimental parameter identification, mainly focused on fuel cell voltage loss indicators. The implementation of the indicators indirect measurement methodology provides an experimental way for the isolation of three main types of voltage losses in the fuel cell: activation, mass transport and ohmic losses. Additionally since these voltage loss indicators relate the operating conditions to the fuel cell voltage, they can be utilized to calibrate and validate CFD models as well as employed in novel control strategies.

This work was preceded by [L. Wang et al. 2003] and followed by [A. Husar, Strahl, and Riera 2012]. The first one is focused in the parametric study of PEM fuel cell performance with the variation of temperature, pressure and humidity, discussing the possible interrelationships between the parameters. Moreover, a three-dimensional fuel cell model is presented and validated by the experimental data. The second one is an accurate explanation of the experimental methodology used to obtain the three different voltage losses through current sweeps, which is the methodology used in this thesis.

6.2. Voltage loss analysis

To obtain the polarization curve from the current sweep it is only needed to recover the i–V value of each of the 10 points obtained from the CS (Fig 22) after they are stabile, the results are shown in Fig 33.

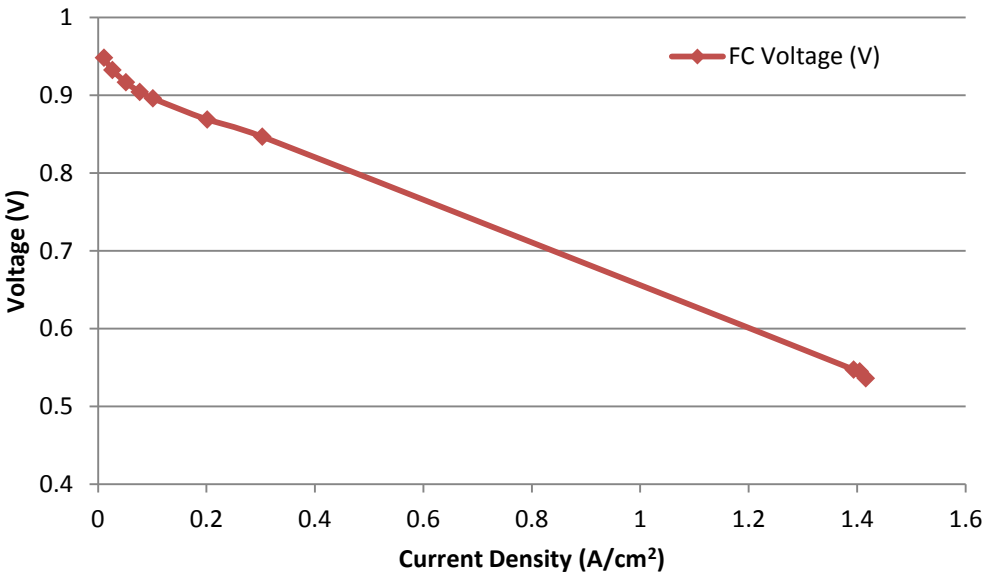

Fig 33: Polarization curve extracted from the Current sweep (80°C, 2.3 – 2.5 bar, Cathode Stoich.=1.5, 1.4 a/cm^2)

The following steps to obtain the voltage losses of the PEMFC have been already described in [A. Husar, Strahl, and Riera 2012], knowing that the theoretical voltage of a fuel cell is [O'Hayre 2009]:

$$V_{fc} = E_{T,P} - \Delta V_{act} - \Delta V_{mt} - \Delta V_{ohm} \qquad [V] \tag{36}$$

First of all the calculation of the theoretical Open Circuit Voltage (OCV) of the fuel cell considering different temperatures and pressure of the anode and the cathode is calculated applying equation 16:

$$E_{T,P} = -\left(\frac{\Delta H^0}{nF} - \frac{T\Delta S^0}{nF}\right) + \frac{RT}{nF}\ln\left[\frac{P_{H_2}P_{O2}^{0.5}}{P_{H2O}}\right] \; [V] \tag{16}$$

Where ΔH^0 is the change in enthalpy and ΔS^0 is the change in entropy of the reaction at standard conditions, which are considered to be 25ºC for the temperature and 1 bar for the pressure. The values at these conditions are, respectively, -285,826 J/mol and -163 J/mol/K. n represents the number of electrons transferred per mole, which in this case is 2 for H_2, F is Faraday's constant (96485,4 J/V/mol) and R is the universal gas constant (8,314472 J/molK). The partial pressures have been calculated with the data from the relative humidity of anode and cathode and depending on the temperature. Knowing that the relative humidity is equal to:

$$\phi = \frac{P_w}{P_{sat}} \tag{37}$$

Where P_w is the partial pressure of the water and P_{sat} is the saturated vapour pressure of the water. The following formula allows us to calculate the saturation pressure (in Pa) for any given temperature between 0°C and 100°C [*ASHRAE* 2013]:

$$p_{sat} = e^{aT^{-1}+b+cT+dT^2+eT^3+fln(T)} \quad [Pa] \tag{38}$$

The partial pressure of the liquid water is 1.

$$P_{H_2O_l} = 1 \tag{39}$$

While in the case of the hydrogen the partial pressure is the difference between the total (1) and the partial pressure of the water.

$$P_{H_2} = 1 - \left(\frac{p_{sat}}{p_{an}}\right) \tag{40}$$

In the same way, the partial pressure of the oxygen is the difference between the total (1) and the partial pressure of the water, taking into account that the inlet is air and not pure oxygen; it means that what remains needs to be divided between nitrogen and oxygen, with the ratio 3.76:1.

$$P_{O_2} = \frac{1 - \left(\frac{p_{sat}}{p_{cat}}\right)}{1 + 3{,}76} \tag{41}$$

The theoretical OCV of the FC ($E_{T,P}$) for the different case of study are:

Table 15: $E_{T,P}$ values [V]

	1.23 – 1.25 bar	2.3 – 2.5 bar
45°C	1.201	1.201
60°C	1.187	1.188
80°C	1.167	1.169

Having the theoretical value of the fuel cell voltage and the real value, from the fast polarization curve gotten from the CS, is possible to calculate the activation losses, the ohmic losses and the mass transport losses.

First of all with the R_{Ohm} value obtained from the high frequency real axis intercept of the EIS it is possible to calculate the ohmic losses of the fuel cell just applying equation 23.

Where i is the current density (A/cm^2) from the 10 stable points of the CS and R is the related resistance (Ωcm^2).

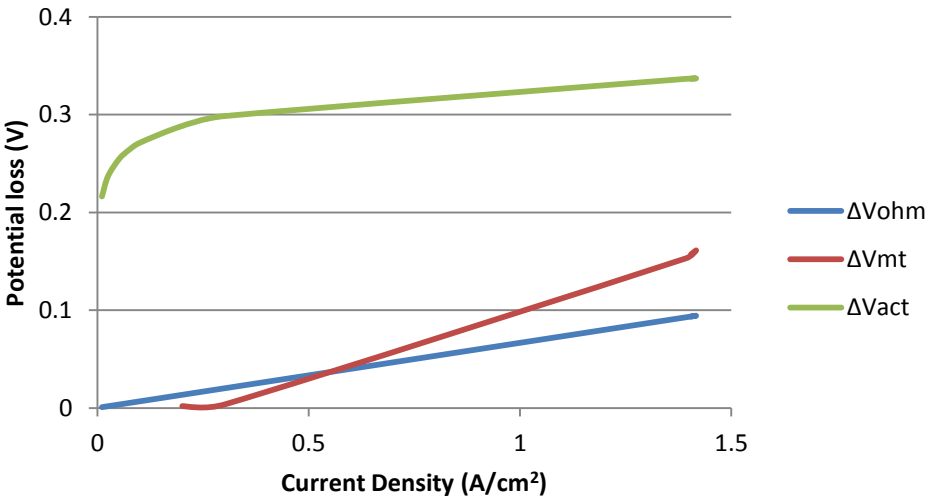

Fig 34: FC voltage losses (1 A/cm^2, 80°C, Stoich. An-Cat:1.3 – 1.5, P An-Cat:2.5 – 2.3 bar)

Subtracting the ohmic losses (ΔV_{Ohm}) from the total losses the result is a curve that contains the activation losses (ΔV_{act}) and the mass transport losses (ΔV_{mt}). Assuming that in the nonlinear part of the curve the only losses are the activation ones [A. Husar, Strahl, and Riera 2012], the first 7 points of fast CS give the activation losses curve equation. On the other hand, the mass transport losses are the result of subtracting the activation losses to the global curve (activation losses and mass transport losses together). The three resulting curves are presented in Fig 34.

From these curves it is possible to obtain the indicators R_{mt} (mass transport related resistance) and the Tafel Slope. R_{mt} is simply the slope of the linearization of the mass transport voltage losses obtained before. The Tafel Slope (eq. 42) is the slope of the linear part of the logarithmic linealization of the activation losses curve.

$$\Delta V_{act} = a + b \cdot log(i) = a + \frac{b \cdot ln(i)}{2.3} \tag{42}$$

Moreover, from the Tafel equation is possible to obtain the values of the charge transfer coefficient (α) and the cathode exchange current density (i_0).

$$b = \frac{RT}{n\alpha F} \rightarrow \alpha = \frac{\mathrm{RT}}{\mathrm{nFb}} \tag{43}$$

$$a = -\frac{RT}{n\alpha F}\ln(i_0) \rightarrow i_0 = e^{-\frac{a}{b}} \tag{44}$$

Where n is the number of electrones involved in the electrode reactions (in this case 2), and b is the Tafel slope.

6.3. Indicators

As a result from the whole process, graphics of the voltage losses and the indicators correlated are presented below.

The voltage losses are presented only for the operational point ($1A/cm^2$), while the indicators are represented for the different current densities.

Only the results concerning PUMA MIND conditions are presented below, the results at low pressure can be find in the annex.

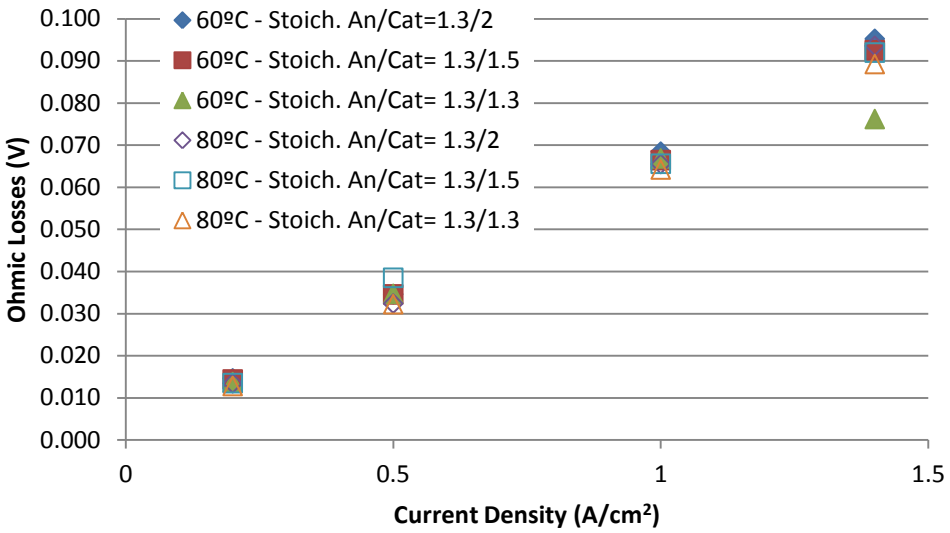

Fig 35: Ohmic losses at 1 A/cm^2 with respect to stoichiometry and temperature

The ohmic losses (Fig 35) are the lowest in all cases, always below the 0.1V at the operational point. Even if they get higher with the temperature, this variation is very low. The variation due to the stoichiometry is almost imperceptible.

Even though the ohmic losses are relatively small compared to the other losses in the fuel cell, there may be some undesirable long-term degradation caused by a dry membrane.

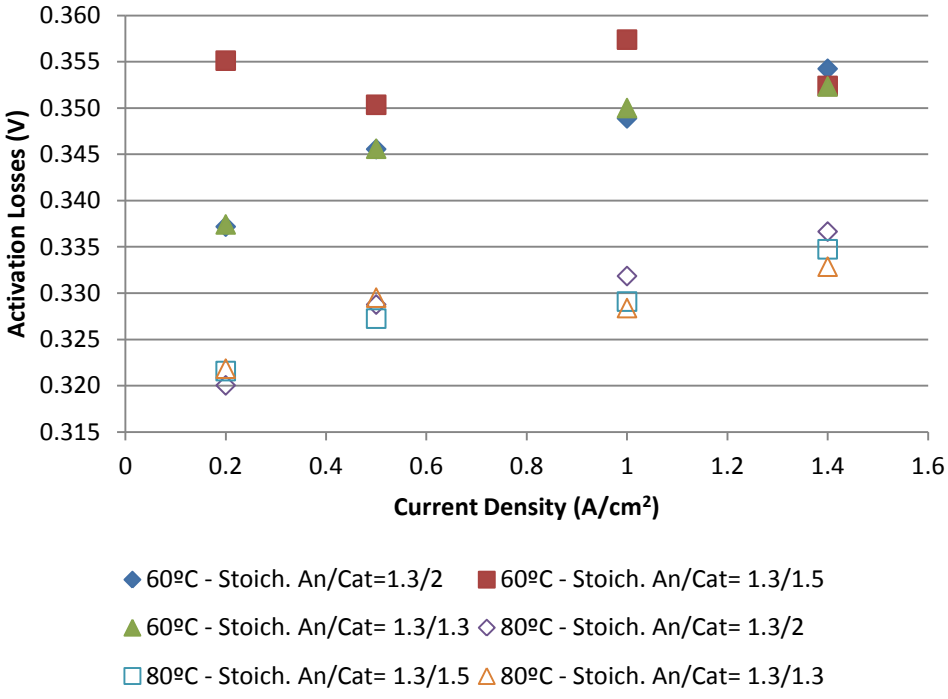

Fig 36: Activation losses at 1 A/cm^2 with respect to stoichiometry and temperature

The activation losses (Fig 36) are the highest. They are followed by the mass transport losses that vary mainly due to stoichiometry, while the activation losses do not vary that much with the stoichiometry. While with temperature increase, the activation losses decrease. The same occurs with the mass transport losses, even if the variation is much larger than that for the activation losses. The range of the mass transport losses is between 0V and 0.6V (in this temperature range), while for the activation losses the range is between 0.32V and 0.36V.

The activation losses decrease whith the temperature since they are directly dependent on the thermodinamic reversible potential ($E_{T,P}$) that, as can be seen in Table 15, decrease with the increasing of the temperature. The lower the $E_{T,P}$, the lower the activation losses are.

On the other hand, the mass transport losses increase with the increase in the current (Fig 37). This last component of the voltage losses contains all the measurement errors, due to the order of decomposition of the voltage losses. As it was expected, they strongly depend on the stochiometry, but they are also temperature dependent. The lower the temperature, the higher the mass transport losses.

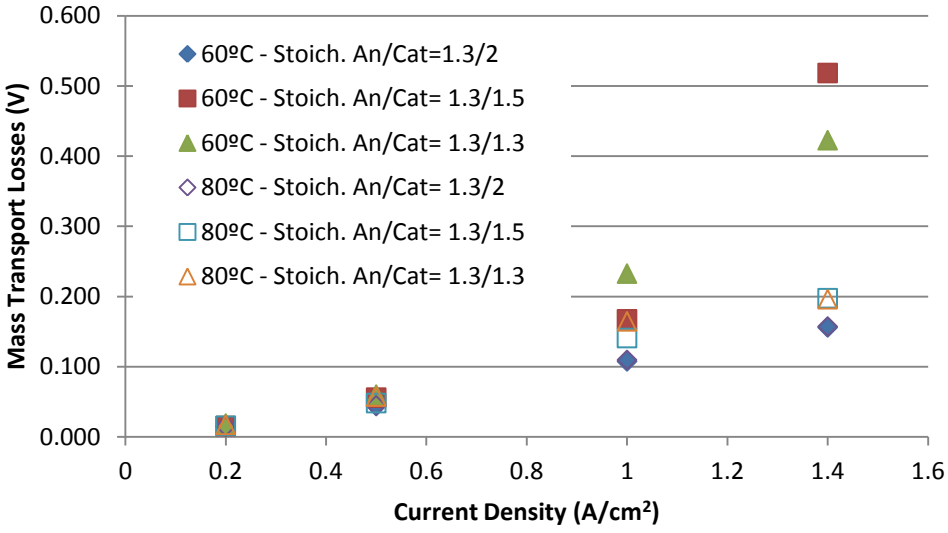

Fig 37: Mass transport losses at 1 A/cm2 with respect to stoichiometry and temperature.

According to the indicators graphs and in line with the voltage losses results, the ohmic resistance is higher at lower temperatures and for higher cathode stoichiometry (Fig 38). What can be seen is that this indicator decreases with higher current densities, even if it stays between 0.063 Ωcm^2 and 0.078 Ωcm^2.

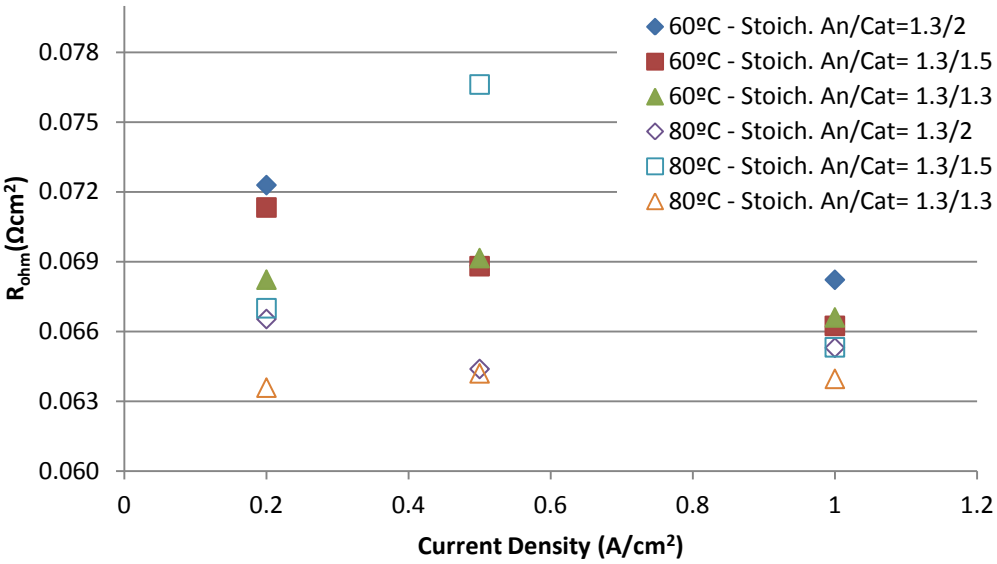

Fig 38: Ohmic resistance as the Ohmic indicator, respect stoichiometry and current density.

The Tafel Slope depends on the current density: the higher the current density, the lower the Tafel Slope (Fig 39). The dependency on temperature or stoichiometry is not that important: for each current density, the indicators at different temperatures and stoichiometries are contained in an order of 0.015. The only appreciation is that at higher temperatures it is a bit smaller, so the activation losses are a bit smaller than at lower temperatures.

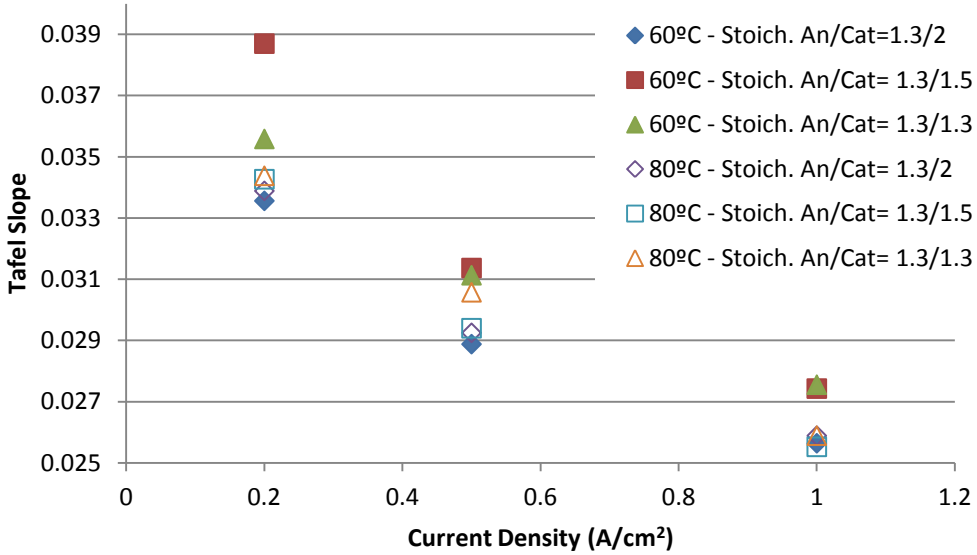

Fig 39: Tafel slope as activation indicator, respect stoichiometry and current density.

The mass transport indicator (represented as a resistance in Fig 40) is higher for higher current densities. The higher the temperature is, the lower

the indicator. According to the stoichiometry, for lower values of the cathode stoichiometry, this indicator is bigger (specially for the stoichiometry 1.3).

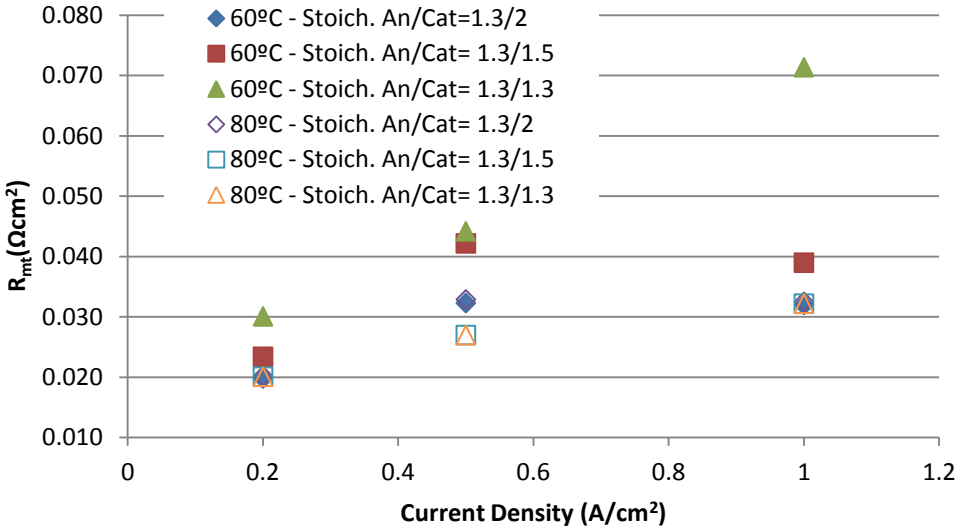

Fig 40: Linear mass transport indicator represented as a resistance, respect stoichiometry and current density.

6.4. Temperature dependence

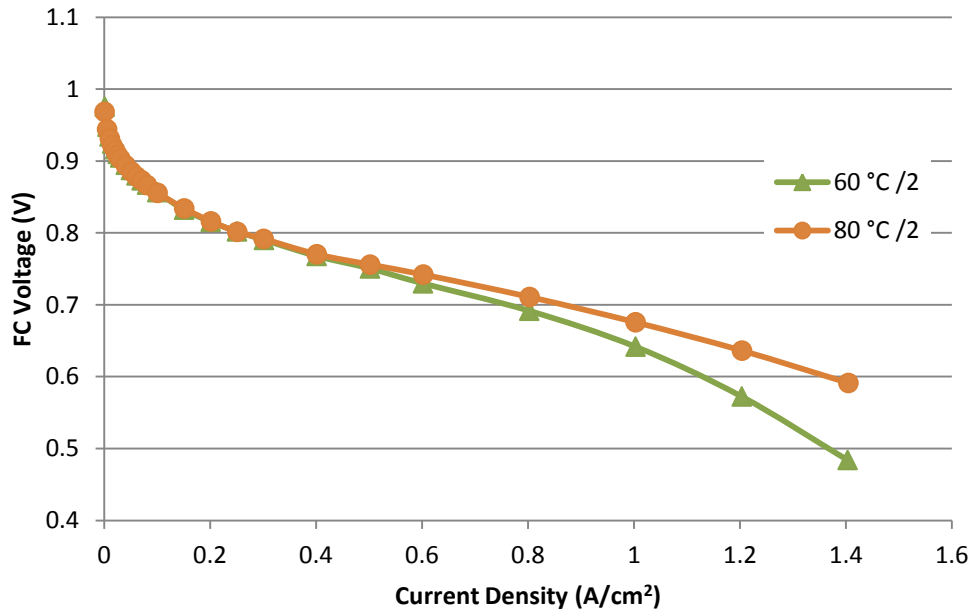

Fig 41: Polarization curve 2.3 – 2.5 bar, cathde stoich. = 2

At higher temperatures, the FC performance is better, as shown in Fig 41, for multiple reasons. First of all, as we have seen before, at high temperatures the activation losses are lower, meaning that the reaction

kinetics is faster. Moreover at more temperature (lower than the saturation condition) there is more water in the membrane, reducing the ionic resistance (R_{ohm}) and improving the proton conductivity.

6.5. Pressure dependence

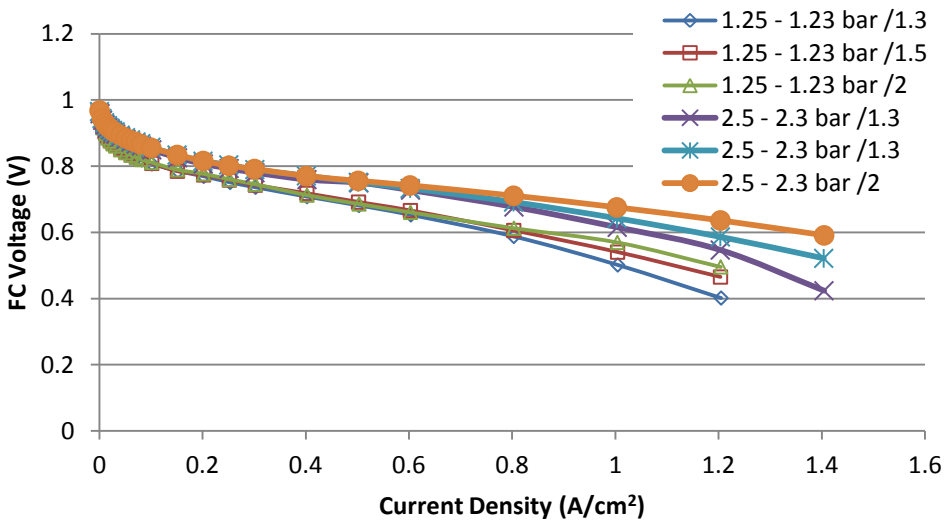

Fig 42: Polarization curve 80°C, varying cathode stoichiometry and pressure

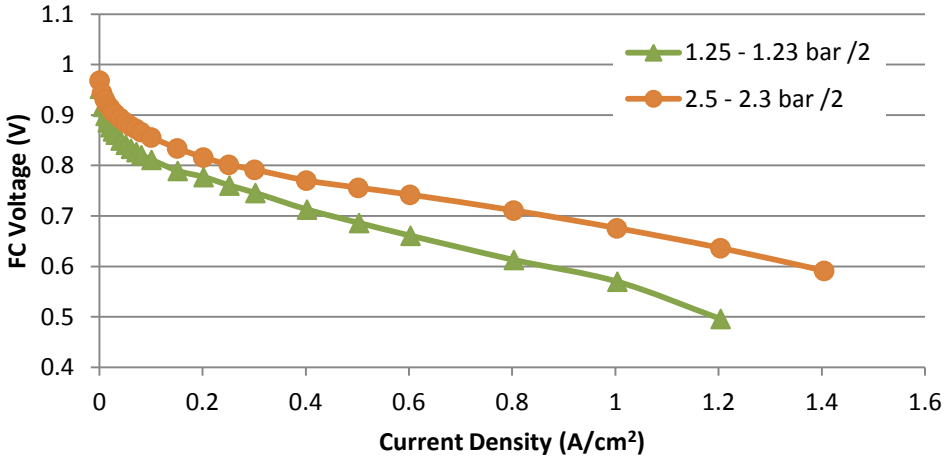

Fig 43: Polarization curve 80°C, cathode stoichiometry=2 and varying pressure

The performance always improves when the operating pressure increases (Fig 42 and Fig 43). This can be explained by an increase of the partial pressures of the reactant and product flows, which causes an improvement of the open circuit voltage according to Nernst Law.

6.6. Stoichiometry dependence

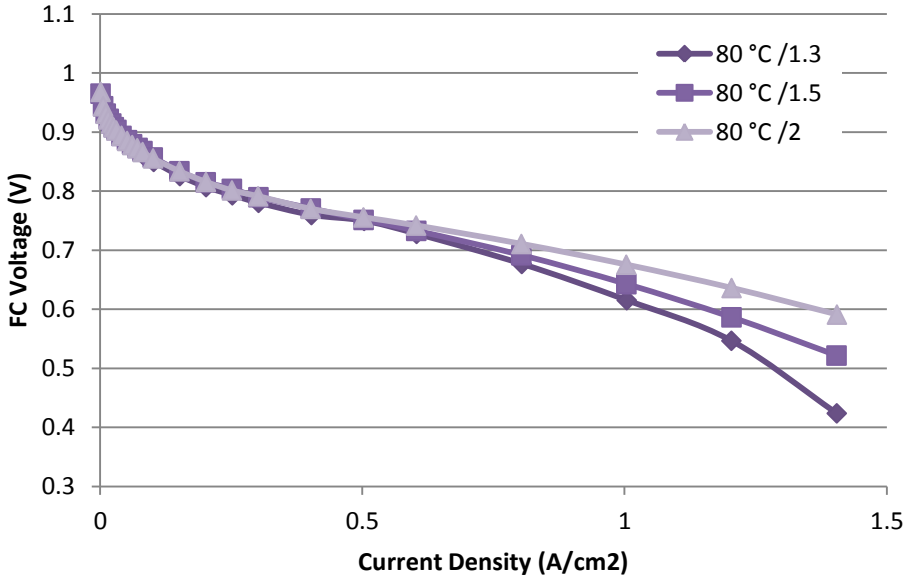

Fig 44: Polarization curve at 80°C, 2.3 – 2.5 bar and varying cathode stoichiometry

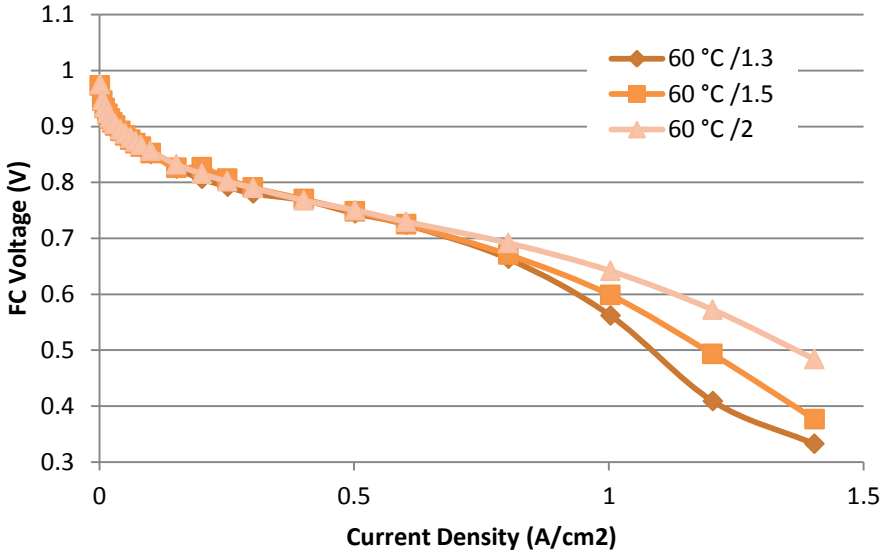

Fig 45: Polarization curve at 60°C, 2.3 – 2.5 bar and varying cathode stoichiometry

In the figures above it is clear that the higher the cathode stochiometry, the better the performance. How it was expected, at higher stoychiometries the mass transport losses (at high current densities) are lower. This is due to the lower oxygen concentration in the catalyst layer for higher stoichiometries.

Fot the lowest stoichiometry (1.3) at high current density there is a deviation from the usual shape of the curve in this region (it should be like

the one in Fig 44) due to the instability of the fuel cell at this temperatues. An increasing temperature at this conditions generates more water and improves the fuel cell conductivity reducing the voltage losses.

Moreover, a variation of the charge transfer coefficient (α) and the cathode exchange current density (i_0) has been observed from the experimental data. A more accurate study has been carried out about this variation.

With this purpose, the variation of the fuel cell voltage with the oxygen concentration has been studied.

Equation 45 [O'Hayre 2009] describes the fuel cell voltage losses depending on the oxigen concentration.

$$V_{FC} = E_{T,P} - \Delta V_{ohm} - \frac{RT}{\alpha nF}\left[ln\left(\frac{C_{O_2}^0}{C_{O_2}}\right) + ln\left(\frac{i}{i_0}\right)\right] \quad (45)$$

From this, two elements can be distinguished:

$$\Delta V_{act} = \frac{RT}{\alpha nF}\left[ln\left(\frac{i}{i_0}\right)\right] \quad (46)$$

$$\Delta V_{mt} = \frac{RT}{\alpha nF}\left[ln\left(\frac{C_{O_2}^0}{C_{O_2}}\right)\right] \quad (47)$$

From the previous equation is possible to obtain the evolution of the oxygen concentration in the cathode catalyst layer.

$$C_{O_2} = C_{O_2}^0 \cdot \frac{i_0}{i} \cdot e^{\frac{\alpha nF}{RT}(E_{TP} - V_{FC} - \Delta V_{ohm})} \quad (48)$$

Where $C_{O_2}^0$ is the molar concentration (mol/m^3) of the Oxigen at the reference conditions. `

$$C_{O_2}^0 = X_{O_2}^0 \cdot \frac{p_{cat} - p_{sat} \cdot RH_{cat}}{RT} \quad (49)$$

Where $X_{O_2}^0$ is the mass fraction of the oxigen at the reference conditions (0.21), p_{sat} is the saturation pressure (Pa) at the correspondent temperature and RH_{cat} in the relative humidity at the cathode, in this case of study, 50%.

In the figures below is possible to see the exponential performance of the oxygen concentration and how it gets dramatically small at high current desities, turning the concentration losses the dominant ones at this conditions.

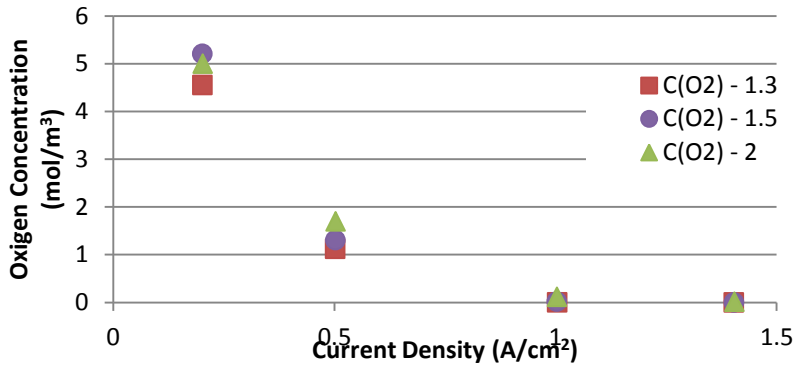

Fig 46: Oxygen concentration in the cathode catalyst layer (60°C)

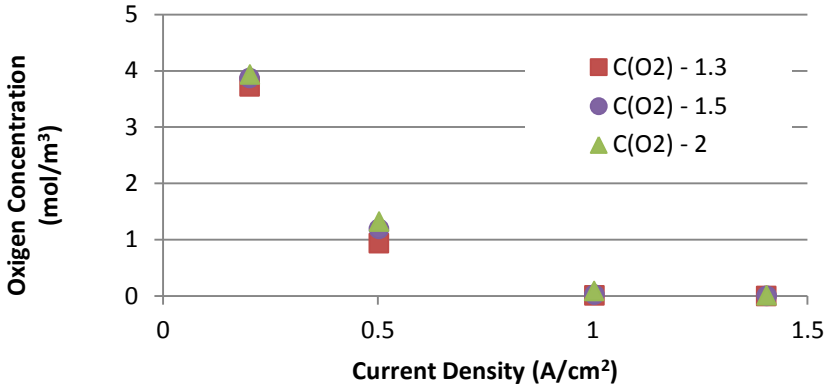

Fig 47: Oxygen concentration in the cathode catalyst layer (80°C)

Furthermore, the concentration is lower at higher temperatures, becouse of the partial pressure of the reactants.

In Fig 48 the oxygen concentration and the mass transport losses are presented together to see the direct relationship between them, even though if one has an exponential trend and the other is linear, both have actually an exponential performance.

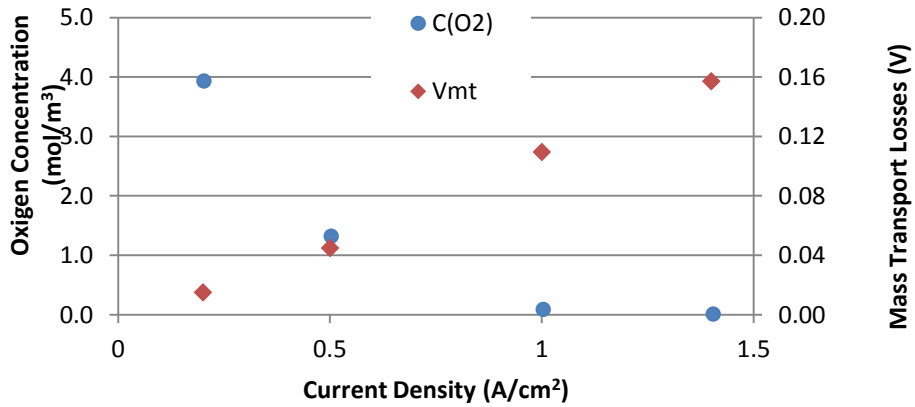

Fig 48: Mass transport voltage losses related with the oxygen concentration in the cathode catalyst

6.7. PC vs CS

The current sweep is a very powerful tool to determine the cause of the losses inside of a fuel cell. The fuel cell can be diagnosed in a time frame of seconds and the internal condition of the fuel cell can be assessed.

As can be seen in Fig 49, compared with the polarization curve, there is a big difference. This is due to the timing of the two experimental methods. A polarization curve can last around 20 min, while the current sweep only takes 2 minutes, thus in the second case the internal condition are not changing. From the figure below is clear that from a polarization loss higher voltage losses result, because the changing internal conditions, as temperature, water content or reactant concentration alter FC performance.

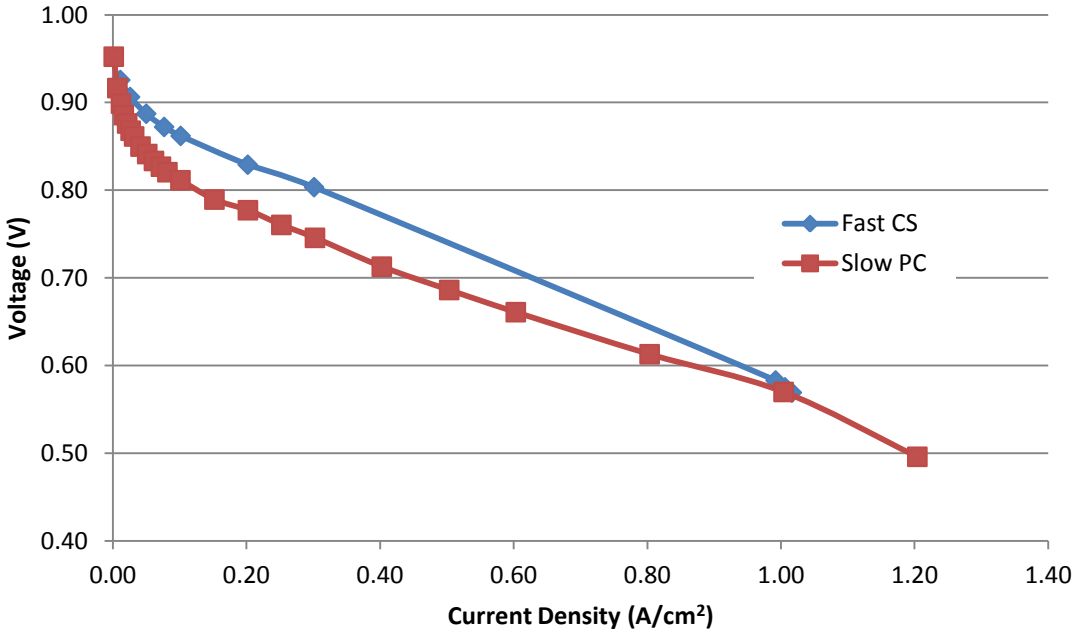

Fig 49: Experimental slow Polarization curve compared to a fast current sweep at 80ºC, cathode's stoichiometry at 2 and 1A/cm^2 (Pressure An-Cat =1.25-1.23).

What must be noted is that all the power generated during the sweep would be lost. Thus if the current sweeps is used as a on-line monitoring tool of the fuel cell internal condition it will affect the performance of the system.

CHAPTER 7: MODEL VALIDATION

7.1. State of art

In the field of fuel cell control, cell or system modelling has played a decisive role in developing, optimizing and testing algorithms and strategies. However, modelling PEMFC based systems is a particularly challenging task due to the interactions between physical phenomena of different nature (thermal, electrical, mechanical, electrochemical, etc.), the presence of numerous nonlinear structures, the spatial distribution of phenomena, the sensitivity of the associated sensors and the limited accessibility of variables, to name some examples. In fact, PEMFC modelling has been studied by several authors and with different approaches; however, many of these models have not been completely experimentally validated and there is still a lack of rigorous studies on parameters identification and their association with performance variables [S. Strahl 2010].

In the field of the Computational Fluid Dynamics modelling two relevant works, [S. Strahl et al. 2014] and [S. Strahl et al. 2014] ,describe the water transport as a decisive factor to study the PEMFC performance. In [Stephan Strahl, Husar, and Franco 2014] a model that describes two-phase water transport, electrochemistry and thermal management is analysed, while one of the focus of the work done in [S. Strahl et al. 2014] is the temperature dependency of the exchange current density, thus implying a water content dependence. The modelling of the water management in the PEMFC's MEA is

important not only to improve the performance of the fuel cell but also to develop new materials to optimize costs and improve durability. In order to develop and simulate dynamic water management strategies that match the application load requirements and the operating conditions, new models need to be based on a broad understanding of water transport in the MEA [S. Strahl 2010].

7.2. Objective

The objective of this chapter of the work is to validate a model proposed by Dr. Stephan Strahl. Since the original version of the model was not built for the specific fuel cell of this work, first of all it has to be adapted. Moreover, the model only includes the MEA assembly, without the anode and cathode channels; this is why this work only covers the validation of the model focusing on activation losses. Activation losses are highly dependent on the reactions in the MEA , while the rest of the fuel cell losses, at higher values of current densities, are more influenced by other losses, first of all, losses due to mass transport, related with the channels implementation.

Aim of this work is to start the adaptation of the Strahl model to the PUMA MIND fuel cell and studies the activation losses at low current densities, as a way to validate the model. This work is just the beginning of the adaptation on the whole model to the single cell in order to have a good parameters identification and their association with performance variables, obtaining a good tool to implement control strategies.

COMSOL® Multiphysics is a software for finite element analysis of physical environments, it allows to simulate the process and to visualize the results. The software is based on the finite element method (in the following shortened as FEM) to solve the implemented model, subdividing the whole physical domain into smaller parts, called finite elements, and using variational methods based on the calculus of variations to solve the problem by minimizing an associated error function.

.

7.3. Geometry

A two-dimensional (in the following shortened as 2D) geometry for the model is considered to be adequate for the model to simulate the system. As consequence it is not possible to simulate the channels due their three-dimensional (in the following shortened as 3D) shape, so the geometric

parameters have been changed according to consideration shown in Chapter 4. Other specific characteristics of the fuel cell have not been implemented because of the timing of this work, so more investigations are needed to be developed in future research activities.

The 2D model is developed because it provides better simulation accuracy than a 1D model and has a higher computational efficiency than a 3D model. The equivalence between the dimensions of the real serpentine and the model is introduced in the calculation of the layers length.

Fig 50 shows the main subdomains of the model: the GDL, both anode and cathode, the MPL, both anode and cathode, the two catalysts and the membrane. As mentioned above, the anode and cathode channels shown in Fig 50 are not included in the present model.

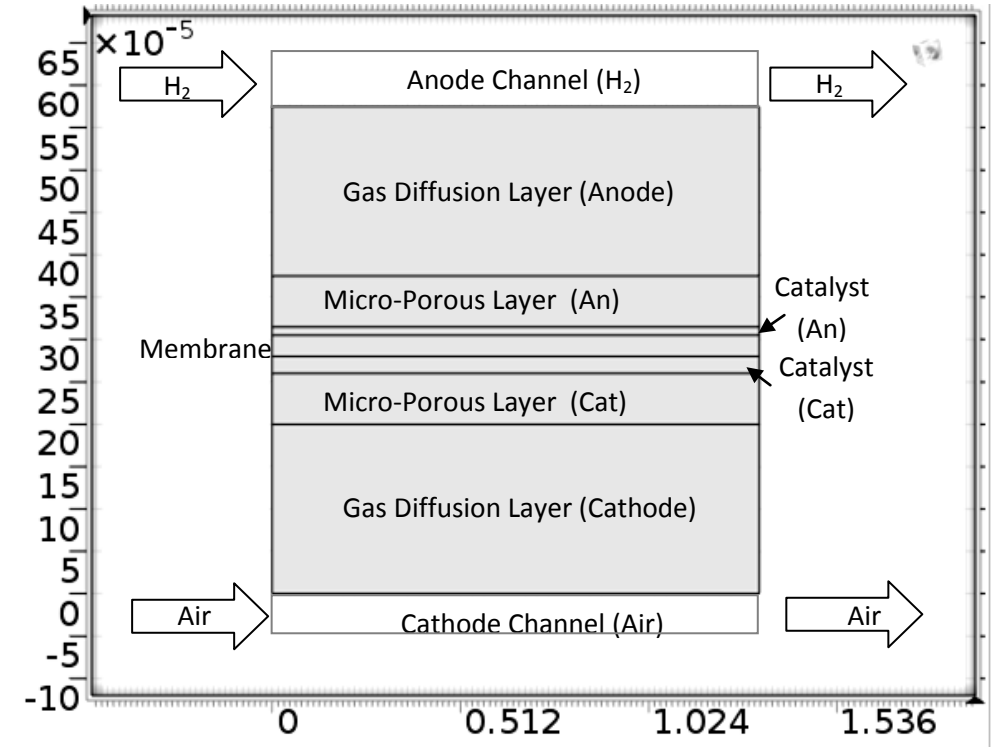

Fig 50: 2D model geometry

7.4. Physics

7.4.1. Transport of concentrated species – Cathode

The COMSOL® module defines the equations for the species mass fractions, including a diffusion model (mixture-averaged or Fick's law). What is studied is the evolution of chemical species transported by convection and diffusion.

The base equation for an individual species *i* is:

$$\nabla \cdot \boldsymbol{j_i} + \rho(\boldsymbol{u} \cdot \nabla)\omega_i = R_i \qquad (50)$$

Where j_i is the diffusive mass flux, ρ is the fluid density, $\boldsymbol{u}$ the velocity and ω_i the respective mass fraction of the gaseous species i (H_2 ,O_2 ,N_2 or H_2O). The source terms R_i on the catalyst layer boundaries describe reactant consumption and water generation based on the electrochemical reactions.

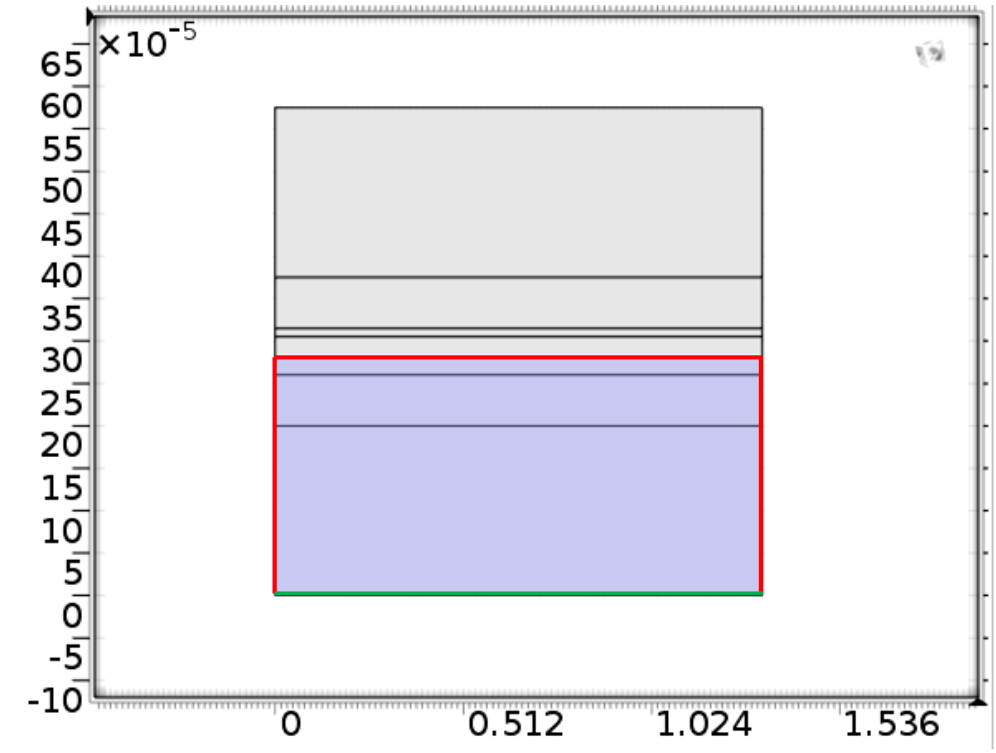

Fig 51: Transport of concentrated species – Cathode geometry

In Fig 51 is possible to see that the part of the FC where this physics is acting is the cathode. The red lines indicates no flow boundary conditions, it means, no convection and diffusion throughout those limits. The green line indicates the inflow boundary, where the inlet mass fraction of oxygen and water are the inputs.

7.4.2. Transport of concentrated species – Anode

This is the same module as in chapter 7.4.1., ruled by the same equation. The only differences are the area affected and the species implied. In this case, as it is possible to see in Fig 52, the anode is where the reactions take place, there is no flow throw the red lines, and the inflow (H_2) is in the superior area, where the channels are supposed to be. Across the yellow line (to the membrane) there is nitrogen flux.

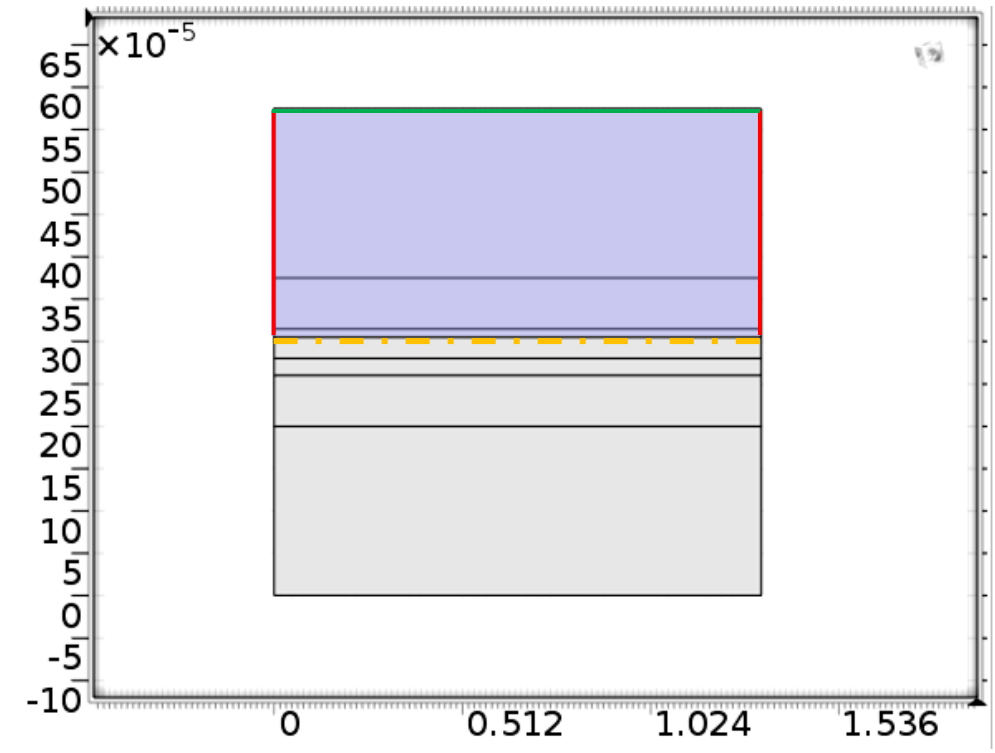

Fig 52: Transport of concentrated species – Anode geometry

7.4.3. Secondary current distribution

The Secondary Current Distribution module describes the current and potential distribution in an electrochemical cell under the assumption that the variations in composition are negligible in the electrolyte. Under this assumption, migration of ions gives the only net contribution to the current in the electrolyte.

$$\nabla \cdot i_l = Q_l \tag{51}$$

$$i_l = -\sigma_l \nabla \phi_l \tag{52}$$

$$\nabla \cdot i_s = Q_s \tag{53}$$

$$i_s = -\sigma_s \nabla \phi_s \tag{54}$$

Where ϕ_l and ϕ_s are respectively the electrolyte potential and the electronic phase potential; σ is the conductivity i the current and Q the charge.

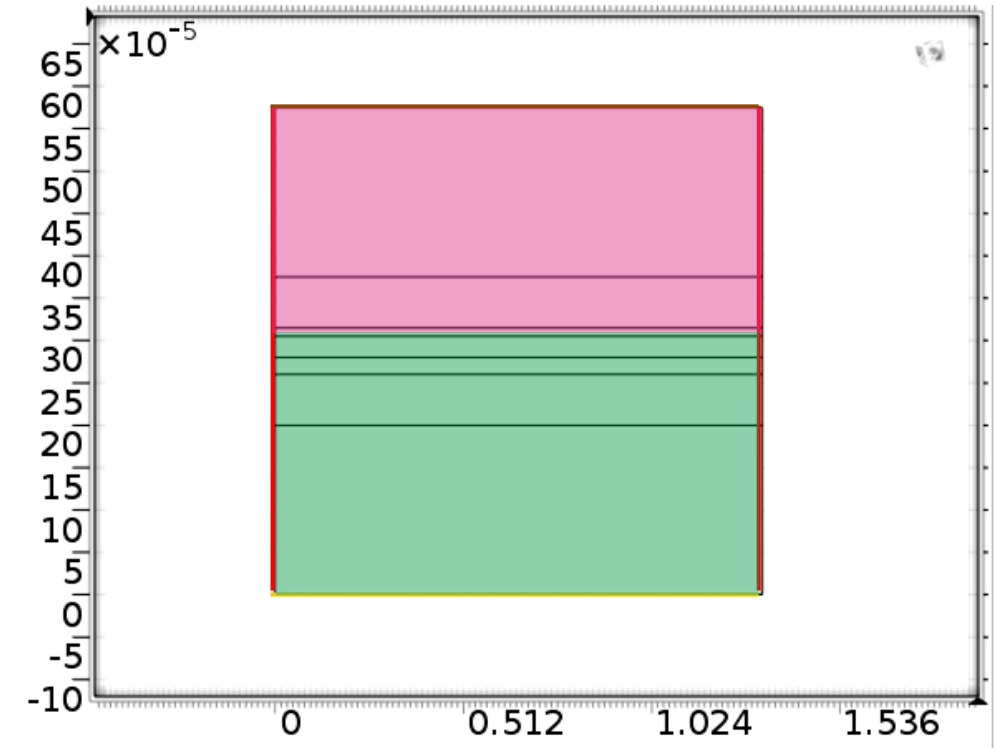

Fig 53: Secondary current distribution geometry

There are two main areas involved in this physics: the anode and the cathode (that includes the membrane). The difference between them are the initial values: both have null electrolyte potential, while the anode has null electric potential as well but the cathode has an electric potential equal to 1V. This is represented in Fig 53 where the brown line indicates the ground (anode) and the yellow line indicates the electrode current. As in the previous figures, the red lines indicate the insulation boundaries.

In this physics is where the reactions that have been studied specifically in this thesis take place. In the cathode and anode catalyst the Butler – Volmer expression (eq. 55) is used to define the electrode kinetics.

$$i_{loc} = i_0 \left(e^{\frac{\alpha_a F \eta}{RT}} - e^{\frac{\alpha_c F \eta}{RT}} \right) \tag{55}$$

In a PEM fuel cell, the value of the exchange current density at the cathode electrode is considerably low compared to the value at the anode electrode, and therefore the anodic activation overvoltage is usually negligible. Thus the anode parameters can be neglected and i_0 is the exchange current density, α_c the cathode charge transfer coefficient, η is the potential and F is Faraday's constant (96485,4 J/V/mol) and R is the universal gas constant (8,314472 J/molK).

In the cathode side, the exchange current density is defined as:

$$i_0 = i_{0_c}\left(\frac{C_{O2}^{\ 0}}{C_{O_2}}\right)^{k_{conc}} \tag{56}$$

Moreover, the α values are defined as [Bezmalinović et al. 2014]:

$$1 = \alpha_c + \alpha_a \tag{57}$$

7.4.4. Transport of liquid water

In this model there is transport of liquid water everywhere except throw the membrane. The initial conditions are constant (5% in the catalyst region and 10% in the anode region). In all the area there is evaporation and condensation, while only in the catalyst (both anode and cathode) there is sorption, it means liquid water that becomes dissolved water in the catalyst and moves throw the membrane, which is what is described in the "Transport of dissolved water" physic.

In Fig 54 is possible to see the zero flux boundaries (red lines), this means that there is no liquid water in the membrane, only dissolved. In yellow the initial condition regions, defined by a PDE coefficient (eq. 59).

$$e_a\frac{\partial^2 s}{\partial t^2} + d_a\frac{\partial s}{\partial t} + \nabla(-c\,\nabla s - \alpha s + \gamma + \beta\,\nabla s + as) = f \tag{58}$$

While in the catalyst (green and blue areas) the sorption is:

$$f = -S_d(M_{H_2O}) \tag{59}$$

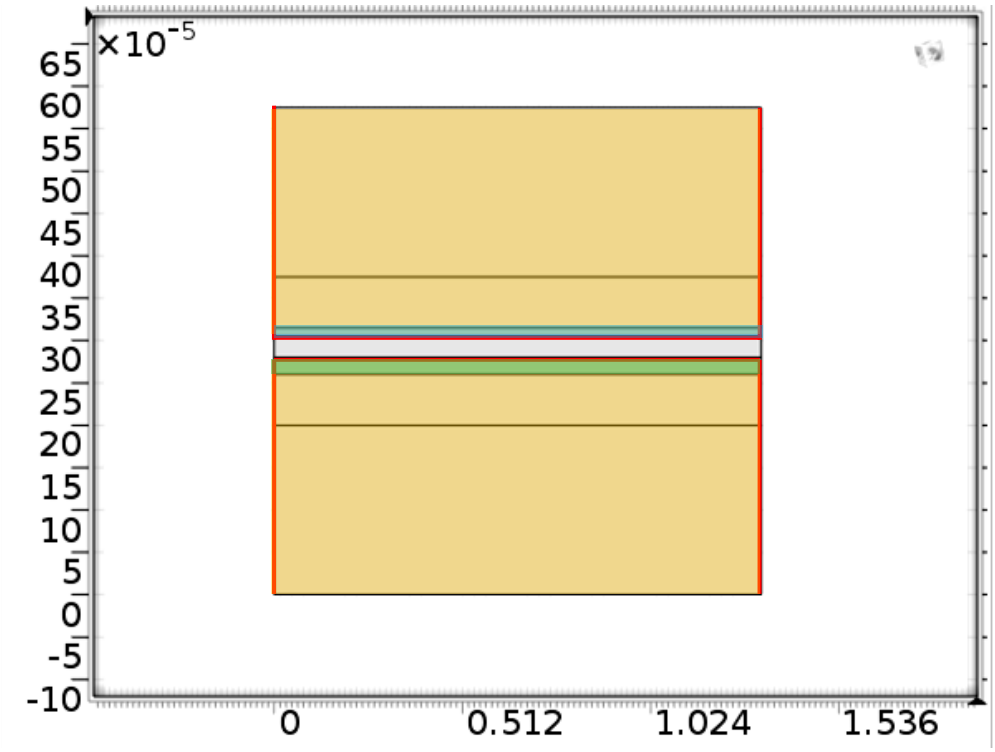

Fig 54: Transport of liquid water geometry

7.4.5. Transport of dissolved water

As it is possible to see in Fig 55 there is transport of dissolved water only throw the catalyst and the membrane (delimited by the red lines). Only in the catalyst there is sorption, which is:

$$f = S_d \tag{60}$$

The initial conditions are:

$$c_d = \frac{\rho_{PEM}\lambda_S(0.1)}{EW_{Naf}} \tag{61}$$

Where $\mathrm{EW_{Naf}}$ is the equivalent weight of the Nafion.

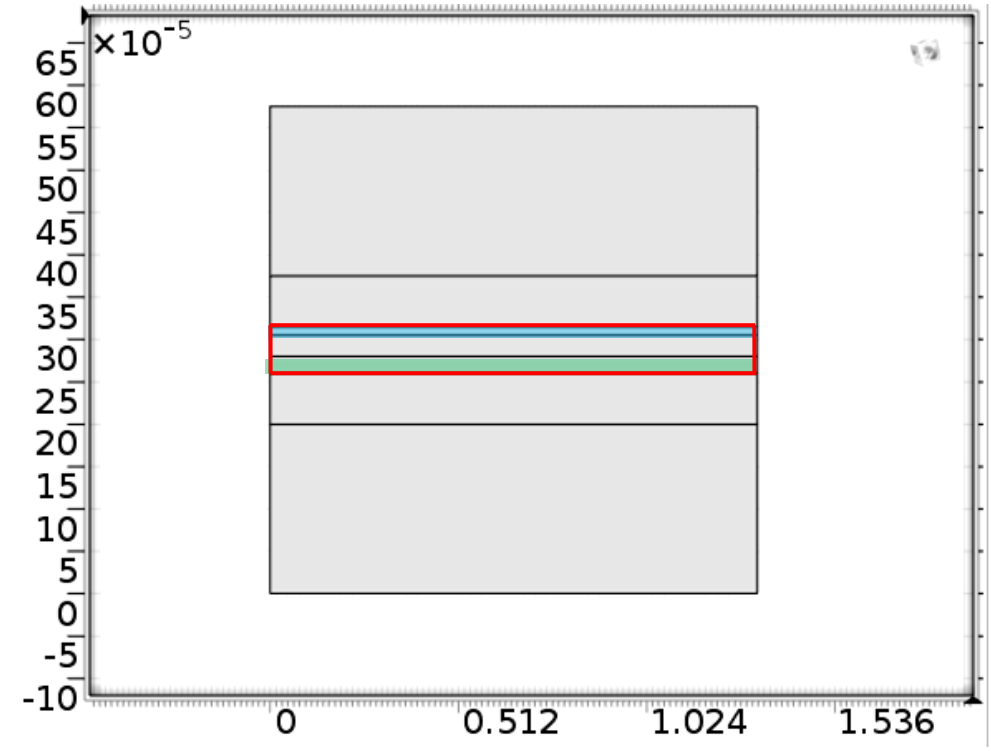

Fig 55: Transport of dissolved water geometry

Table 16: Model physics summary

Physic	Equation
Transport of concentrated species – Cathode	$\nabla \cdot j_i + \rho(u \cdot \nabla)\omega_i = R_i$
Transport of concentrated species – Anode	$\nabla \cdot j_i + \rho(u \cdot \nabla)\omega_i = R_i$
Secondary distribution current	$\nabla \cdot i_l = Q_l$ $i_l = -\sigma_l \nabla \phi_l$ $\nabla \cdot i_s = Q_s$ $i_s = -\sigma_s \nabla \phi_s$
Transport of liquid water	$f = -S_d(M_{H2O})$
Transport of dissolved water	$f = S_d$

7.5. Model solver

7.5.1. Mesh generation

Because the subdomain geometry is kept simple, a high quality mapped mesh can be generated that consists only of rectangular elements, as illustrated in Fig 56. Rectangular elements normally show a better convergence behaviour than triangular shapes, and therefore also reduce the solution time.

To generate this mesh, the *Predefined mesh size* in *Mesh > Mapped Mesh Parameters* has to be set to *Extremely fine*.

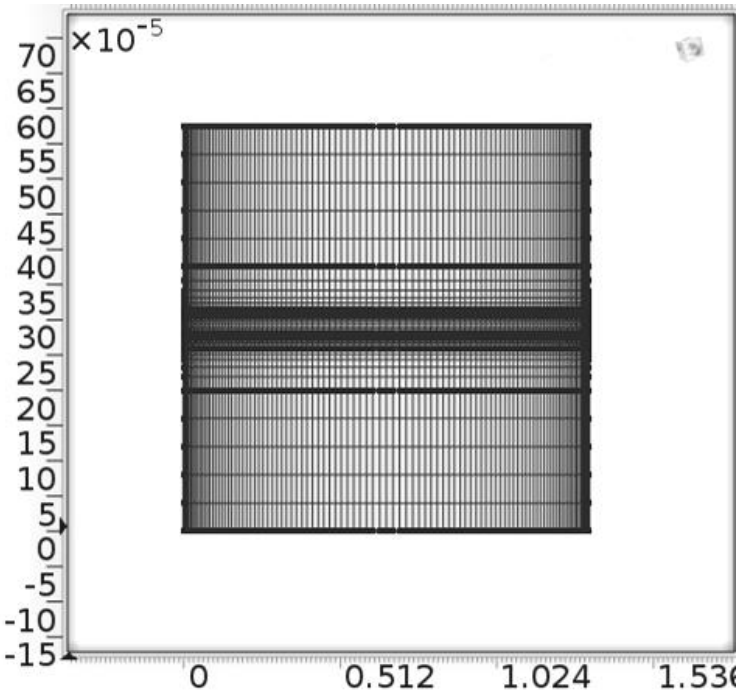

Fig 56: Model mesh

7.5.2. Solver

The model has two options to solve the system: stationary and time dependent. In this work, only the stationary option has been studied. Into this stationary option two steps are followed: first of all the system solves the three main physics of the system, the ones that already exist in the COMSOL predefined modules (Transport of concentrated species – Cathode, Transport of concentrated species – Anode and Secondary current distribution). Then, the solution of this first partial simulation is taken as the initial conditions to develop the other physics (Transport of liquid water and transport of dissolved water) that have been implemented manually.

This makes the model easier to solve, since the three main physics have a quicker solver, even though the majority of the time simulation is spent to

solve the initial conditions of the model. Solving the model in two steps allows the COMSOL® to have a solid base to start solving the other two physics that have been inserted manually, which always takes more time and carries more complications.

The first three physics defines electrochemical behaviour of a fuel cell, while the other two try to define the water transport and management throw experimental coefficients and expressions.

The aim of this simulation is to obtain the polarization curve, in order to validate the model with the experimental results. This is the reason why in the solver a parametric sweep of the external current density is included. This sweep only covers until i=0.3 A/cm^2, this is low current densities, to observe the polarization losses. More points are taken in the first 0.1 A/cm^2: between 0.01 A/cm^2 and 0.1 A/cm^2 a point is evaluated every 0.01 A/cm^2, between 0.1 A/cm^2 and 0.3 A/cm^2 a point is evaluated every 0.05 A/cm^2.

7.6. Results

After changing the geometric parameters (chapter 7.3.) the model has been ran in order to see the accuracy compared with the experimental results.

Simulations for all the slow experimental polarization curves have been done.

Table 17: Slow polarization curve conditions

	Pressure	
	1.23 – 1.25 bar	1.3 – 1.5 bar
Stoich. An-Cat: 1.3-2	45°C, 60°C, 80°C	60°C, 80°C
Stoich. An-Cat: 1.3-1.5	45°C, 60°C, 80°C	60°C, 80°C
Stoich. An-Cat: 1.3-1.3	45°C, 60°C, 80°C	60°C, 80°C

In the following tables the variables changed for every simulation are showed. Simulations have been done separately: first at high pressure and then low pressure. For each pressure state, the two or three different temperatures have been simulated, changing the ohmic resistance, the cathode exchange current density and the charge transfer coefficient. This values result from the mean value of the same variable obtained from the current sweeps data elaboration.

Table 18: Simulation variables (Pressure 2.3 – 2.5 bar)

	80°C			60°C		
	2	1.5	1.3	2	1.5	1.3
R_{Ohm} (Ωcm^2)	0.066	0.069	0.064	0.069	0.068	0.067
α_c	0.542	0.543	0.509	0.493	0.457	0.457
I_{0c} (A/cm^2)	7.3E-06	7.7E-06	8.9E-06	3.5E-06	7.9E-06	7.2E-06

Table 19: Simulation variables (Pressure 1.23 – 1.25 bar)

	80°C			60°C			45°C		
	2	1.5	1.3	2	1.5	1.3	2	1.5	1.3
R_{Ohm} (Ωcm^2)	0.096	0.075	0.075	0.074	0.070	0.070	0.073	0.075	0.073
α_c	0.480	0.520	0.533	0.424	0.445	0.446	0.658	0.602	0.716
I_{0c} (A/cm^2)	6.9 E-06	2.8 E-06	2.5 E-06	6.4 E-06	3.7 E-06	4.6 E-06	5.1 E-08	2.9 E-07	2.9 E-08

Only some of these results are presented in this chapter, the others can be find at the Annex 2.

In Fig 57 is possible to see a simulation ran at the same conditions as for the experimental test (I_{0c}=6.9E-06 A/cm^2). The firs appreciation that has to be done is that the curve is quite higher (0.15) than the experimental one.

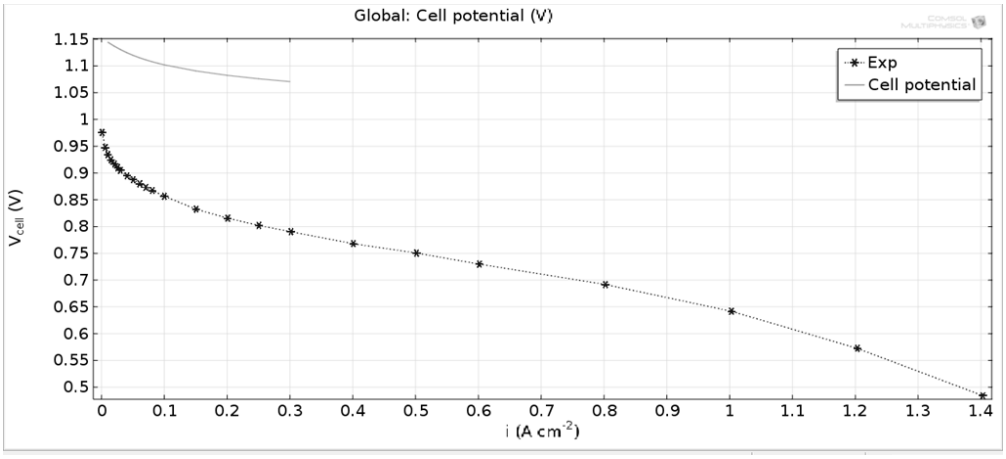

Fig 57: Polarization curve (60°C, Cat. Stoich. = 2, p=2.3-2.5 bar)

To discover which parameter makes this curve differ from the experimental one, different simulations varying only one parameter have been done. The result is that, for a lower cathode exchange current density (I_{0c}=1·E-9 A/cm^2), the curve follows better the shape of the experimental one (Fig 58).

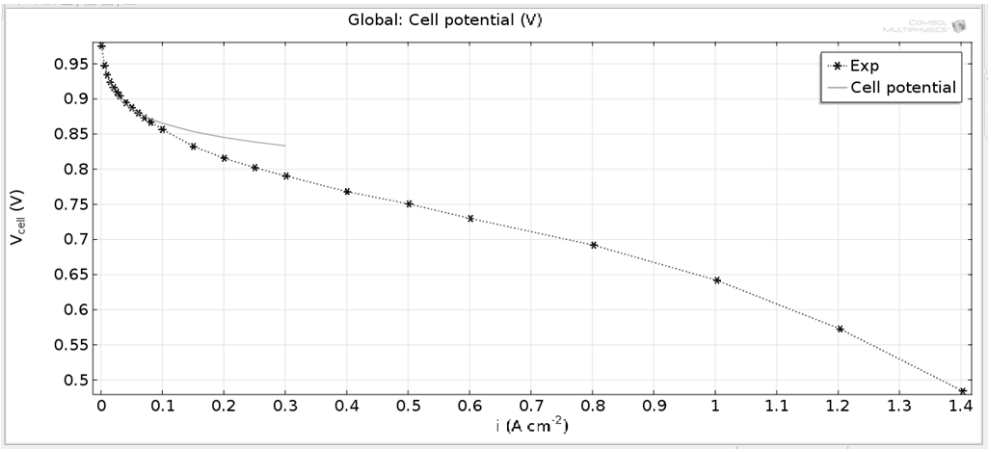

Fig 58: Polarization curve (60°C, Cat. Stoich. = 2, p=2.3-2.5 bar, I_{0c}=1·E-9 A/cm^2)

Other changes have been done, and one surprising thing is that, maintaining all the values as in the previous case, and changing the number of the cells of the FC, from 1 to 20 (the original value) the curve does not change, as it is possible to see in Fig 59.

This means that the role of the number of the cells is not relevant in this model, and in the future work, this should change to adapt well the model to a single cell.

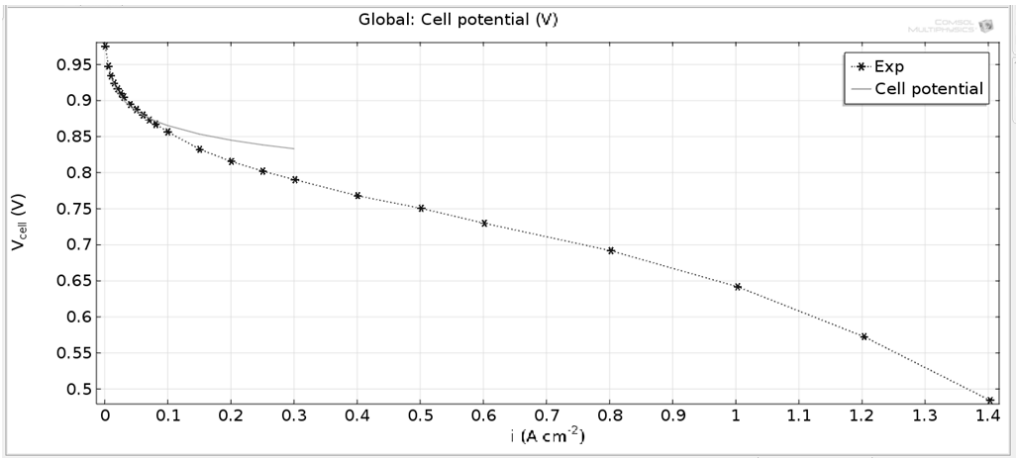

Fig 59: Polarization curve (60°C, Cat. Stoich. = 2, p=2.3-2.5 bar, I0c=1·E-9 A/cm^2, n=20)

The same tests have been done at 80°C, changing all the corresponding parameters. The results are similar as the ones at 60°C. At the cathode current density obtained from the experimental data (7.3E-06) the curve is almost 0.15 higher than the experimental one (Fig 60).

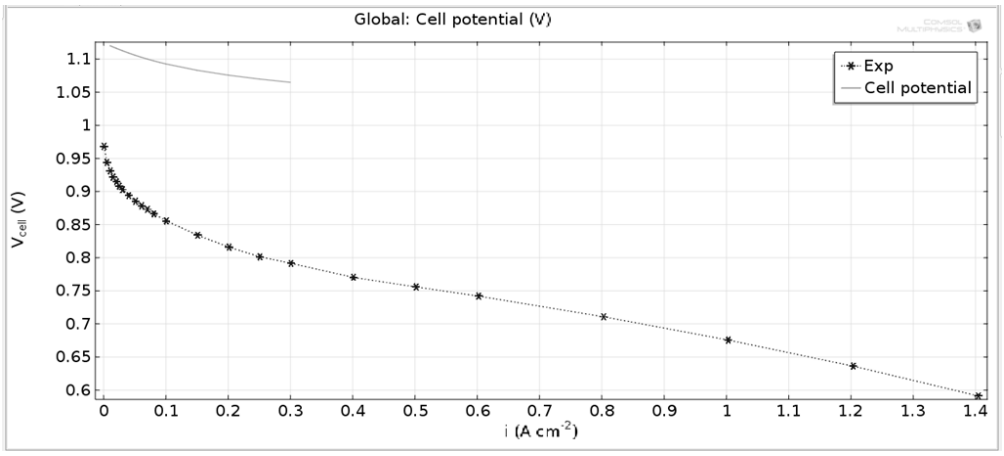

Fig 60: Polarization curve (80°C, Cat. Stoich. = 2, p=2.3-2.5 bar)

The lower this parameter is, the more accurate is the simulated curve. In the following figures, the results with a I_{0c} of 1·E-8 A/cm^2 (Fig 61) and 1·E-9 A/cm^2 (Fig 62) are showed. As in the previous case, the one that is more similar to the experimental one is the one at 1·E-9 A/cm^2.

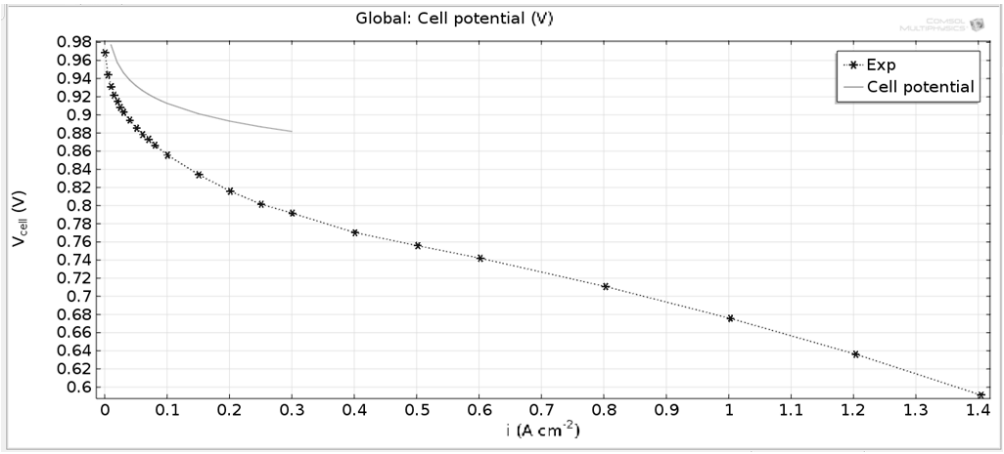

Fig 61: Polarization curve (80°C, Cat. Stoich. = 2, p=2.3-2.5 bar, I_{0c}=1·E-8 A/cm^2)

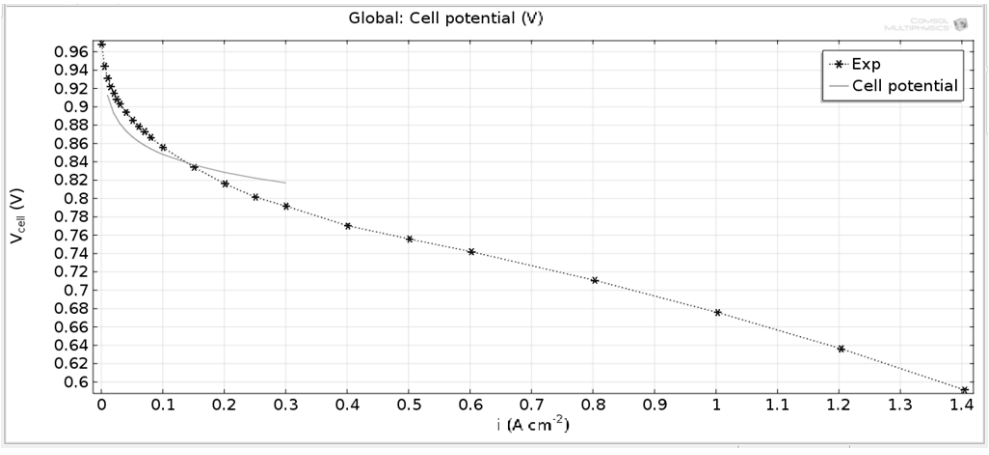

Fig 62: Polarization curve (80°C, Cat. Stoich. = 2, p=2.3-2.5 bar, I_{0c}=1·E-9 A/cm^2)

CHAPTER 8: CONCLUSIONS

In this work, an exhaustive experimental study on PEMFC voltage loss and a first adaptation of a two dimensional CFD model has been presented.

The experimental study supposes an important progress in the consolidation of the study methodology of the voltage losses designed in [a. Husar, Strahl, and Riera 2012] opening at the same time new research topic for future research related with the variation of the internal variables to improve fuel cell performance.

This methodology allows for the internal observation of a fuel cell from the analysis of its output. Isolating the fuel cell losses of the single cell and determining the three indicators (Tafe Slope, ohmic resistance and mass transport resistance), internal conditions of the system can be determined. The Tafel Slope works as an internal kinetic reactions indicator, thus reading those values it is possible to know how fast the internal reactions are. The ohmic resistance gives information about the internal resistance of the fuel cell, which does not depend much the operating condition, but about the water content in the membrane (ionic resistance): if there is no water in the membrane the voltage drops because there is no proton conduction. This is a good indicator to study the membrane degradation due to dry performance. The mass transport resistance indicates the concentration gradients due to the electrode reactants gas consumption, thus changing the partial pressure of the reactants.

All the tests and the subsequent data elaboration developed along the all thesis provides relevant information about the performance of the fuel cell related with external conditions as temperature, pressure or stoichiometry. External variables that, with a good control system, can be set to optimize the oparating condition, finding an equilibrium between the maximum efficiency, the reduction of the parasitic loads and the lifetime of the fuel cell.

Better performance of the fuel cell has been observed at higher temperatures (80°C), higher pressures (2.3 bar in the cathode and 2.5 bar in the anode) and higher cathode stoichiometry (2). At high temperatures the activation losses are lower, due to the higher internal ativity, as well as the ohmic losses (lower resistance at higher temperatures) and mass transport losses. The analysis done in this studio goes further, so beyond this main conclusion, there is a range of operational condition where the fuel cell performance is quite good (60°C and cathode stoichiometry of 1.5) and other where the fuel cell voltage decreases dramatically (cathode stoichiometry of 1.3) or where the fuel cell can not work at stable conditions (at lower temperatures than 60°C). Regarding the pressure, higher pressure is recommended since the results are dramatically better than at low pressure, however at a cost of more energy needed for the compressor.

Moreover, the experimental study supposes a data set useful for a further efficiency and durability studio, as well as a starting point to develop a CFD model robust to improve the fuel cell control.

The model adapted in this work needs additional adjustments to properly reproduce the single cell performance. In this regard, the studies done in this work make available to future research useful observation about the existent model as the adaptation of the model for a single cell, working at a higher temperature range with variable exchange current density and variable charge transfer coefficient.

As a whole, the work presented in this thesis applies a comprehensive experimental approach which describes and implements methodologies and experimental procedures to characterize and model a single cell PEMFC. Automating this method an on-line monitoring can be achieved to minimize the fuel cell losses throw a temperature control.

CHAPTER 9: FUTURE WORK

This thesis is a contribution to the work of the Control team at the *Institut de Robòtica i Informàtica Industrial (UPC – CSIC)* in to the European project PUMA MIND. This work is mainly focused on improving the current models with the integration of multiscale aspects of the relevant phenomena not only pertaining to fuel cell system performance but also to degradation phenomena that occur inside the fuel cell [A. P. Husar 2012].

Moreover, as it is said in the model validation chapter, this work needs to be complemented with an accurate creation, study and validation of a 2D model able to describe the single cell operation and useful for the fuel cell control. This means adapting the existent model [Strahl, 2015], including anode and cathode channels, in order to analyze, especially, the mass transport losses. The model will include voltage loss indicators, with special attention to the parameters and indicators that, from this study, is possible to say that are variable, contrarily to the studies done until now. The model would show of the compressor, in order to optimize the operational costs, maintaining a good performance and avoiding excessive degradation. The final objective would be to design and implement an effective high performance controller.

A scholarship to work on this development of a dynamic model of the thermal supply of gases of a fuel cell has already been adjudicated.

BIBLIOGRAPHY

Barbir, Frano. 2005. "PEM Fuel Cells: Theory and Practice (Sustainable World Series)." *Energy*, 456.

Bezmalinović, Dario, Stephan Strahl, Vicente Roda, and Attila Husar. 2014. "Water Transport Study in a High Temperature Proton Exchange Membrane Fuel Cell Stack." *International Journal of Hydrogen Energy* 39 (20): 10627–40. doi:10.1016/j.ijhydene.2014.04.186.

Husar, A, S Strahl, and J Riera. 2011. "Experimental Characterization and Identification of the Voltage Losses in an Open Cathode PEM Fuel Cell Stack," 2009–12.

Husar, A., S. Strahl, and J. Riera. 2012. "Experimental Characterization Methodology for the Identification of Voltage Losses of PEMFC: Applied to an Open Cathode Stack." *International Journal of Hydrogen Energy* 37 (8). Elsevier Ltd: 7309–15. doi:10.1016/j.ijhydene.2011.11.130.

Husar, Attila Peter. 2012. "Universitat Politècnica de Catalunya Doctoral Thesis : PERFORMANCE INDICATORS FOR THE DYNAMIC Attila Peter Husar Directors :," no. March.

IRI. 2012. "Atomatic Control Research." http://www.iri.upc.edu.

Larminie, James, and Andrew Dicks. 2003. *Fuel Cell Systems Explained*. Chichester [etc.] : John Wiley. http://cataleg.upc.edu/record=b1240691~S1*cat.

Matthey, Johnson. 2015. "Fuel Cell Today." http://www.fuelcelltoday.com/.

O'Hayre, Ryan P. 2009. *Fuel Cell Fundamentals*. Hoboken : John Wiley and Sons. http://cataleg.upc.edu/record=b1350072~S1*cat.

PUMA-MIND. 2014. "PUMA MIND." http://www.pumamind.eu/.

Santarelli, M. G., and M. F. Torchio. 2007. "Experimental Analysis of the Effects of the Operating Variables on the Performance of a Single PEMFC." *Energy Conversion and Management* 48 (1): 40–51. doi:10.1016/j.enconman.2006.05.013.

Santarelli, M. G., M. F. Torchio, and P. Cochis. 2006. "Parameters Estimation of a PEM Fuel Cell Polarization Curve and Analysis of Their Behavior with Temperature." *Journal of Power Sources* 159 (2): 824–35. doi:10.1016/j.jpowsour.2005.11.099.

Strahl, S. 2010. "Characterization, Development and Experimental Validation of a Dynamic PEM Fuel Cell System Model." Hochschule Regensburg - Universitat Politècnica de Catalunya.

http://202.127.29.4/shao_gnss_ac/publications/clock/Study of GPS satellites clock%A1%AFs behaviour.pdf.

Strahl, S., A. Husar, P. Puleston, and J. Riera. 2014. "Performance Improvement by Temperature Control of an Open-Cathode PEM Fuel Cell System." *Fuel Cells* 14 (3): 466–78. doi:10.1002/fuce.201300211.

Strahl, Stephan, Attila Husar, and Alejandro a. Franco. 2014. "Electrode Structure Effects on the Performance of Open-Cathode Proton Exchange Membrane Fuel Cells: A Multiscale Modeling Approach." *International Journal of Hydrogen Energy* 39 (18). Elsevier Ltd: 9752–67. doi:10.1016/j.ijhydene.2014.03.218.

The ASHRAE Handbook Fundamentals... 2013. Atlanta, GA : American Society of Heating, Refrigerating and air-Conditioning Engineers. http://cataleg.upc.edu/record=b1445222~S1*cat.

Wang, Lin, Attila Husar, Tianhong Zhou, and Hongtan Liu. 2003. "A Parametric Study of PEM Fuel Cell Performances." *International Journal of Hydrogen Energy* 28 (11): 1263–72. doi:10.1016/S0360-3199(02)00284-7.

ANNEX

A1. LOW PRESSURE RESULTS

As mentioned in chapter 5.5 the results at low pressure and low temperatures (45°C) are not taken in to account for the successive studios since the fuel cell is highly unstable thus the coefficients related (as shown in the following figures) can not be considered to compare with the other results.

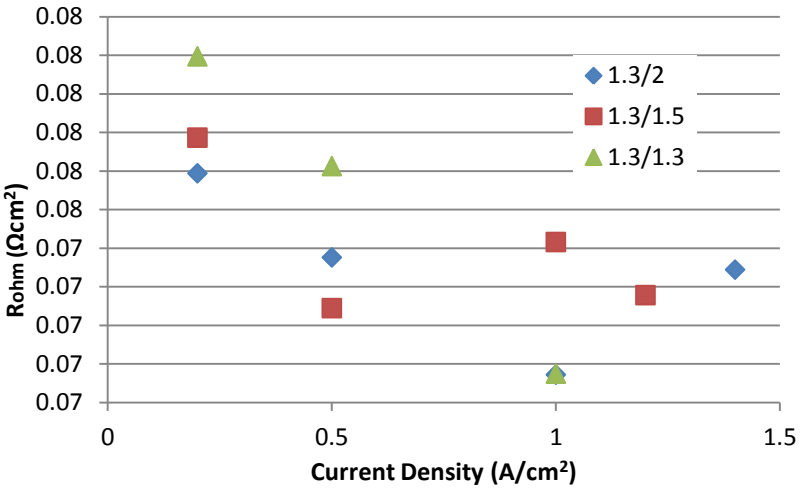

Fig 63: Ohmic resistance as the Ohmic indicator, respect stoichiometry and current density (1.23 – 1.25 bar, 45°C)

At high current densities the fuel cell is higly unstable, thus the temperature rises and this is why the ohmic resistance does not decrease, but increases, as can be seen in Fig 63.

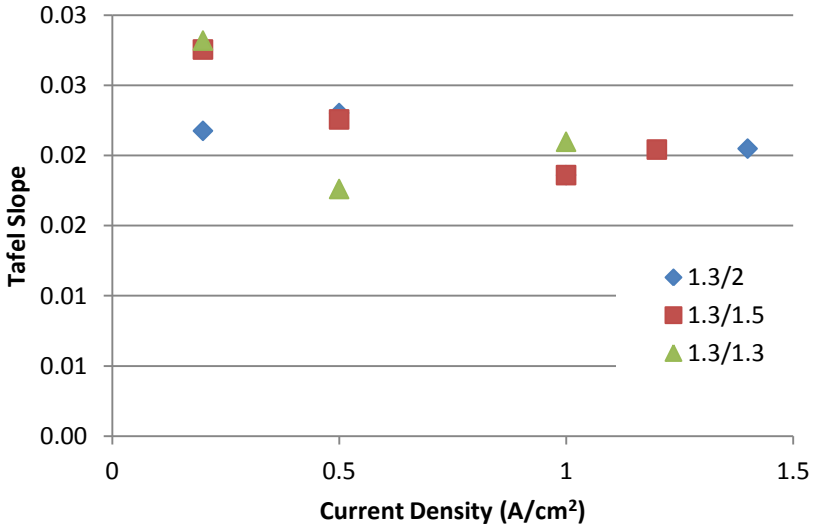

Fig 64: Tafel slope as the activation indicator, respect stoichiometry and current density (1.23 – 1.25 bar, 45°C)

With the Tafel slope (Fig 64) occurs the same, even if the variation is almost insignificant (the Tafel slope is almost constant); it tends to reduce,

but at high current densities it increases, due to the rising temperature respect to the input one (45°C).

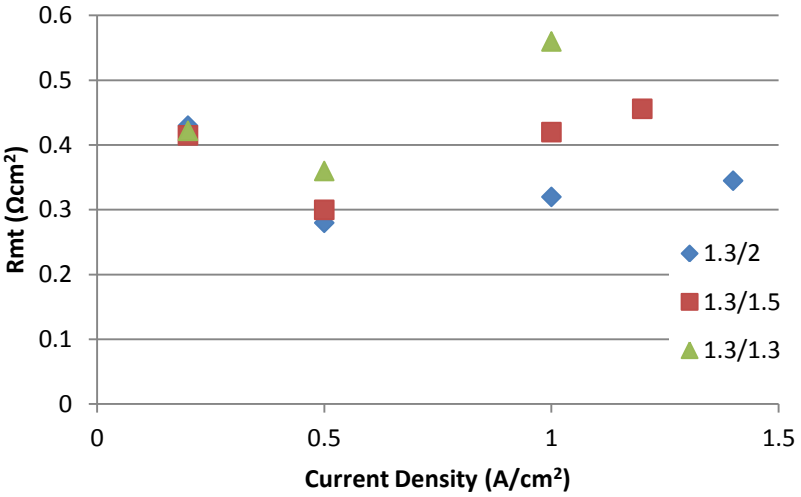

Fig 65: Mass transport resistance as the mass transport losses indicator, respect stoichiometry and current density (1.23 – 1.25 bar, 45°C)

In Fig 65 is clear the instability of the fuel cell operation: the mass transport indicator does not follow a pattern, especially at high current densities.

The tests done at low temperature lead to discard that temperature as a possible temperature for the fuel cell performance. The future studies are carried out comparing only the results at 60°C and 80°C.

In the following figures the results at 60°C and 80°C are presented and compared between them.

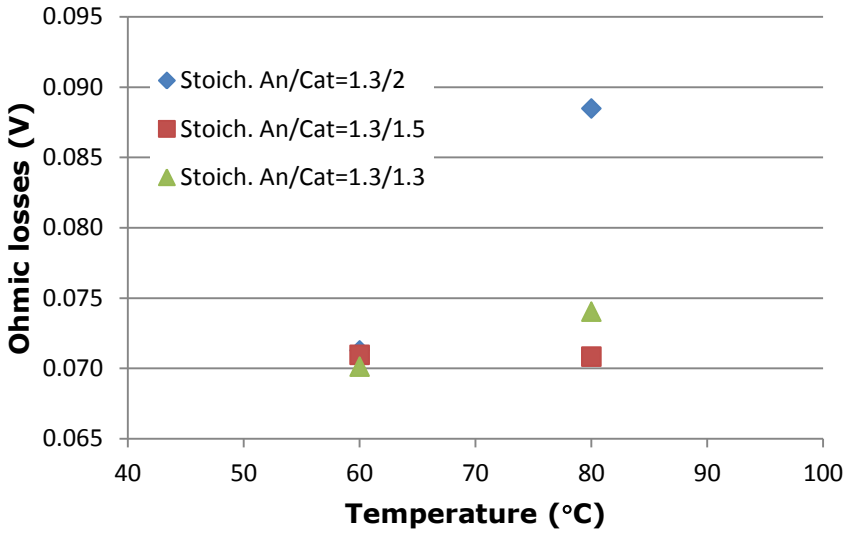

Fig 66: Ohmic losses at 1A/cm^2 respect to stoichiometry and temperature (Pressure An-Cat =1.25-1.23 bar).

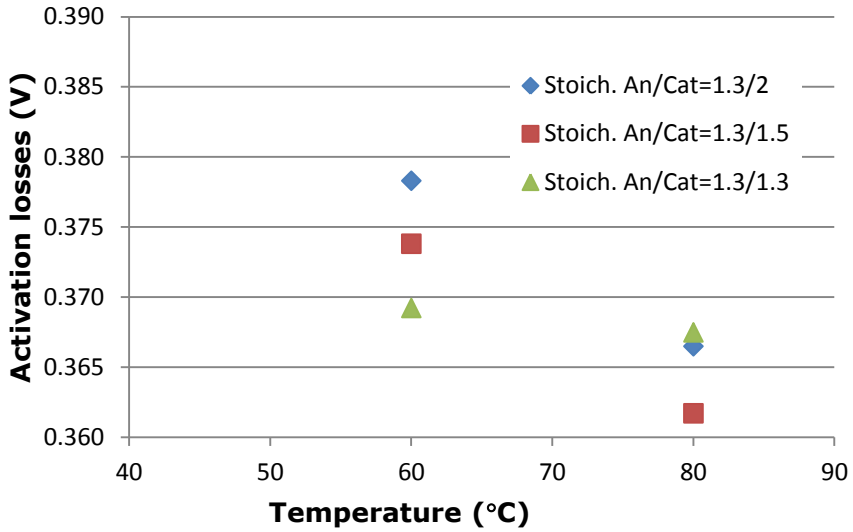

Fig 67: Activation losses at 1A/cm^2 respect to stoichiometry and temperature (Pressure An-Cat =1.25-1.23).

As can be seen in Fig 66 and Fig 67 the activation losses decrease with the temperature, while the ohmic losses are almost constant. They should decrease with the temperature (as in for the case at high temperature) but it does not happen, specially for the case of cathode stoichiometry 2, which value is strange, but it is calculated directly from the value obtained from the EIS, so the probability of a calculation error is reduced.

In Fig 68 is possible to see how the mass transport losses are lower at high temperatures, how is explained in chapter 6.

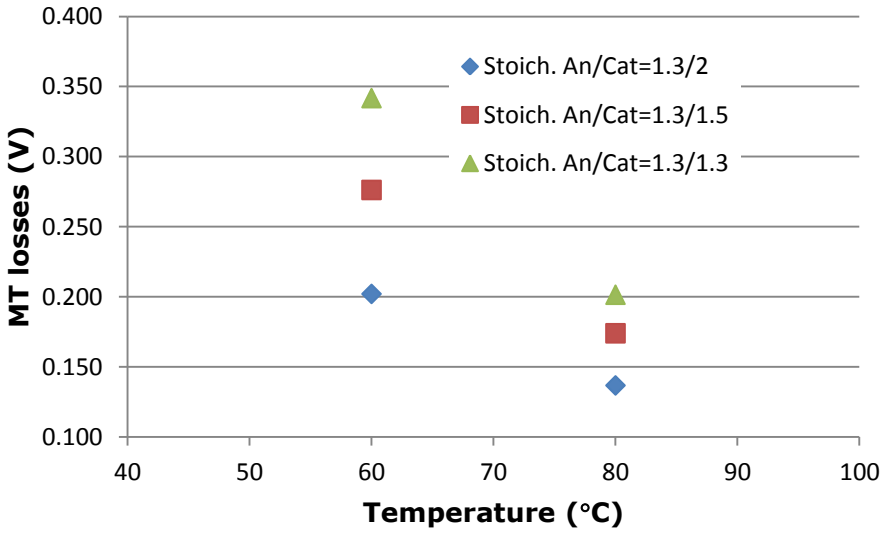

Fig 68: Mass transport losses at 1A/cm^2 respect to stoichiometry and temperature (Pressure An-Cat =1.25-1.23).

Observing the indicators (Fig 69, Fig 70, Fig 71) is possible to observe the same performance as for high pressure, except for the ohmic losses, which are higher at high temperatures, even if the values are almost constant.

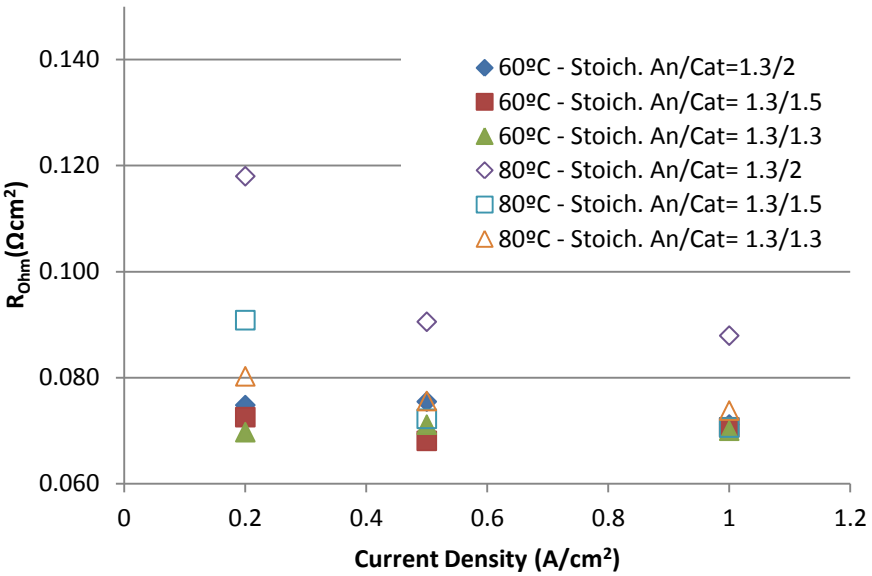

Fig 69: ohmic resistance as the ohmic indicator, respect stoichiometry and current density (Pressure An-Cat =1.25-1.23).

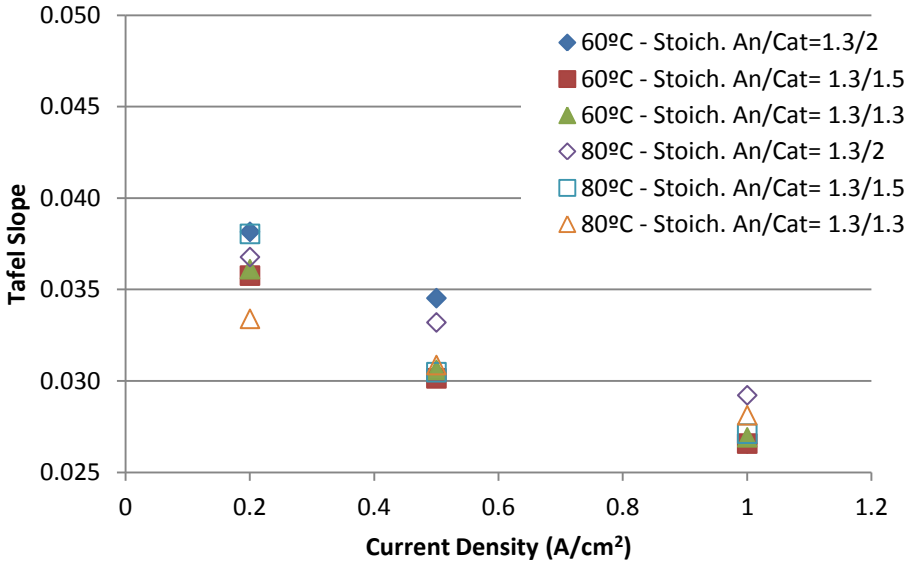

Fig 70: Tafel slope as activation indicator, respect stoichiometry and current density (Pressure An-Cat =1.25-1.23).

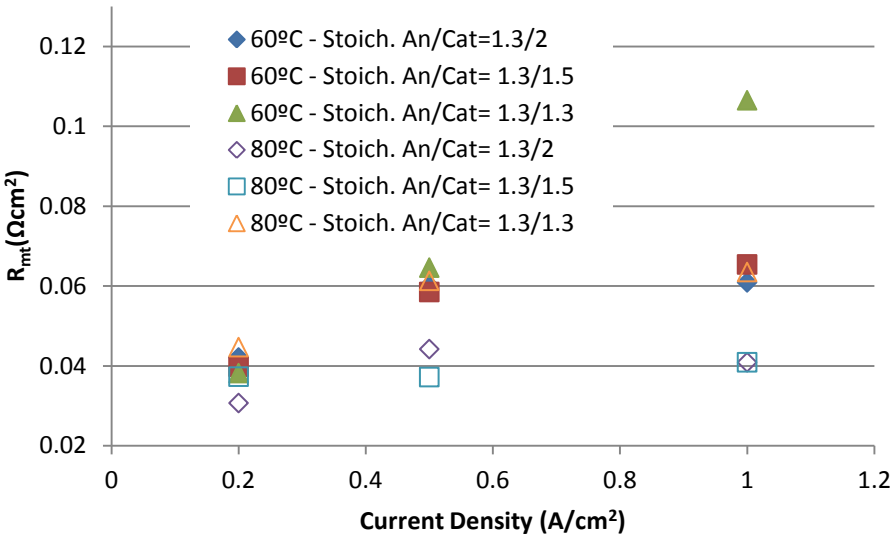

Fig 71: Mass Transport Resistance as mass transport losses indicator, respect stoichiometry and current density (Pressure An-Cat =1.25-1.23).

A2. COMSOL® MODEL

A2.1. Parameters

Parameter	Expression	Description
depth	A_geo/l_ch_a	In-plane Depth
l_ch_a	1.325[m]	Anode channel length
d_GDL	0.2e-3[m]	Thickness GDL
d_MPL	6e-5[m]	Thickness MPL
d_PEM	d_MEA-d_CCL-d_ACL	Thickness PEM, Nafion 1.1mil
d_CCL	2e-5[m]	Thickness CCL
d_ACL	1e-5[m]	Thickness ACL
d_MEA	5.5e-5[m]	ACL+CCL+PEM
d_ch_c	1e-3[m]	Channel width cathode
wO2_0	0,23	O2 mass fraction
wH2Ov_c_0	0,003	H2Ov mass fraction
P_ca	2.3[atm]	Cathode Pressure
k_air	0.027 [W/(m*K)]	Thermal cond, air
k_GDL	1.7 [W/(m*K)]	Thermal cond, GDL
k_PEM	0.15[W/m/K]	Thermal cond, PEM
eps_GDL	0,5	Porosity, GDL
eps_MPL	0,2	Porosity,MPL
eps_CL	eps_MPL	Porosity, CL
rho_GDL	440 [kg/m^3]	Density, GDL
C_p	1260[J/kg/K]	Heat capacity, stack
M_air	0.029[kg/mol]	Mean molar mass, air
C_p_air	1012[J/kg/K]	Heat capacity, air
T0	298[K]	Initial temp
i_ext	0.5 [A/cm^2]	External applied current density
V_cell	0.75[V]	Cell Voltage
n_cell	1	Number of cells
E_th	1.2[V]	Theoretical potential
gamma	1/d_CCL	
T_ext	T0	Channel temp
h_air	50[W/m^2/K]	Heat transfer coefficient
A_geo	25[cm^2]	
R	8.314 [J/(mol*K)]	Universal gas constant
F	96485[C/mol]	Faraday constant
M_H2	0.002[kg/mol]	Molar mass, H2
M_O2	0.032[kg/mol]	Molar mass, O2
M_N2	0.028[kg/mol]	Molar mass, N2
M_H2O	0.018[kg/mol]	Molar mass, H2O

a_diatomic	2,75E-04	
a_H2Ov	3,64E-04	
b_diatomic	1,823	
b_H2Ov	2,334	
wO2_in	0,21	Inlet Massfraction, O2 cathode
wH2Oc_in	0,007	Inlet Massfraction, H2O cathode
wH2_in	0,999	Inlet Massfraction, H2 anode
wH2Oa_in	1-wH2_in	Inlet Massfraction, H2O anode
P_an_in	2.5[bar]	Inlet pressure, anode
mu_H2	8.76e-6[Pa*s]	Viscosity, H2
K_GDL	1e-12[m^2]	Permeability, GDL
K_MPL	1e-15[m^2]	Permeability, MPL
K_CL	1e-16[m^2]	Permeability, CL
T	353[K]	Cell Temp
mu_Air	1.983e-5[Pa*s]	Viscosity, Air
sigma_GDL	5000[S/m]	Conductivity GDL
R_ohm	0.064[V/A]	Ohmic resistance
sigma_PEM	d_PEM*n_cell/(R_ohm*A_geo)	Membrane conductivity
alpha_c	0,509	Cathode charge transfer coefficient
i_0_a	1e-2[A/cm^2]	Anode exchange current density
i_0_c	1e-7[A/cm^2]	Cathode exchange current density
Delta_S	-265.87 [J/K/mol]	Entropy
k_conc	(1+1/alpha_c)	Concentration loss parameter
sigma_H2O	0.0625 [kg/s^2]	Surface tension, H2O_l
rho_H2O_l	970 [kg/m^3]	Density, H2O_l
mu_H2O_l	3.517e-4 [Pa*s]	Dynamic viscosity, H2O_l
theta_GDL	100*pi/180	Water contact angle, GDL
theta_MPL	100*pi/180	Water contact angle, MPL
theta_CL	89.9*pi/180	Water contact angle, CL
E_a	0.449 [eV]	Evaporation energy
k_B	1.380648e-23 [J/K]	Boltzmann constant
k_cond	1000*depth [1/m] [1/s]	Condensation rate constant
k_ev	1*depth[1/m] [1/s]	Evaporation rate constant
k_sorp_0	0.1[1/s]	Sorption dynamic
EW	1.1[kg/mol]	Equivalent molar weight Nafion
rho_PEM	1.95e3 [kg/m^3]	Density, Nafion

A2.2. Simulation Results

In this chapter of the appendix the low pressure simulation results are presented. As for the cases at high pressure, the model fits better the experimental results for lower current densities than the determined experimentally.

The variables modified in these simulations are described in chapter 7.6.

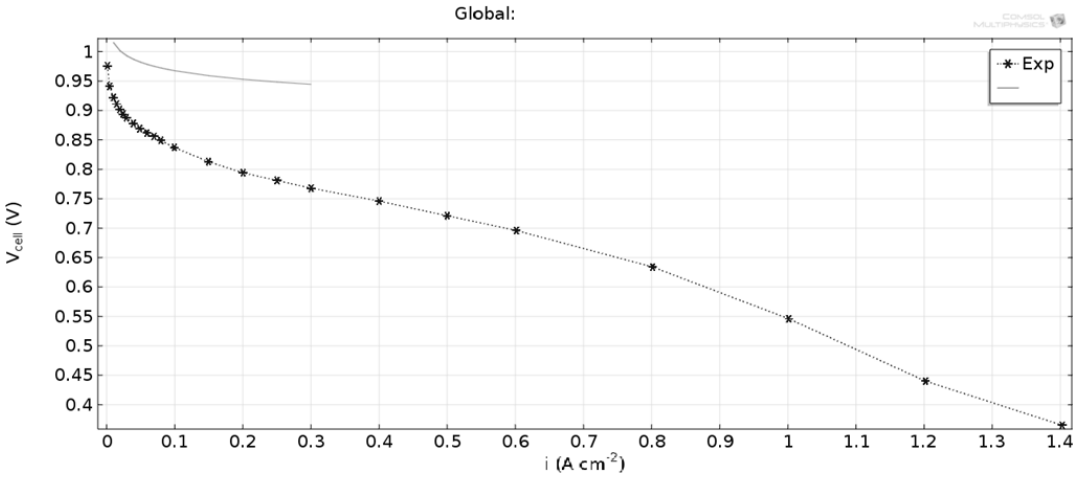

Fig 72: Polarization curve (45°C, Cat. Stoich. = 2, p=1.23-1.25 bar)

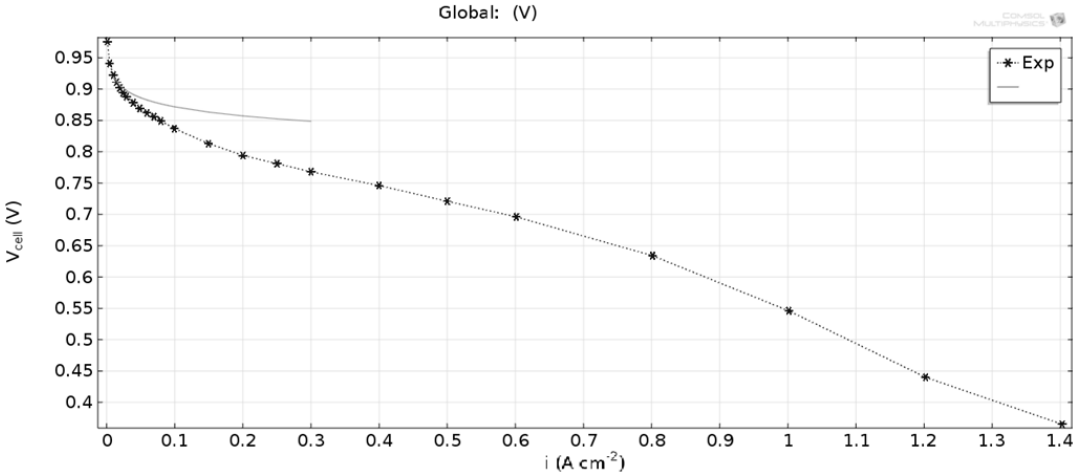

Fig 73: Polarization curve (45°C, Cat. Stoich. = 2, p=1.23-1.25 bar, I_{0c}=1·E-11 A/cm^2)

The main difference is that at 45°C, where the fuel cell his highly unstable, the exchange current densities are lower (order E-7 or E-8), but the mismatch between the experimental data and the model is still of E-3 (arriving in these cases to I_{0c}=1·E-11 A/cm^2 to obtain a more similar result).

In the figures above the results at 45°C and cathode stoichiometry of 2 are presented at different exchange current densities, while in the figures below only the results at experimental conditions are presented, because the

performance of the curve varying the exchange of the current density is the same as in the previous case.

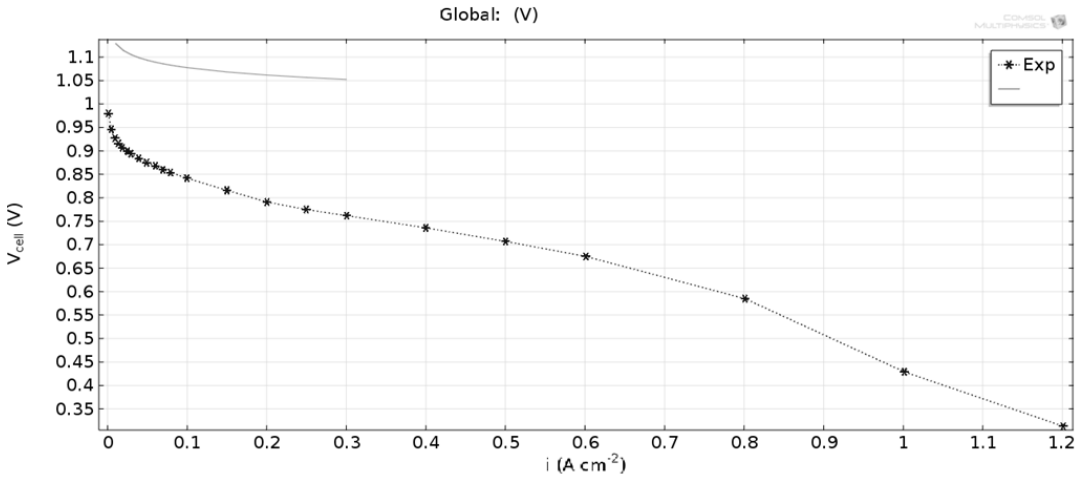

Fig 74: Polarization curve (45°C, Cat. Stoich. = 1.5, p=1.23-1.25 bar)

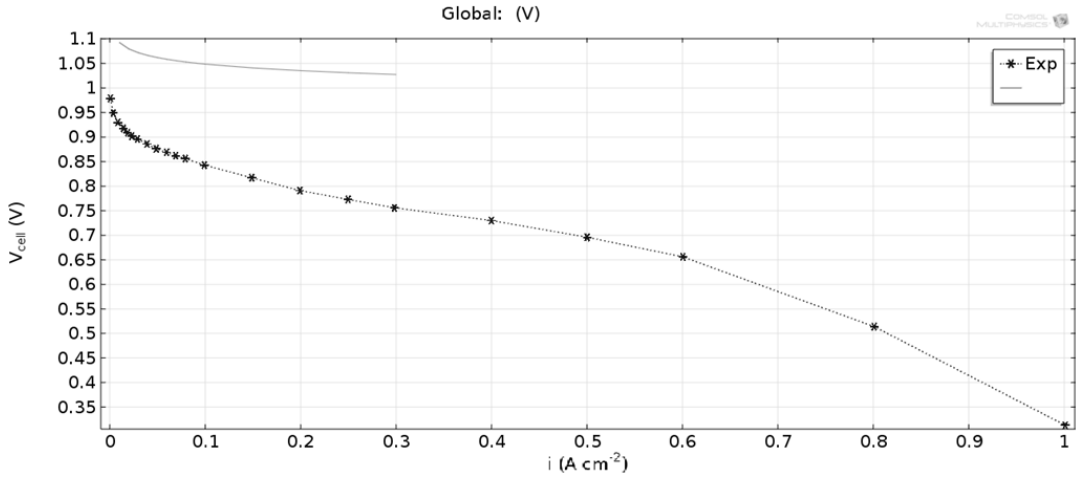

Fig 75: Polarization curve (45°C, Cat. Stoich. = 1.5, p=1.23-1.25 bar)

At 60°C and 80°C the same problem with the exchange current density occurs, but in these cases, as in the ones described in chapter 7.6, the order of the exchange current density is of E-6, and the adjustment with the experimental curve is achieved at an exchange current density of E-9.

At these temperatures the results are presented for each stoichiometry (2, 1.5 and 1.3), but only the results of the simulation at the cathode stoichiometry of 2 are presented also for lower exchange current densities (E-9).

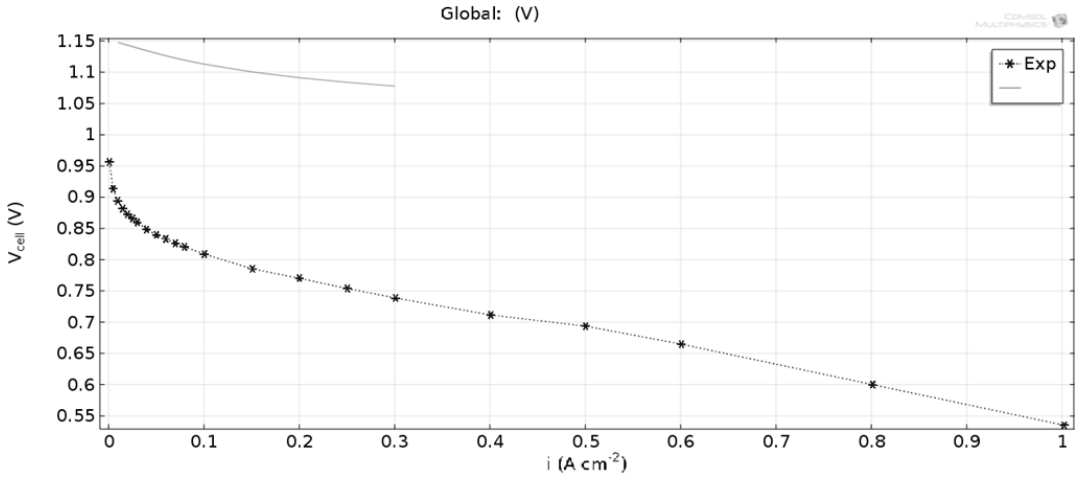

Fig 76: Polarization curve (60°C, Cat. Stoich. = 2, p=1.23-1.25 bar)

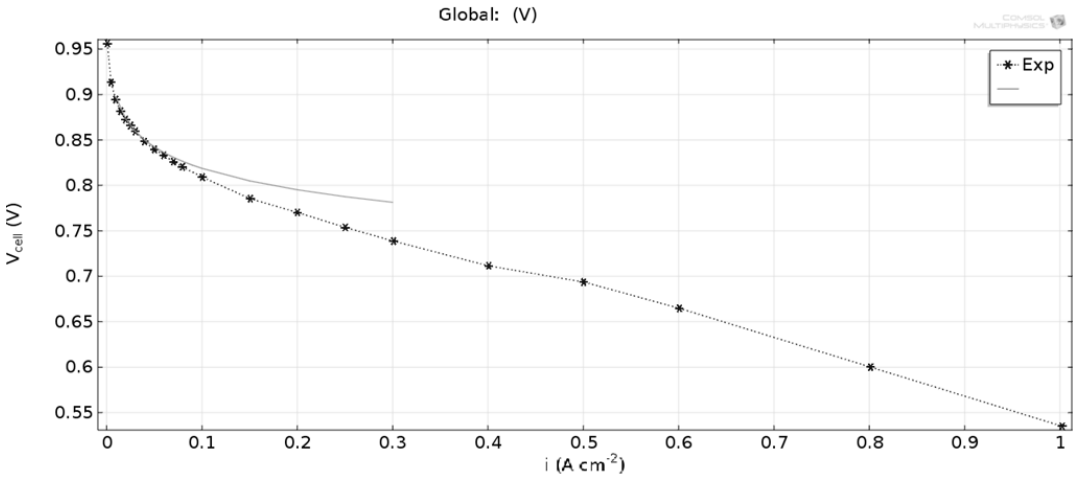

Fig 77: Polarization curve (60°C, Cat. Stoich. = 2, p=1.23-1.25 bar, I_{0c}=1·E-9 A/cm^2)

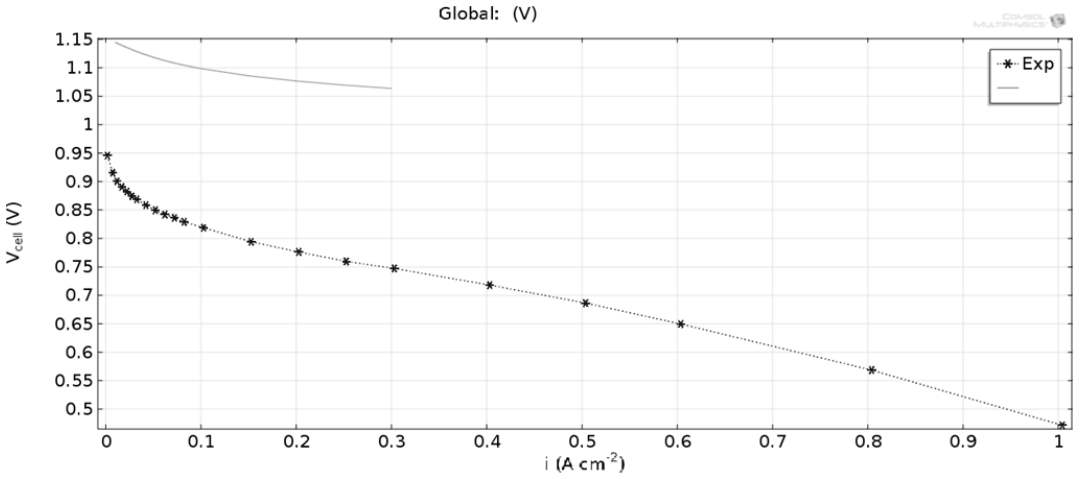

Fig 78: Polarization curve (60°C, Cat. Stoich. = 1.5, p=1.23-1.25 bar)

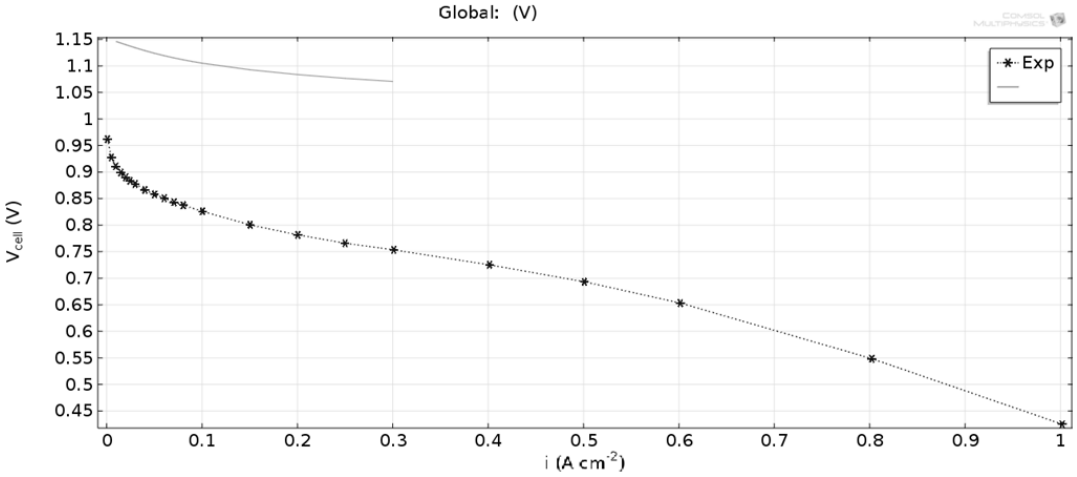

Fig 79: Polarization curve (60°C, Cat. Stoich. = 1.3, p=1.23-1.25 bar)

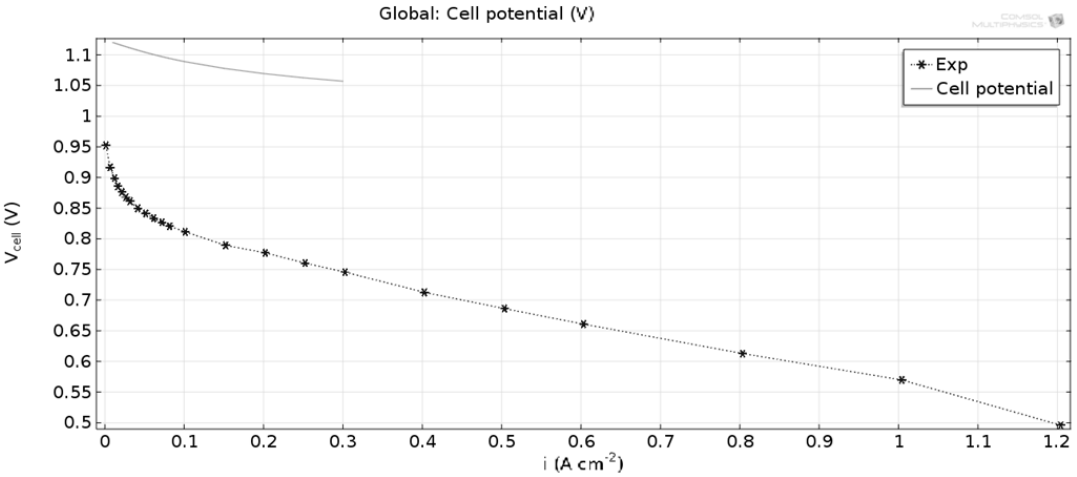

Fig 80: Polarization curve (80°C, Cat. Stoich. = 2, p=1.23-1.25 bar)

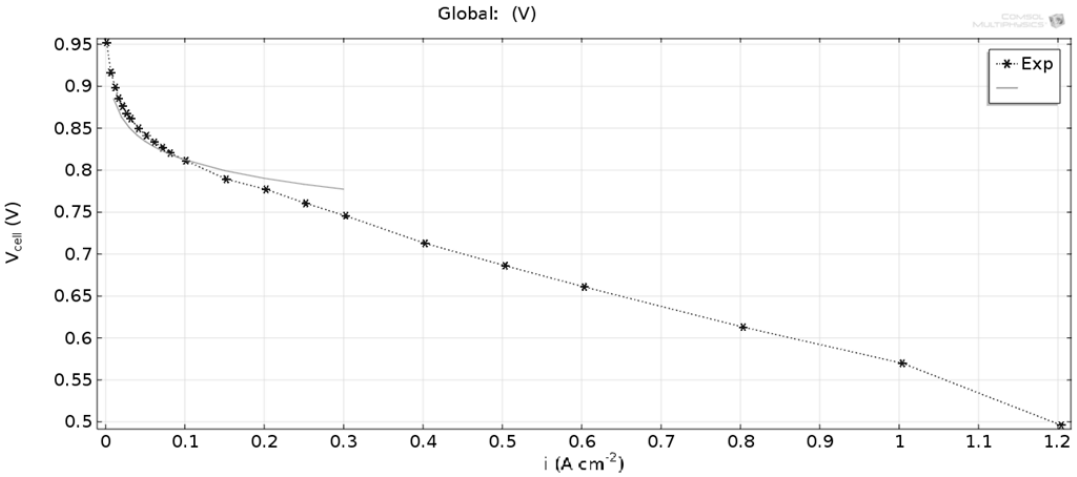

Fig 81: Polarization curve (80°C, Cat. Stoich. = 2, p=1.23-1.25 bar, I_{0c}=1·E-9 A/cm^2)

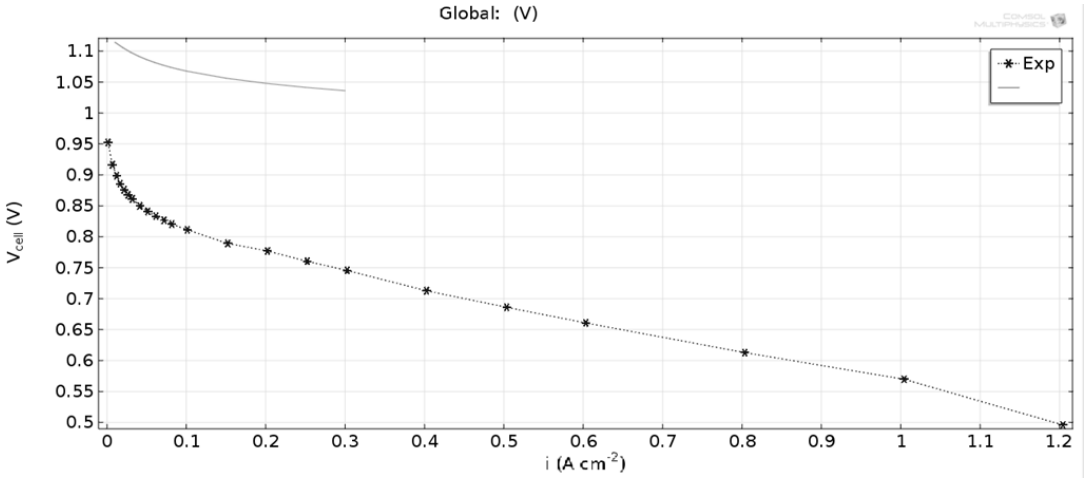

Fig 82: Polarization curve (80°C, Cat. Stoich. = 1.5, p=1.23-1.25 bar)

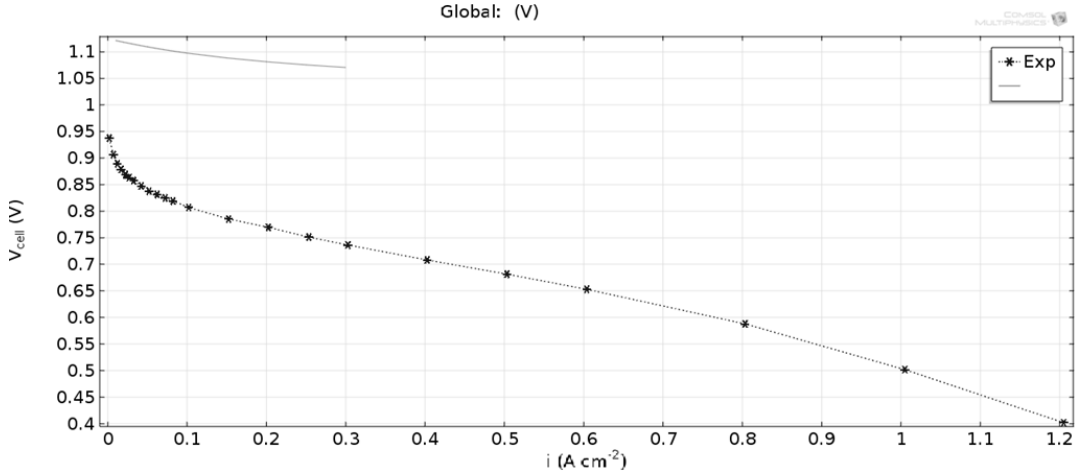

Fig 83: Polarization curve (80°C, Cat. Stoich. = 1.3, p=1.23-1.25 bar)